ROCK POWERED LIFE IN THE SAMAIL OPHIOLITE:

AN ANALOG FOR EARLY EARTH

by

Elizabeth Marie Fones

A dissertation submitted in partial fulfillment
of the requirements for the degree

of

Doctor of Philosophy

in

Microbiology

MONTANA STATE UNIVERSITY
Bozeman, Montana

July 2021

ACKNOWLEDGEMENTS

First, I would like to thank my advisor, Dr. Eric Boyd, for sharing his feedback, time, effort, guidance, and patience. I would also like to thank my other committee members including Drs. Alexis Templeton, Dan Colman, Jovanka Voyich, and Seth Walk for their support and for lending their expertise to my dissertation project. I also extend my gratitude to all collaborators I have had the privilege of working with, including all other members of Rock Powered Life and Oman Drilling Project teams. I also wish to thank Dr. Bonnie Baxter, Jaimi Butler, and their students for enjoyable collaborations at Great Salt Lake. I thank Dr. David Mogk and the staff of I-CAL at Montana State University for their help with mineralogical characterizations.

I am especially grateful to mom, dad, and Robert for their support, love, humor, and guidance throughout my life. I also have greatly appreciated the love and support of Eric Dunham and his family over the past several years. I thank my labmates/friends, past and current, for being helpful, encouraging, and inspiring: Max, Melody, Dan, Erik A., Eric D., Devon, Rachel, Maria, Lisa, Mason, and Alexis. I would also like to thank the MBI staff, especially Ileana Yates-Johnson, for their help over the years. Many thanks to my friends and family, both far and near, who have supported me.

Finally, I am thankful for funding sources that have supported my research, including MSU's Cole Tierney Award, the College of Agriculture's FY19 Equipment Award, MSU's Student Research Travel Grant, Bigelow Laboratory's SCGC Single Cell Sequencing Award, the Joint Genome Institute's FY21 Community Science Program Award, and the MBI Department's Beverly Ferguson Graduate Student Award.

TABLE OF CONTENTS

TABLE OF CONTENTS CONTINUED

TABLE OF CONTENTS CONTINUED

LIST OF TABLES

Table Page

LIST OF TABLES CONTINUED

LIST OF FIGURES

Figure Page

LIST OF FIGURES CONTINUED

LIST OF FIGURES CONTINUED

ABSTRACT

Serpentinization is a geochemical process wherein the oxidation of Fe(II)-bearing minerals in ultramafic rock couples with the reduction of water to generate H_2, which in turn can reduce inorganic carbon to biologically useful substrates such as carbon monoxide and formate. Serpentinization has been proposed to fuel a subsurface biosphere and may have promoted life's emergence on early Earth. However, highly reacted waters exhibit high pH and low concentrations of potential electron acceptors for microbial metabolism, including CO_2. To characterize how serpentinization shapes the distribution and diversity of microbial life, direct cell counts, microcosm-based activity assays, and genomic inferences were performed on environmental rock and water samples from the Samail Ophiolite, Oman. Microbial communities were shaped by water type with cell densities and activities generally declining with increasing pH. However, cells inhabiting highly reacted waters exhibited adaptations enabling them to minimize stresses imposed by serpentinization, including preferentially assimilating carbon substrates for biomolecule synthesis rather than dissimilating them for energy generation, maintaining small genomes, and synthesizing proteins comprised of more reduced amino acids to minimize energetic costs and maximize protein stability in highly reducing waters. Two distinct lineages of a genus of methanogens, *Methanobacterium*, were recovered from subsurface waters. One lineage was most abundant in high pH waters exhibiting millimolar concentrations of H_2, yet lacked two key oxidative [NiFe]-hydrogenases whose functions were presumably replaced by formate dehydrogenases that oxidize formate to yield reductant and CO_2. This allows cells to overcome CO_2/oxidant limitation in high pH waters via a pathway that is unique among characterized Methanobacteria. Finally, gabbro cores from the Stillwater Mine (Montana, U.S.A) were used to develop methods for detecting the activities of cells inhabiting mafic to ultramafic igneous rocks while controlling for potential contaminants. Optimized protocols were applied to rock cores from the Samail Ophiolite, where rates of biological formate and acetate metabolism were higher in rocks interfacing less reacted waters as compared with more extensively reacted waters, and in some cases may greatly exceed activities previously measured in fracture waters. This dissertation provides new insights into the distribution, activities, and adaptations exhibited by life in a modern serpentinizing environment.

CHAPTER ONE

GENERAL INTRODUCTION

Overview

Serpentinization is an abiotic geochemical process that has been proposed to have supported life on early Earth (1, 2). During serpentinization, hydration and oxidation of ferromagnesian minerals (e.g. olivine and pyroxene) in ultramafic rock can couple with the reduction of water to generate H_2 (3). High concentrations of H_2 can serve as an electron donor for microbial life or can abiotically reduce dissolved inorganic carbon (DIC) to reduced carbon substrates including CO, $HCOO^-$, and CH_4 (4, 5), additional potent reductants capable of fueling microbial metabolism. Moreover, ultramafic rocks are common throughout the solar system, suggesting that serpentinization could occur on other planetary bodies where similar rocks encounter liquid water (2). If serpentinization helped facilitate the transition from an abiotic world to a biotic one on early Earth, it could potentially facilitate or have facilitated this same transition on other planetary bodies. However, the oxidation of Fe(II) in serpentinization generates highly reducing conditions in waters that are limited in potential oxidants necessary to support life, including dissolved inorganic carbon (DIC) (6-8). Additionally, consumption of H^+ via the dissolution of primary minerals causes pH to rise with increasing reaction progress (8). As such, the process of serpentinization can create dueling benefits (replete reductant supply) and challenges (high pH and limited oxidant supply including DIC) for subsurface microbial life, both today and early in Earth's history.

Previous studies of serpentinizing systems have shown low densities of microbial cells (often $<10^6$ cells mL^{-1}) in environments impacted by serpentinization (9-13). In serpentinite springs of the Voltri Massif, Italy, Cabeço de Vide, Portugal, and the Cedars peridotite body, California, USA, as few as 10^2 cells mL^{-1} were detected (14-16), with cell densities tending to decrease in waters interpreted to have been more heavily influenced by serpentinization reactions (12, 14, 15). Despite relatively low cell densities, genomic inferences, microcosm-based assays, and isotopic analyses suggest that microorganisms inhabiting serpentinizing environments can utilize abiotic products of the process including hydrogen, carbon monoxide, formate, methane, and acetate in their carbon and/or energy metabolisms (9, 10, 12, 14, 17-21). Highly reacted, hyperalkaline waters in serpentinizing environments tend to not only harbor low cell densities, but also host microbial communities that are less diverse than those inhabiting waters with circumneutral pH (6, 10, 11, 22), consistent with the polyextremophilic and DIC/oxidant limited conditions commonly found at pH > 10 in these systems. More specifically, the decrease in diversity among communities inhabiting hyperalkaline waters tends to be associated with a shift toward a predominance of strict anaerobes, a finding that is in line with the highly reduced nature of these fluids (6, 22). Among the anaerobes commonly detected in hyperalkaline serpentinized waters are putative acetogens and methanogens affiliated with the hydrogenotrophic and autotrophic genus, *Methanobacterium* (6, 9, 14, 19, 23).

Acetogens and hydrogenotrophic methanogens are often advocated as having the most ancient of extant metabolisms (24, 25). There are numerous rationales for the primacy of acetogens and hydrogenotrophic methanogens, including their reliance on the Wood-Ljungdahl (WL) pathway of carbon fixation for central metabolism (26). The WL pathway canonically

couples H_2 oxidation with CO_2 reduction and is putatively ancient as it the only CO_2-fixation pathway that yields ATP (26-28). The ability of acetogens and hydrogenotrophic methanogens to use CO_2 as sole carbon source and electron acceptor via the WL pathway may have alleviated a major barrier for early autotrophic life. CO_2 is presumed to have been readily available on early Earth whereas organic carbon and other potential oxidants (e.g., oxygen, nitrate, ferric iron, and sulfate) are likely to have been far more limiting prior to the advent of oxygenic photosynthesis and the subsequent Great Oxidation Event (29, 30). Indeed, the WL pathway has been proposed to have originally emerged in an ancient serpentinizing environment (2, 26, 31-33). However, highly reacted waters in modern serpentinizing environments exhibit extremely low concentrations of DIC (6, 7, 14, 15, 23) and it is not yet understood how methanogens or other autotrophs such as acetogens could have overcome this limitation.

The present work seeks to characterize how serpentinization reaction progress shapes the distribution and diversity microbial life in subsurface fracture fluids and ultramafic rocks of the Samail Ophiolite, Sultanate of Oman. The Samail Ophiolite is the largest, best-exposed continental site of active serpentinization in the world and therefore provides an accessible field location for investigating how serpentinization shapes microbial communities. In particular, this work will evaluate how cells are distributed throughout subsurface rocks and fracture waters in the Samail Ophiolite, their potential metabolisms and activities, and the adaptations that enable them to overcome stresses imposed by highly-reacted waters in a serpentinizing environment. The Samail Ophiolite is composed of both mafic and ultramafic rocks (largely gabbros and peridotites, respectively) undergoing active, low temperature serpentinization and resulting in distinct water types that have been influenced by host bedrock lithology, mixing, and the extent

of water–rock interactions. Results will be discussed in the context of possible adaptations allowing life to persist under polyextremophilic conditions imposed by a modern serpentinizing environment that may be reminiscent of early Earth.

Life in Modern Serpentinizing Environments

Serpentinization occurs wherever ultramafic rock encounters liquid water, including locations where water circulates through ultramafic mantle rocks via hydrothermal flow and in terrestrial ophiolites where sections of oceanic crust and underlying mantle are tectonically emplaced on continental margins. As such, serpentinization has the potential to support a vast subsurface chemosynthetic microbial biosphere on Earth and other rocky bodies throughout the solar system such as Mars, Europa, and Enceladus (34-37). However, access to these environments is limited to mid-ocean spreading ridges and several globally distributed terrestrial ophiolites. As mentioned in the *General Introduction*, the Samail Ophiolite in Oman is the largest, best-exposed continental site of active serpentinization in the world and thereby provides an accessible natural setting for robustly investigating the habitability of a subsurface serpentinizing environment. Deep wells (~75 m – 475 m deep) drilled by the Oman Ministry of Regional Municipalities and Water Resources prior to the year 2000 interface gabbro and peridotite bedrock and host a range of geochemical characteristics inferred to represent varying degrees of serpentinization reaction progress and water mixing (6-8). This subsurface microbial observatory was expanded between 2016 and 2018 by the Oman Drilling Project (oman.drilling.ac.uk) by drilling multiple new boreholes (300 – 400 m deep) into a large body of mantle peridotite (38). This permitted further investigations into life that not only inhabit waters

influenced by active hydrous alteration of ultramafic mantle rock but that may also inhabit pore spaces and microfractures in the rocks themselves.

Per the model outlined by Leong and Shock, 2020, in modern continental serpentinizing environments, slightly acidic (pH ~5.5) oxic rainwater infiltrates a shallow subsurface aquifer and reacts with ultramafic rocks in a system that is open to atmospheric exchange (8). Dissolution of primary minerals in the ultramafic rocks consumes H^+ (derived from atmospheric CO_2 via $CO_2 + H_2O \rightarrow HCO_3^- + H^+$) and drives an increase in pH. At increased pH, equilibration with atmospheric CO_2 increases dissolved HCO_3^- concentrations, and Mg^{2+} released from primary minerals accumulates in solution. The resulting waters are circumneutral to slightly basic (pH 7-9) and rich in Mg^{2+} and HCO_3^-, commonly referred to as Type I or magnesium bicarbonate-type waters (39-41). As waters percolate more deeply into the subsurface, they continue to react with ultramafic rock and lose contact with the atmosphere. Waters become increasingly reduced as atmosphere-derived gases such as O_2 and CO_2 are exhausted (due to either biological or geochemical reduction) and the oxidation of Fe(II) in primary minerals continues to couple with the reduction of water to generate H_2 that can reach millimolar concentrations. High concentrations of H_2 can drive the reduction of DIC to substrates such as CO, $HCOO^-$, CH_4, and acetate (CH_3COOH). pH increases as H^+ is no longer delivered from atmospheric CO_2. High pH and the accumulation of divalent cations from dissolution of primary minerals (Ca^{2+} and Mg^{2+}) saturate carbonate minerals. Precipitation of dolomite ($CaMg(CO_3)_2$) and magnesite ($MgCO_3$) further depletes DIC and Mg^{2+}. The resulting anoxic waters exhibit pH >10, are highly reducing, and rich in Ca^{2+}, OH^-, and reduced substrates such as H_2 and CH_4.

These highly reacted end-member fluids are commonly referred to as Type II or calcium hydroxide-type waters (39-41).

Few studies to date have compared the microbial communities inhabiting Type I waters, Type II waters, and zones of mixing between these end-member fluids. Rempfert et al., 2017, examined the influence of geochemistry on the taxonomic composition of microbial communities in waters exhibiting a broad range of geochemical characteristics sampled from the Samail Ophiolite via 16S rRNA gene sequencing (6). The results indicate that the pH of waters influenced microbial diversity and shaped the taxonomic composition of microbial communities, with communities inhabiting hyperalkaline (pH > 10) fracture waters exhibiting distinct taxonomic assemblages and lower diversity as compared with those from alkaline and circumneutral (pH ~7–10) waters. Moreover, physiological inferences based on homology of 16S rRNA gene sequences to cultivated representatives suggested that the metabolisms supporting dominant populations inhabiting Type II waters include the anaerobic, low energy-yielding processes of methanogenesis, acetogenesis, and fermentation, which was in line with 16S rRNA gene sequences recovered from Type II waters in the Samail Ophiolite by Miller et al., 2016 (6, 23). However, aside from these observations, it remained unclear how serpentinization reaction progress influences the habitability of subsurface rock- and water-hosted ecosystems at the level of the distribution and densities of microbial cells, their functional potentials, and their rates of substrate utilization/production. This, in turn, limited understanding of the adaptations enabling microbial life to inhabit environments impacted by serpentinization.

Serpentinization and the Emergence of the Wood-Ljungdahl Pathway

The Wood-Ljungdahl (WL) pathway, also known as the reductive acetyl-CoA pathway, is a carbon fixation pathway that canonically couples H_2 oxidation with CO_2 reduction in bacterial acetogens and archaeal methanogens. The results of Weiss et al., 2016, which included phylogenetic analyses for 6.1 million protein coding genes from sequenced bacterial and archaeal genomes to infer the physiology of the last universal common ancestor (LUCA) of Bacteria and Archaea, suggest that the WL pathway was a property of LUCA (24). Unlike other CO_2 fixation pathways, the WL pathway is exergonic (26-28). The overall energy-harvesting reactions catalyzed by acetogenic and methanogenic cells utilizing the WL pathway (i.e., $4H_2 + 2CO_2 \rightarrow CH_3COOH + 2H_2O$ and $4H_2 + CO_2 \rightarrow CH_4 + 2H_2O$, respectively) are identical to spontaneous abiotic reactions triggered by serpentinization (2, 26). Furthermore, metallic and metallic-sulfur clusters in enzymes and electron carriers central to the WL pathway (i.e., the C-cluster in carbon monoxide dehydrogenase (CODH), the A-cluster of acetyl-CoA synthase (ACS), ferredoxins, [NiFe]-hydrogenase, and [Fe]-hydrogenase) are structurally similar to minerals commonly found in serpentinizing environments (26). As such, these proteins may represent a biological refinement of minerals that themselves exhibit catalytic activity. In this view, according to Russel, Hall, and Martin, 2010, “the first energy-harnessing biochemical pathways underpinning microbial growth were not invented by microbes, but were instead biologically catalyzed versions of pre-existing exergonic, although likely sluggish, geochemical processes generating methane and/or acetate” (2). Additionally, Boyd et al., 2020, point out that early autotrophs employing the WL pathway putatively were putatively reliant on iron sulfur cluster(s) containing ferredoxin proteins as central electron carriers, yet the reduction potential of

H_2 (approximately -0.41 V) is not typically low enough to efficiently reduce the low potential ferredoxins that are required by acetogens and methanogens (approximately -0.41 V to -0.50 V) without more recently evolved mechanisms (i.e., electron bifurcation or ion translocation) to lower their potential (42, 43). The combination of high pH conditions and high H_2 concentrations, which are naturally generated via serpentinization reactions that would have been widespread on early Earth, yield H_2 reduction potentials low enough to efficiently reduce these low potential ferredoxins. This further supports the proposition that the earliest autotrophic life may have emerged in an alkaline serpentinizing environment.

Highly reacted fluids in modern serpentinizing environments commonly host high relative abundances of methanogens and putative acetogens inferred to be dependent on the WL pathway for central metabolism. However, these environments are characterized by vanishingly low quantities of DIC, and it is not yet understood how these cells overcome CO_2 limitation for use as an oxidant or carbon source under these conditions. This warranted further investigation as to how these cells survive under the polyextremophilic conditions exhibited by highly reacted Type II waters as a model for how life may have emerged and diversified on early Earth.

Overarching Goals and Hypotheses:

This work seeks to develop new understanding of how serpentinization reaction progress shapes microbial communities in a modern serpentinizing environment. Previous studies have largely focused on the benefits of H_2 and reduced carbon compounds generated via serpentinization reactions in supporting microbial metabolism. However, this dissertation seeks to comprehensively evaluate the habitability of a subsurface serpentinizing environment, including investigations into how the polyextremophilic conditions generated via extensive

serpentinization reactions (i.e., hyperalkaline fluids that are highly reducing and limited in potential oxidants including DIC) constrain microbial life and to characterize the adaptations enabling cells to overcome physiological stresses imposed by highly reacted fluids.

First, I aimed to characterize how serpentinization reaction progress shapes microbial communities at the levels of cell densities, community functional potentials, carbon cycling activities, and genomic features. Specifically, I hypothesized that microbial community functional potential is shaped primarily by fluid pH (a proxy for serpentinization reaction progress) and that reduced carbon compounds generated as a consequence of serpentinization reactions (i.e., formate and carbon monoxide) fuel the carbon and energy needs of resident microorganisms. Further, I hypothesized that increasing pH and the accompanying lack of potential oxidants including DIC in highly reacted waters would constrain microbial cell densities and activities as compared to circumneutral, less extensively reacted waters. Finally, cells would exhibit adaptations to minimize energetic and physiologic stress imposed by highly reducing, carbon-limited conditions in high pH waters.

To evaluate these interrelated hypotheses, subsurface well waters spanning a range in pH conditions were sampled and subjected to geochemical and biological analyses in Chapter 2. To evaluate the distribution of cells in fracture waters of this subsurface environment, cells from waters collected from five wells that intersected differing bedrock rock types and that had differing geochemical compositions were enumerated via epifluorescence microscopy. Filtered biomass from each of seven wells (including two depths for the well exhibiting the highest pH, NSHQ14) was subjected to DNA extraction and metagenomic sequencing and assembly. These metagenomes were ordinated based upon the relative abundances of metabolic proteins they

were inferred to encode. These same metagenomes were probed for homologues of genes inferred to be involved in CO_2 utilization via the WL pathway and in the metabolism of formate and carbon monoxide. Metagenomes were then evaluated for evidence of adaptation to the polyextremophilic conditions present in the high pH waters, including genome streamlining and the preferential use of more reduced amino acids under more reducing external conditions. Finally, a ^{14}C-radiolabeled tracer approach was used to quantify the rate that formate, carbon monoxide, and DIC were dissimilated for energy harvesting and assimilated for biomolecule synthesis. To evaluate the hypothesis that cells preferentially used carbon substrates for biomass generation (as opposed to dissimilation for energy harvesting) as a potential adaptation to carbon limitation among high pH waters, the rate of substrate dissimilation for energy generation was compared with the rate of substrate assimilation to biomass for each substrate.

Second, 16S rRNA gene sequences affiliated with an autotrophic and hydrogenotrophic genus of methanogens, *Methanobacterium*, had been previously detected at high relative abundance in fracture waters exhibiting high pH in the Samail Ophiolite (6, 23) and other globally distributed sites of serpentinization (6, 9, 14, 19, 23). This was intriguing due to the potential emergence of the WL pathway utilized by methanogens in a serpentinizing environment on early Earth. However, it is not well understood how autotrophic methanogens overcome the extremely low concentrations of DIC present in highly reacted waters. In Chapter 3, I began to address this question by reconstructing methanogen genomes from the same metagenomic data described in Chapter 2. I compared methanogenesis pathways in the metagenome assembled genome (MAG) recovered from a well hosting circumneutral (pH ~ 7.6) subsurface fracture waters with MAGs recovered from a well hosting hyperalkaline waters (pH

~11.1 and 11.3) to specifically, investigate the hypothesis that methanogen cells inhabiting circumneutral waters could couple H_2/CO_2 in their carbon and energy metabolisms whereas those inhabiting hyperalkaline waters would be reliant upon oxidation of formate or CO to yield intracellular CO_2 that could then be reduced to CH_4 for energy generation or acetyl-CoA for biomolecule synthesis. I then tested these genomic predictions using microcosm-based experiments wherein I traced the cellular reduction of DIC versus formate to methane using ^{14}C-radiolabeled bicarbonate and formate, respectively. Finally, I evaluated the hypothesis that methanogen cells were continuing to diversify their genomes in hyperalkaline waters by identifying genomic differences between 69 single amplified genomes (SAGs) recovered from waters exhibiting high pH (~11.3).

In Chapter 4, I sought to evaluate the hypothesis that microbial cells are not only distributed throughout the fracture fluids of the Samail Ophiolite, which is the source of waters sampled from wells in work outlined in Chapters 2 and 3, but also within the pore spaces and microfractures of the mafic to ultramafic rocks of the ophiolite and that their activities can be measured via laboratory experiments. However, robust approaches are required to detect the activities of viable cells residing in low-porosity igneous rocks while excluding potential false positives attributable to drill-site and laboratory contaminants. This is particularly true considering the hypothesized low abundances of cells in these samples. I initiated my studies by first characterizing a gabbro test core from the Stillwater Mine, Montana, USA, with respect to its minerology and developing a series of controls to maximize my ability to detect the activities of viable cells inhabiting this core sample while minimizing the introduction of contaminating cells.

Production of CH_4 from acetate (acetoclastic methanogenesis) was chosen as the target activity for protocol optimization since this process should be sensitive to O_2, allowing us to evaluate whether the procedures used to handle the Stillwater Complex core samples were sufficient to preserve and measure the anaerobic activities to be targeted for measurement in Oman rock cores. Acetoclastic methanogenesis might be expected in this type of rock type based on the recovery of DNA sequences affiliated with acetoclastic methanogens in other mafic and ultramafic rock-hosted sites (9, 13, 44, 45). Additionally, methane generation from acetate may first include oxidation (e.g., to CO_2) performed by one cell type and reduction of this product to methane by another. This approach may thereby increase the measurable rate of methane production in microcosms as compared with measuring inorganic carbon reduction to methane alone. In addition to targeting a process likely to be active in the subsurface, I also determined the incubation temperature at which cells exhibited the highest rates of activity to evaluate the hypothesis that the cells were most active at temperatures of the Stillwater Mine. The protocols developed using cores from the Stillwater Complex were then applied to rock cores collected during drilling operations of two new boreholes that host waters of contrasting geochemical conditions in the Samail Ophiolite. The rate of biological disproportionation of acetate to CH_4 and CO_2 was measured in two core sections and compared with the rates of acetate metabolism in waters recovered from the same boreholes. Additionally, formate to CH_4 and oxidation to CO_2 were also selected as target metabolisms in the core sections from the Samail Ophiolite. This is because Chapter 2 revealed that genes encoding formate dehydrogenases were highly abundant in all metagenomes and were more abundant than genes that encode proteins required to oxidize CO (i.e., Mo- or Ni-CODH) or required for the dissimilatory reduction of inorganic carbon via

the processes of methanogenesis or acetogenesis. Chapters 2 and 3 also indicated that the rates of biological formate utilization (i.e., to CO_2, CH_4, and biomass) among cells inhabiting fracture fluids of the Samail Ophiolite nearly always outpaced rates of CO and inorganic carbon utilization. Thus, microcosm assays were used to measure rates of formate metabolism among cells inhabiting core samples from the Samail Ophiolite.

Chapter 5 summarizes the findings of Chapter 2 through Chapter 4. In this section, the major findings of each of the previous three chapters are discussed in terms of the benefits and limitations imposed on microbial life inhabiting modern day environments undergoing serpentinization. Finally, I discuss future research directions that could further our understanding of the extent, activities, and diversification of life in subsurface serpentinizing environments. The implications of this work are discussed in context of the evolution of life on Earth and the potential for discovering life on other planetary bodies.

Additional Ph.D. Research

In addition to three primary-author manuscripts comprising research for my dissertation project, I have co-authored the following five manuscripts in refereed journals during my Ph.D. studies:

1. Templeton, A.S., Ellison, E.T., Glombitza, C., Morono, Y., Rempfert, K.R., Hoehler, T.M., Zeigler, S.K., Kraus, E., Spear, J.R., Nothaft, D.B., **Fones, E.M.**, Boyd, E.S., Munro-Ehrlich, R.M., Mayhew, L.E., Cardace, D., Matter, J.M., Kelemen, P.B., & the Oman Drilling Project Science Party. Accessing the subsurface biosphere within rocks undergoing active low-temperature serpentinization in the Samail Ophiolite (Oman Drilling Project). In Revision in J. Geophys. Res. Biogeosci.

2. Dunham, E.C., **Fones, E.M.**, Fang, Y., Lindsay, M.R., Steuer, C., Fox, N., Willis, M., Walsh, A., Colman, D.R., Baxter, B.K., Lageson, D., Mogk, D., Rupke, A., Xu, H., & Boyd, E.S. An ecological perspective on dolomite formation in Great Salt Lake, Utah. Front. Earth Sci. 2020; 8: 24.

3. Payne, D.*, Dunham, E.C.*, Mohr, E.*, Miller, I.*, Arnold, A.*, Erickson, R.*, **Fones, E.M.***, Lindsay, M.R., Colman, D.R., & Boyd, E.S. Geologic legacy spanning >90 years explains unique Yellowstone hot spring geochemistry and biodiversity. Environ. Microbiol. 2019; 21: 4180-4195. *Authors contributed equally to this work.

4. Poudel, S., Dunham, E.C., Lindsay, M.R., Amenabar, M.J., **Fones, E.M.**, Colman, D.R., & Boyd, E.S. Origin and evolution of flavin-based electron bifurcating enzymes. Front. Microbiol. 2018; 9: 1762.

5. Sward, E.W., **Fones, E.M.**, Spaan, R.R., Pallister, K.B., Haller, B.L., Guerra, F.E., Zurek, O.W., Nygaard, T.K., & Voyich, J.M. (2018). *Staphylococcus aureus* SaeR/S-regulated factors decrease monocyte-derived tumor necrosis factor–α to reduce neutrophil bactericidal activity. J. Infect. Dis. 2018; 217: 943-952.

References

1. Schulte M, Blake D, Hoehler T, McCollom T. Serpentinization and its implications for life on the early Earth and Mars. Astrobiology 2006; 6: 364-376.

2. Russell M, Hall A, Martin W. Serpentinization as a source of energy at the origin of life. Geobiology 2010; 8: 355-371.

3. McCollom TM, Klein F, Robbins M, Moskowitz B, Berquó TS, Jöns N *et al*. Temperature trends for reaction rates, hydrogen generation, and partitioning of iron during experimental serpentinization of olivine. Geochim. Cosmochim. Acta. 2016; 181: 175-200.

4. Seewald JS, Zolotov MY, McCollom T. Experimental investigation of single carbon compounds under hydrothermal conditions. Geochim. Cosmochim. Acta. 2006; 70: 446-460.

5. McCollom TM, Seewald JS. Abiotic synthesis of organic compounds in deep-sea hydrothermal environments. Chem. Rev. 2007; 107: 382-401.

6. Rempfert KR, Miller HM, Bompard N, Nothaft D, Matter JM, Kelemen P *et al*. Geological and geochemical controls on subsurface microbial life in the Samail Ophiolite, Oman. Front. Microbiol. 2017; 8: 56.

7. Canovas PA, Hoehler T, Shock EL. Geochemical bioenergetics during low-temperature serpentinization: An example from the Samail ophiolite, Sultanate of Oman. J. Geophys. Res. Biogeosci. 2017; 122: 1821-1847.

8. Leong JAM, Shock EL. Thermodynamic constraints on the geochemistry of low-temperature, continental, serpentinization-generated fluids. Am. J. Sci. 2020; 320: 185-235.

9. Crespo-Medina M, Twing KI, Sánchez-Murillo R, Brazelton WJ, McCollom TM, Schrenk MO. Methane dynamics in a tropical serpentinizing environment: the Santa Elena Ophiolite, Costa Rica. Front. Microbiol. 2017; 8: 916.

10. Twing KI, Brazelton WJ, Kubo MD, Hyer AJ, Cardace D, Hoehler TM *et al*. Serpentinization-influenced groundwater harbors extremely low diversity microbial communities adapted to high pH. Front. Microbiol. 2017; 8: 308.

11. Brazelton WJ, Morrill PL, Szponar N, Schrenk MO. Bacterial communities associated with subsurface geochemical processes in continental serpentinite springs. Appl. Environ. Microbiol. 2013; 79: 3906-3916.

12. Lang SQ, Früh-Green GL, Bernasconi SM, Lilley MD, Proskurowski G, Méhay S *et al*. Microbial utilization of abiogenic carbon and hydrogen in a serpentinite-hosted system. Geochim. Cosmochim. Acta. 2012; 92: 82-99.

13. Schrenk MO, Kelley DS, Bolton SA, Baross JA. Low archaeal diversity linked to subseafloor geochemical processes at the Lost City Hydrothermal Field, Mid-Atlantic Ridge. Environ. Microbiol. 2004; 6: 1086-1095.

14. Brazelton WJ, Thornton CN, Hyer A, Twing KI, Longino AA, Lang SQ *et al*. Metagenomic identification of active methanogens and methanotrophs in serpentinite springs of the Voltri Massif, Italy. PeerJ 2017; 5: e2945.

15. Morrill PL, Kuenen JG, Johnson OJ, Suzuki S, Rietze A, Sessions AL *et al*. Geochemistry and geobiology of a present-day serpentinization site in California: The Cedars. Geochim. Cosmochim. Acta. 2013; 109: 222-240.

16. Tiago I, Chung AP, Veríssimo A. Bacterial diversity in a nonsaline alkaline environment: heterotrophic aerobic populations. Appl. Environ. Microbiol. 2004; 70: 7378-7387.

17. Brazelton WJ, Nelson B, Schrenk MO. Metagenomic evidence for H_2 oxidation and H_2 production by serpentinite-hosted subsurface microbial communities. Front. Microbiol. 2012; 2: 268.

18. Morrill PL, Brazelton WJ, Kohl L, Rietze A, Miles SM, Kavanagh H *et al*. Investigations of potential microbial methanogenic and carbon monoxide utilization pathways in ultra-basic reducing springs associated with present-day continental serpentinization: the Tablelands, NL, CAN. Front. Microbiol. 2014; 5: 613.

19. Woycheese KM, Meyer-Dombard DAR, Cardace D, Argayosa AM, Arcilla CA. Out of the dark: transitional subsurface-to-surface microbial diversity in a terrestrial serpentinizing seep (Manleluag, Pangasinan, the Philippines). Front. Microbiol. 2015; 6: 44.

20. Neubeck A, Sun L, Müller B, Ivarsson M, Hosgörmez H, Özcan D *et al*. Microbial community structure in a serpentine-hosted abiotic gas seepage at the Chimaera Ophiolite, Turkey. Appl. Environ. Microbiol. 2017; 83: e03430-03416.

21. Lang SQ, Früh-Green GL, Bernasconi SM, Brazelton WJ, Schrenk MO, McGonigle JM. Deeply-sourced formate fuels sulfate reducers but not methanogens at Lost City hydrothermal field. Sci. Rep. 2018; 8: 1-10.

22. Suzuki S, Ishii Si, Wu A, Cheung A, Tenney A, Wanger G *et al*. Microbial diversity in The Cedars, an ultrabasic, ultrareducing, and low salinity serpentinizing ecosystem. Proc. Natl. Acad. Sci. 2013; 110: 15336-15341.

23. Miller HM, Matter JM, Kelemen P, Ellison ET, Conrad ME, Fierer N *et al*. Modern water/rock reactions in Oman hyperalkaline peridotite aquifers and implications for microbial habitability. Geochim. Cosmochim. Acta. 2016; 179: 217-241.

24. Weiss MC, Sousa FL, Mrnjavac N, Neukirchen S, Roettger M, Nelson-Sathi S *et al*. The physiology and habitat of the last universal common ancestor. Nat. Microbiol. 2016; 1: 1-8.

25. Martin WF, Weiss MC, Neukirchen S, Nelson-Sathi S, Sousa FL. Physiology, phylogeny, and LUCA. Microb. Cell 2016; 3: 582.

26. Russell MJ, Martin W. The rocky roots of the acetyl-CoA pathway. Trends Biochem. Sci. 2004; 29: 358-363.

27. Berg IA. Ecological aspects of the distribution of different autotrophic CO_2 fixation pathways. Appl. Environ. Microbiol. 2011; 77: 1925.

28. Ljungdahl L. The autotrophic pathway of acetate synthesis in acetogenic bacteria. Annu. Rev. Microbiol. 1986; 40: 415-450.

29. Moore EK, Jelen BI, Giovannelli D, Raanan H, Falkowski PG. Metal availability and the expanding network of microbial metabolisms in the Archaean eon. Nat. Geosci. 2017; 10: 629-636.

30. Lyons TW, Reinhard CT, Planavsky NJ. The rise of oxygen in Earth's early ocean and atmosphere. Nature 2014; 506: 307-315.

31. Martin W, Baross J, Kelley D, Russell MJ. Hydrothermal vents and the origin of life. Nat. Rev. Microbiol. 2008; 6: 805-814.

32. Sojo V, Herschy B, Whicher A, Camprubi E, Lane N. The origin of life in alkaline hydrothermal vents. Astrobiology 2016; 16: 181-197.

33. Martin WF, Sousa FL. Early microbial evolution: the age of anaerobes. Cold Spring Harb. Perspect. Biol. 2016; 8: a018127.

34. Chassefiére E, and Leblanc, F. Constraining methane release due to serpentinization by the observed D/H ratio on Mars. Earth Planet. Sci. Lett. 2011; 310: 262-271.

35. Glein CR, Baross JA, Waite JH. The pH of Enceladus' ocean. Geochim. Cosmochim. Acta. 2015; 162: 202-219.

36. Waite JH, Glein CR, Perryman RS, Teolis BD, Magee BA, Miller G *et al*. Cassini finds molecular hydrogen in the Enceladus plume: evidence for hydrothermal processes. Science 2017; 356: 155-159.

37. Vance S, Melwani Daswani M. Serpentinite and the search for life beyond Earth. Philos. Trans. R. Soc. A. 2020; 378: 20180421.

38. Kelemen P, Matter J, Teagle D, Coggon J, Team ODPS. Proceedings of the Oman Drilling Project: Scientific Drilling in the Samail Ophiolite, Sultanate of Oman. International Ocean Discovery Program 2020; Phase 1 and 2.

39. Paukert AN, Matter JM, Kelemen PB, Shock EL, Havig JR. Reaction path modeling of enhanced in situ CO_2 mineralization for carbon sequestration in the peridotite of the Samail Ophiolite, Sultanate of Oman. Chem. Geol. 2012; 330: 86-100.

40. Barnes I, O'Neil JR. The relationship between fluids in some fresh alpine-type ultramafics and possible modern serpentinization, western United States. Geol. Soc. Am. Bull. 1969; 80: 1947-1960.

41. Neal C, Stanger G. Past and present serpentinisation of ultramafic rocks; an example from the Semail Ophiolite Nappe of Northern Oman. The Chemistry of Weathering. 1985. Springer. pp 249-275.

42. Boyd ES, Amenabar MJ, Poudel S, Templeton AS. Bioenergetic constraints on the origin of autotrophic metabolism. Philos. Trans. R. Soc. A. 2020; 378: 1471-2962.

43. Buckel W, Thauer RK. Energy conservation via electron bifurcating ferredoxin reduction and proton/Na+ translocating ferredoxin oxidation. Biochim. Biophys. Acta Bioenerg. 2013; 1827: 94-113.

44. Orcutt BN, Bach W, Becker K, Fisher AT, Hentscher M, Toner BM *et al*. Colonization of subsurface microbial observatories deployed in young ocean crust. ISME J. 2011; 5: 692-703.

45. Lever MA, Rouxel O, Alt JC, Shimizu N, Ono S, Coggon RM *et al*. Evidence for microbial carbon and sulfur cycling in deeply buried ridge flank basalt. Science 2013; 339: 1305-1308.

CHAPTER TWO

PHYSIOLOGICAL ADAPTATIONS TO SERPENTINIZATION IN THE SAMAIL OPHIOLITE, OMAN

Contribution of Authors and Co-Authors

Manuscript in Chapter 2

Author: Elizabeth M. Fones
Contributions: Contributed to experimental design and conducted the experiments. Contributed to the writing the manuscript.

Co-Author: Daniel R. Colman
Contributions: Contributed to bioinformatics analyses and writing the manuscript.

Co-Author: Emily A. Kraus
Contributions: Contributed to collecting samples, conducting experiments, and writing the manuscript.

Co-Author: Daniel B. Nothaft
Contributions: Contributed to collecting samples, conducting experiments, and writing the manuscript.

Co-Author: Saroj Poudel
Contributions: Contributed to bioinformatics analyses and writing the manuscript.

Co-Author: Kaitlin R. Rempfert
Contributions: Contributed to collecting samples, conducting experiments, and writing the manuscript.

Co-Author: John R. Spear
Contributions: Contributed to sample collection and writing the manuscript.

Co-Author: Alexis S. Templeton
Contributions: Contributed to project design, sample collection, and writing the manuscript.

Co-Author: Eric S. Boyd
Contributions: Contributed to experimental design, sample collection, and writing the manuscript.

Manuscript Information Page

Elizabeth M. Fones, Daniel R. Colman, Emily A. Kraus, Daniel B. Nothaft, Saroj Poudel, Kaitlin R. Rempfert, John R. Spear, Alexis S. Templeton, and Eric S. Boyd

The International Society for Microbial Ecology Journal

Status of Manuscript:

____ Prepared for submission to a peer-reviewed journal

____ Officially submitted to a peer-reviewed journal

____ Accepted by a peer-reviewed journal

__x__Published in a peer-reviewed journal

Nature Publishing Group

Issue date: July 2019, doi: 10.1038/s41396-019-0391-2

Physiological Adaptations to Serpentinization in the Samail Ophiolite, Oman

Elizabeth M. Fones[1,4], Daniel R. Colman[1,4], Emily A. Kraus[2,4], Daniel B. Nothaft[3,4], Saroj Poudel[1,4], Kaitlin R. Rempfert[3,4], John R. Spear[2,4], Alexis S. Templeton[3,4], and Eric S. Boyd[1,4,*]

[1]*Department of Microbiology & Immunology, Montana State University, Bozeman, MT*
[2]*Department of Civil and Environmental Engineering, Colorado School of Mines, Golden, CO*
[3]*Department of Geological Sciences, University of Colorado, Boulder, CO*
[4]*NASA Astrobiology Institute, Mountain View, CA*

[*]Author of correspondence: Eric S. Boyd (*eboyd@montana.edu*)

Department of Microbiology & Immunology

Montana State University

PO Box 173520

Bozeman, MT 59717

Phone: (406) 994-7046

Fax: (406) 994-4926

Hydration of ultramafic rock during the geologic process of serpentinization can generate reduced substrates that microorganisms may use to fuel their carbon and energy metabolisms. However, serpentinizing environments also place multiple constraints on microbial life by generating highly reduced hyperalkaline waters that are limited in dissolved inorganic carbon. To better understand how microbial life persists under these conditions, we performed geochemical measurements on waters from a serpentinizing environment and subjected planktonic microbial cells to metagenomic and physiological analyses. Metabolic potential inferred from metagenomes correlated with fluid type, and genes involved in anaerobic metabolisms were enriched in hyperalkaline waters. The abundance of planktonic cells and their rates of utilization of select single-carbon compounds were lower in hyperalkaline waters than alkaline waters. However, the ratios of substrate assimilation to dissimilation were higher in hyperalkaline waters than alkaline waters, which may represent adaptation to minimize energetic and physiologic stress imposed by highly reducing, carbon-limited conditions. Consistent with this hypothesis, estimated genome sizes and average oxidation states of carbon in inferred proteomes were lower in hyperalkaline waters than in alkaline waters. These data suggest that microorganisms inhabiting serpentinized waters exhibit a unique suite of physiological adaptations that allow for their persistence under these polyextremophilic conditions.

The earliest forms of life on Earth are commonly thought to have relied on redox reactions involving hydrogen (H_2) and single-carbon (C1) compounds to fuel their carbon and energy metabolisms [1]. The geologic process of serpentinization may have served as a source of these substrates for early life [2]. During serpentinization, the oxidation of ferromagnesian minerals (e.g., olivine) in mafic and ultramafic rocks couples with the reduction of water to produce H_2 [3]. High concentrations of dissolved H_2 can drive the reduction of dissolved inorganic carbon (DIC) to reduced carbon compounds such as formate ($HCOO^-$), carbon monoxide (CO), and methane (CH_4) through reactions similar to the Sabatier process [3, 4]. However, increased serpentinization reaction progress also yields increasingly high pH waters that can be metal-rich and limited in available oxidants [5]. Moreover, divalent cations in serpentinized waters and in minerals common in ultramafic rocks interact with CO_2 to precipitate mineral carbonates (e.g., $MgCO_3$, $CaCO_3$), thereby yielding low concentrations of DIC in highly reacted waters [5,6,7]. Despite the potential for serpentinization to have fueled the metabolisms of life on early Earth, the specific adaptations that allow for life under these conditions are not well understood.

Previous studies of serpentinizing systems have shown low densities of microbial cells (often $<10^6$ cells mL^{-1}) in environments impacted by serpentinization [8,9,10,11,12]. In serpentinite springs of the Voltri Massif, Italy, Cabeço de Vide, Portugal, and the Cedars peridotite body, California, USA, as few as 10^2 cells mL^{-1} were detected [13,14,15]. Despite relatively low densities, microbial cells inhabiting environments influenced by serpentinization appear to be capable of using products of this process. For example, sequencing of community DNA extracted from a hyperalkaline seep community in the Tablelands Ophiolite

(Newfoundland, Canada), a hydrothermal chimney community at Lost City Hydrothermal Field (LCHF; mid-Atlantic Ocean), and the Coast Range Ophiolite Microbial Observatory (CROMO; California, USA) revealed genes that code for a variety of hydrogenase and CO dehydrogenase (CODH) proteins [9, 16], suggesting that organisms within these communities are capable of utilizing H_2 and CO in their carbon and/or energy metabolisms. Similarly, biological ^{13}CO consumption was observed in microcosm experiments containing water and sediments from hyperalkaline springs in the Tablelands Ophiolite [17]. Additional metagenomic sequencing data coupled with experimental evidence demonstrating transformation of isotopically labeled acetate ($^{13}CH_3COO^-$) to methane ($^{13}CH_4$), as well as $^{13}CH_4$ transformation to isotopically labeled bicarbonate ($H^{13}CO_3^-$), points to active CH_4 cycling in serpentinite springs of the Voltri Massif, Italy [13]. A high relative abundance of 16S ribosomal RNA (rRNA) genes closely related to known methanogens (up to 90% of the total archaeal population) coupled with detection of all key genes involved in hydrogenotrophic methanogenesis, acetoclastic methanogenesis, and formatotrophic methanogenesis in metagenomes from the Santa Elena Ophiolite, Costa Rica, reveals the putative importance of methanogens in this and potentially other environments undergoing active serpentinization [8]. Similarly, physiological inference based on homology of 16S rRNA genes suggests that organisms capable of H_2 oxidation, CO oxidation, and CH_4 cycling inhabit a serpentinizing seep in the Zambales Ophiolite, Philippines [18], and putative H_2 and CH_4 oxidizers have similarly been identified via homology of 16S rRNA genes in a serpentinite-hosted seep at the Chimaera Ophiolite, Turkey [19]. The isotopic signature of lipid biomarkers combined with metagenomic insights suggest that $HCOO^-$ serves as a source of electrons for sulfate reducers, but not methanogens, in the LCHF [20]. Together, these data

suggest that microbial communities from globally distributed environments impacted by serpentinization harbor the functional capacity to utilize products of serpentinization to support their energy and carbon metabolisms.

The Samail Ophiolite in the Sultanate of Oman is the largest, best-exposed ophiolite in the world, thereby providing an accessible field location for studying the physiological adaptations that allow microorganisms to inhabit environments impacted by serpentinization [21]. The ophiolite is composed of both mafic and ultramafic rocks (largely gabbros and peridotites, respectively) that are purported to be undergoing active serpentinization, resulting in distinct water types influenced by host bedrock lithology, mixing, and the extent of water–rock interactions [5]. Rempfert et al. examined the influence of geochemistry on the taxonomic composition of microbial communities in fracture waters sampled from wells drilled in the Samail Ophiolite via 16S rRNA gene sequencing [5]. The results indicate that the pH of waters influenced microbial diversity and shaped the taxonomic composition of microbial communities, with communities inhabiting hyperalkaline (pH > 10) fracture waters exhibiting distinct taxonomic assemblages and lower diversity as compared with those from alkaline and circumneutral (pH ~7–10) waters. Moreover, physiological inferences based on homology of 16S rRNA gene sequences to cultivated representatives suggested that the metabolisms supporting dominant populations inhabiting hyperalkaline waters include the anaerobic, low energy-yielding processes of methanogenesis, acetogenesis, and fermentation [5, 22]. However, aside from these observations, it remains unclear how variation in the geochemical composition of waters in the Samail Ophiolite influences the abundances of microbial cells, their functional

potential, and their rates of substrate utilization/production. This, in turn, limits understanding of the adaptations that enable microbial life to inhabit environments impacted by serpentinization.

In the present study, we examined microbial communities in fracture waters sampled from subsurface wells in the Samail Ophiolite that span a pH gradient of approximately 7.6–11.3. This pH gradient serves as a general proxy for serpentinization reaction progress [5, 23], with waters with circumneutral pH (~7.6–10) having more recently infiltrated the ophiolite, and hyperalkaline (pH > 10) waters representing a contrasting fluid type whose composition has likely been influenced by long-term interaction with minerals in the ophiolite [5]. We subjected waters to geochemical analyses and planktonic communities to cell enumeration, metagenomic sequencing, and determination of potential rates of CO, $HCOO^-$, and HCO_3^- dissimilation (oxidation or reduction) and assimilation to biomass. Insights into the abundance, potential activities, and inferred genomic features of microorganisms in serpentinized waters are discussed in the context of possible adaptations allowing life to persist in polyextremophilic conditions that may be reminiscent of those on early Earth.

Methods

Site Description, Water Sampling.

The classification scheme used here to describe major water types in the Samail Ophiolite, Sultanate of Oman, has been reported previously (5). A submersible pump was used to collect water samples in February 2017 from seven previously drilled wells in the Samail Ophiolite (Table 1). Briefly, waters were collected from beneath the air-water interface in each well at depths specified in Table 2, including two depths for NSHQ14: 50 m (NSHQ14B) and 85 m (NSHQ14C). After pumping ~ 100 liters of water through the tubing, biomass was collected

for DNA extraction using in-line 0.2 µm Millipore polycarbonate filters in 47 mm Pall polycarbonate filter housings.

Quantification of major cations (SO_4^{2-}, NO_3^-) via ion chromatography and ferrous iron concentrations were collected as described previously (5). Water temperature, conductivity, pH, oxidation-reduction potential (ORP), and the concentration of dissolved oxygen were measured in the field with a Hach (Loveland, CO) HQ40D Portable Multi Meter (5). Water samples for dissolved gas analysis were collected via the bubble strip method described previously (24). Methods for determining DIC concentrations and dissolved gas concentrations are reported in the Supplemental Online Materials.

DNA Extraction and Shotgun Metagenomic Sequencing.

Filtered biomass was subjected to DNA extraction using a Zymo (Irvine, CA) Research Xpedition Soil/Fecal DNA MiniPrep Extraction kit according to manufacturer instructions. Triplicate DNA extractions were pooled for metagenomic library preparation, quantified, and normalized to a total of 1 ng for library preparation using the Nextera XT library preparation kit (Illumina Inc., San Diego, CA). DNA from WAB71 and WAB105 were below the 1 ng threshold and were thus bead-cleaned with Kapa Pure Beads (Roche, Pleasanton, CA) to bind all fragmented DNA of 150 bp in length or more. DNA was then concentrated by elution off the beads into a smaller volume of nuclease-free water before library preparation using the Nextera protocols. Following tagmentation and amplification, products were pooled at equimolar concentrations and sequenced on the Illumina HiSeq 2500 Rapid Run platform (2x250 bp). Raw sequence reads were quality filtered, trimmed of adapters, and assembled as described in Supplemental Online Materials.

Comparisons of Genomic Functional Potential.

To assess differences in functional potential among metagenomes, encoded proteins (> 10 amino acids) inferred from metagenomes were clustered into putative homologous protein family bins (>30% amino acid identity) using CD-HIT v.4.6 (25), following previously described methods (26). Representative proteins from the 30% protein bin clusters were annotated against the Kyoto Encyclopedia of Genes and Genomes (KEGG) function database (27) using the KEGG Automatic Annotation Server (28). A subset of the KEGG orthology (KO) assignments were extracted that encompassed the 'Metabolism' functional subcategory (n=10,628), and the abundances of these KOs were used to construct a table of protein bin counts within metagenomes using custom MATLAB scripts (scripts available at: https://github.com/dcolman1/matlab_scripts). The abundance table was then subjected to principal coordinate analysis in R (29) following normalization to total metagenome protein counts, as described previously (26).

Enrichment of Functional Genes and Correlational Analyses Among Metagenomes.

Correlational analyses were conducted to determine the association of annotated proteins involved in energy metabolism to overall differences in protein coding gene profiles. Statistically significant ($p < 0.05$) correlations of 'Energy Metabolism' KO abundances with protein coding gene dissimilarities were determined using the 'env.fit' function within the vegan R package (30). The distribution of target protein-coding functional genes (formate dehydrogenases [FDH], CODH, methyl-coenzyme reductases [MCR], and acetyl-CoA synthases [ACS]) were assessed by querying the metagenomes using BLASTp with bait sequences for the active site subunits for each of the proteins or protein complexes. The specified proteins were chosen as targets to

identify and characterize the distribution/abundance of populations putatively involved in the metabolism of $HCOO^-$, CO, and HCO_3^-/CH_4, as determined via microcosm-based activity assays (described below). Positive matches within the metagenome databases were considered as those with an E-value > 1x10-6, >30% amino acid homology, and >60% of the length of the BLASTp bait sequence. The number of homologs detected in each metagenome was then normalized to total assembly size. Functional gene homologs were assigned taxonomic identities by BLAST querying the functional genes against the IMG database (31).

Estimation of Metagenome-Assembled Genome (MAG) Sizes.

Genome completeness and MAG sizes (in Mbp) were estimated using the CheckM software package (v.1.0.5) (32). Estimated genome sizes were then extrapolated from the draft MAG sizes and percent estimated completion of sufficiently complete MAGs (>40% estimated completeness). Relative abundances were estimated for each population represented by the MAGs, based on the percentage of raw reads mapped to each MAG using the 'profile' command within CheckM.

Oxidation State of Carbon in Inferred Proteomes.

The average oxidation state of carbon (Z_c) was calculated for each protein sequence encoded by the eight metagenomes assembled for this study based on an algorithm described previously (33) using a custom python script (script available at: https://github.com/spoudel1/Oxidation_state_of_carbon/blob/master/oxidationstate.py). CheckM was used to obtain the read coverage for each contig, and the average read coverage for each protein sequence was then determined by the contig read-mapping quantification described above. The Z_c of each protein sequence was then weighted by protein length and the average

read coverage of the genes encoding the specified protein sequences using a custom python script (script available at: https://github.com/spoudel1/Oxidation_state_of_carbon/blob/master/readfile.py).

Enumeration of Planktonic Cells.

Five wells (WAB105, WAB104, WAB55, WAB71, and NSHQ14) were selected as targets for cell counts to include three representative water types spanning a pH gradient from ~8 to 11. Subsamples of homogenized waters were preserved in the field by addition of 0.22 µm filtered formaldehyde to a final concentration of 10% vol./vol. Samples were maintained at ambient temperature during transport to the laboratory and were then placed at 4°C for storage. Stored samples were homogenized and an aliquot of water was stained with 4′,6-diamidino-2-phenylindole (DAPI) and counterstained with SYBR Gold nucleic acid stains (Invitrogen, Carlsbad, CA). Stained cells were filtered onto 0.22 µm Isopore black polycarbonate membrane filters (EMD Millipore, Burlington, MA) and viewed at 1000x under oil immersion for direct enumeration using an EVOS FL Imaging System fluorescent microscope (Thermo Fisher Scientific, Waltham, MA).

Substrate Transformation Rate Potentials.

Waters from the same five wells as those chosen for cell counts were used to determine potential rates of transformation of select 1-carbon substrates via microcosm assays as described previously (34). Ten mL of unfiltered water collected in pre-evacuated Cali-5 Bond bags (Calibrated Instruments, McHenry, MD) were injected into N_2 purged, autoclaved, butyl rubber stoppered 24 mL serum bottles. Vials were prepared in triplicate and kept at ambient temperature during transport to the lab. Abiological controls were prepared in triplicate for each well as

described above, except serum vials were inoculated with water that had been filtered (0.22 μm). Each microcosm vial contained a 1 mM final concentration of $HCOO^-$, HCO_3^-, and CO with 5 μCi ^{14}C-$HCOO^-$, ^{14}C-HCO_3^-, and ^{14}C-CO. Following incubation at 37°C, samples were acidified and headspace ^{14}C-CO_2 and ^{14}C-biomass were measured as described previously (34). ^{14}C-CH_4 measurements were performed by trapping a known volume of headspace gas using a specially fabricated scintillation vial containing a butyl rubber septum with Cytoscint ES scintillation cocktail. The radioactivity measured in counts per minute associated with each of the samples was measured on a PerkinElmer Tri Carb 2900TR Liquid Scintillation Analyzer (PerkinElmer, Waltham, MA), converted to disintegrations per minute using a quench curve, and used to calculate the maximum rates of biological substrate transformation.

Results

Site Characterization and Geochemistry.

Subsurface waters were sampled from seven previously drilled wells intersecting gabbro or peridotite bedrock of the Samail Ophiolite in February 2017 (Table 1). The pH of waters ranged from 7.6 to 11.3 (Table 1). High pH waters exhibited negative ORP (Table 2) and were generally enriched in compounds that microorganisms could potentially use as reductants, such as H_2 and CH_4 (Table 3). However, high pH waters were generally depleted in compounds that microorganisms could potentially use as oxidants, such as SO_4^{2-}, NO_3^-, and DIC (Table 3).

Planktonic Cell Abundances.

Planktonic cell concentrations were on the order of 10^5 cells mL^{-1} in waters from wells sampled in 2017 (Fig. 1). Average cell concentrations were higher in waters sampled from

alkaline peridotite wells (3.77×10^5 cells mL^{-1} and 4.03×10^5 cells mL^{-1} in WAB105 and WAB104, respectively) than in those sampled from hyperalkaline peridotite wells (2.58×10^5 cells mL^{-1} and 1.16×10^5 cells mL^{-1} in WAB71 and NSHQ14, respectively) (Table S3). The highest concentration of cells (7.28×10^5 cells mL^{-1}) was observed in the contact well, WAB55.

Functional Potential of Microbial Communities.

Sixteen metagenome assemblies were produced from DNA extracted from filtered biomass collected from eight subsurface wells in 2015 (Table S1), and from seven subsurface wells including two different depths in well NSHQ14 in 2017 (Table S2). Ordination of matrices describing the dissimilarity in the composition and relative abundance of protein bins inferred from metagenomes revealed patterns of clustering that were consistent with water types and their associations with different host-rock lithologies (Fig. 2A, Fig. S1). For example, communities inhabiting hyperalkaline and contact wells formed clusters, indicating similar functional potential among communities from these water types. Furthermore, metagenomes from the two depths sampled from NSHQ14 (NSHQ14C: 85m and NSHQ14B: 50m) formed a cluster with metagenomes from other hyperalkaline wells but were distinct from each other (Fig. 2A). Lastly, the communities from the wells containing alkaline peridotite waters (WAB105 and WAB104) exhibited highly dissimilar protein coding potentials, despite similar geochemistry of the well waters (Fig. 2A).

Enrichment of Functional Genes Involved in Single Carbon (C1) Metabolism.

The abundances of specific proteins were correlated with overall inferred proteome dissimilarity to identify functions that distinguished protein encoding potential between

communities. The metagenomes from hyperalkaline peridotite wells exhibited enrichment of protein encoding genes that were distinct from those of the other water types (Fig. 2B). Of note was the enrichment of anaerobic, nickel-dependent CODH subunits (CdhA, CdhB) and other encoded proteins typically involved in anaerobic microbial metabolisms (archaeal-type ATP synthase subunits and the anaerobic sulfite reductase subunit A, AsrA) in the hyperalkaline peridotite hosted water communities. In contrast, genes encoding proteins that were enriched in the non-hyperalkaline peridotite well communities included those involved in respiratory and electron transport chains (NADH dehydrogenases Nuo and Ndh; succinate dehydrogenase Sdh; quinol-cytochrome oxidoreductase Qcr; and Pet: required for proper assembly of the cytochrome oxidase), O_2 respiration (cyclooxygenase: Cox; and cytochrome oxidase subunit I: Cyo), and dissimilatory NO_2^- reduction (nitrite reductase: Nir). In addition, several genes coding for proteins involved in methanogenesis or F_{420} biosynthesis (a cofactor involved in methanogenesis) were enriched in the alkaline peridotite well communities.

Enrichment of certain functionalities suggested that the metabolism of C1 compounds potentially distinguished well communities (i.e., via CO utilization and methanogenesis). Consequently, a targeted assessment of the distribution and enrichment of genes coding for proteins involved in single carbon metabolism was conducted. In general, FDH homologs were the most prevalent among the functional genes surveyed, followed by CODH, ACS, and MCR (Fig. 3). MCR homologs were detected in low abundance in the dataset and were identified in only three of the communities: those hosted by wells WAB188 and NSHQ14 (both samples B and C).

Potential Rates of C1 Compound Transformation.

Maximum potential rates of $HCOO^-$, CO, and HCO_3^- substrate transformation were determined via microcosm assays using ^{14}C enriched substrates (Table S4). Significantly ($p < 0.05$) higher rates of substrate utilization were observed in biological assays as compared with abiological (0.22 µm filtered) controls in microcosms from multiple wells for all substrates and all transformations tested (Fig. 4). Rates of substrate use for energy generation (i.e., dissimilatory oxidation or reduction) were negatively correlated with pH for all substrates tested; but these differences were not statistically significant ($p > 0.05$) for reduction of HCO_3^- to CH_4 and for oxidation of $HCOO^-$ to CO_2 (Fig. 4A, 4B). However, rates of CO oxidation to CO_2 exhibited a significant inverse linear correlation with the pH of well waters (Pearson R = -0.94, $p < 0.05$) (Fig. 4C).

Rates of substrate assimilation to biomass were also determined in the same microcosm assays. The rate of $HCOO^-$ assimilation to biomass was correlated positively with pH (Pearson R= 0.90, $p < 0.05$); rates of assimilation of the other substrates were variable with respect to the pH of the water where the communities were sampled. The rate of CO assimilation to biomass was the highest in microcosms containing water from the contact well (WAB55) and was lower in microcosms containing waters from the alkaline and hyperalkaline peridotite wells. Rates of CO assimilation to biomass were the only metabolic rates that correlated positively with the concentration of cells in well waters (Pearson R = 0.88, $p < 0.05$). Rates of HCO_3^- assimilation did not significantly vary with pH.

The ratios of rates of HCO_3^- reduction to CH_4 vs. rates of HCO_3^- assimilation to biomass decreased in communities inhabiting increasingly high pH well waters (Pearson R = 0.87) (Fig. 4D). Likewise, the ratios of rates of $HCOO^-$ oxidation to CO_2 vs. rates of $HCOO^-$ assimilation to

biomass decreased among communities inhabiting increasingly high pH well waters (Pearson R = 0.84). No relationship was observed between ratios of the rate of CO assimilation to the rate of CO oxidation and well water pH.

Estimated Genome Size and Weighted Oxidation State of Carbon (Z_c) in Proteomes.

The mean size of MAGs ranged from 4.0 Mbp (WAB105) to 2.1 Mbp (NSHQ14C) and exhibited a significant (Pearson R = -0.82, $p < 0.05$) inverse linear correlation with pH (Fig. 5B). Smaller MAGs from hyperalkaline well waters generally exhibited a larger relative abundance than those from alkaline well waters (Fig. 5A). The Z_c in inferred proteomes of MAGs ranged from -0.01 (WAB104) to -0.28 (NSHQ14C) and exhibited a significant (Pearson R = -0.72, $p < 0.05$) inverse linear correlation with the pH of the water from which the communities were sampled (Fig. 5C).

Discussion

Wells intersecting gabbro and peridotite bedrock in the Samail Ophiolite provided access to subsurface waters with a range of geochemical compositions that can be interpreted to reflect the extent of serpentinization reaction progress and the degree of fluid mixing in each well (5). These wells were drilled upwards of 20 years ago by the Oman Ministry of Regional Municipalities and Water Resources and are unlikely to still be experiencing the effects of drilling-related disturbances. The range of geochemical characteristics associated with these waters and the planktonic microbial communities they host thus provided an opportunity to examine the physiological adaptations that permit life in serpentinizing systems at the level of

cell abundance, metabolic potential, potential rates of substrate transformation, and genomic characteristics.

Higher cell concentrations were observed in alkaline peridotite subsurface well waters than in hyperalkaline peridotite well waters (Fig. 1). This finding is consistent with previous reports of low cell concentrations in hyperalkaline waters of the Cedars peridotite body (13, 14) and in high-H_2 chimneys of the LCHF (11) but contrary to findings of higher cell concentrations in hyperalkaline waters compared to freshwaters associated with the Tablelands Ophiolite (10). Geochemical analyses performed on hyperalkaline waters collected from the Samail Ophiolite revealed low concentrations of substrates that could potentially serve as oxidants for cells, including DIC (Table 3). Thus, relatively low cell numbers in hyperalkaline waters may be due, in part, to stress imposed on cells by high pH as well as oxidant and inorganic carbon limitation in highly reacted waters, as has been suggested previously (35-37).

The highest concentration of cells was observed in the "contact" well (WAB55) (Fig. 1) that is hosted by peridotite but is within 1 km of the surface boundary between peridotite and gabbro (the paleo-crust-mantle transition) in the ophiolite (5). The relatively high permeability of gabbro coupled with faulting observed at this boundary has been hypothesized to facilitate mixing between more oxidized gabbro-reacted waters and more reduced peridotite-reacted waters in the "contact" wells (5). Mixing may provide microorganisms with higher concentrations of oxidants and reductants that are in disequilibrium when compared to alkaline or hyperalkaline waters, thereby providing additional chemical energy for cells to fuel their metabolisms (38) and thus to replicate. This in turn may promote a higher cell concentrations, a higher taxonomic diversity, as has been suggested previously (5), and a more robust and

functionally diverse community like those recently suggested for hydrothermal environments sourced by mixing of end-member waters (39).

Distinct functional potentials inferred from metagenomes were observed among microbial communities sampled from well waters spanning a pH gradient from ~7.6-11.3 (Fig. 2A). This is consistent with clustering of microbial community compositions by water type, as noted previously based on 16S rRNA gene data (5). Genes involved in anaerobic metabolisms were enriched in metagenomes from hyperalkaline waters (Fig. 2B), which is expected given the low concentrations of dissolved oxygen previously reported in these waters (5). This observation is also consistent with previous physiological inferences from 16S rRNA genes extracted from waters in the Samail Ophiolite, which suggested that the metabolisms supporting dominant populations inhabiting hyperalkaline waters include the anaerobic processes of methanogenesis, acetogenesis, and fermentation (5). Specifically, communities inhabiting hyperalkaline waters showed enrichment of genes encoding Ni-CODH in their metagenomes, enzymes that are typically associated with anaerobic Bacteria and Archaea (40, 41) including those that catalyze the processes of methanogenesis and acetogenesis (42). Additionally, other genes typically involved in anaerobic metabolisms were enriched in hyperalkaline waters, including the anaerobic sulfite reductase subunit A, AsrA, and archaeal-type ATP synthase subunits, the latter of which were also found to be enriched in a serpentinizing spring in The Cedars (California, USA) (37). In contrast, community genomes from alkaline waters were enriched in genes coding for Mo-CODH which is typically associated with aerobes (40, 41). This finding is potentially consistent with the higher redox potential and the generally higher concentrations of dissolved oxygen in these waters (5).

Genes encoding FDH were highly abundant in all metagenomes and were more abundant than genes that encode proteins required to oxidize CO (i.e., Mo- or Ni-CODH) or required for the dissimilatory reduction of inorganic carbon via the processes of methanogenesis or acetogenesis (i.e., MCR, ACS; Fig. 3). Consistent with enrichment in FDH encoding genes, rates of $HCOO^-$ assimilation or oxidation were higher than rates of assimilation or dissimilation of HCO_3^- and CO from all well waters sampled (Fig. 4), suggesting that $HCOO^-$ may be a preferred carbon and/or electron source among microorganisms in the Samail Ophiolite. The rates of $HCOO^-$ assimilation to biomass were the only rates that correlated positively with the pH of waters where the communities were sampled (Fig. 4A). This indicates that microorganisms may be adapted to *i*) efficiently utilize $HCOO^-$ as a carbon source in DIC-limited hyperalkaline waters or *ii*) take advantage of formate as a carbon/energy source in waters that may favor abiogenic formate production. The most abundant MAG (31% relative abundance) in the highest pH well, NSHQ14C, was inferred to encode an FDH protein that was most closely related to that of *Desulfitibacter alkitolerans* (61% identity; Table S5), an anaerobic bacterium that can utilize $HCOO^-$ as an electron donor and carbon source when paired with inorganic electron acceptors such as sulfite (43). Abiotic CO_2 reduction to $HCOO^-$ is favored during the serpentinization of olivine under high H_2 conditions (44). Indeed, experimental low-temperature serpentinization of dunite from the Samail Ophiolite resulted in formation of $HCOO^-$ and depletion of CO_2 (45). Thus, $HCOO^-$ may serve as a bioavailable form of carbon under these conditions. Consistent with the observations presented here, prior work has indicated that abiogenic $HCOO^-$ may serve as an important source of carbon for life in the DIC-limited environments associated with the LCHF, an alkaline serpentinizing system (20).

Despite previous evidence indicating that the process of methanogenesis is common in environments undergoing active serpentinization (12, 13, 18, 46-48), genes encoding subunits of methyl coenzyme reductase (MCR), an enzyme complex that catalyzes the final step of methanogenesis (49), were not highly abundant in metagenomes from waters sampled from the Samail Ophiolite (Fig. 3). The only metagenomes from alkaline or hyperalkaline environments where MCR was detected were from NSHQ14B and NSHQ14C. NSHQ14C also demonstrated significant rates of methanogenesis in microcosm assays (Fig. 4B). The inferred McrA protein homologs identified in the NSHQ14B and NSHQ14C metagenomes were related (88 percent identities) to those encoded by *Methanobacterium* sp. (Table S5), a hydrogenotrophic genus of methanogens (50). Sequences closely related to *Methanobacterium* sp. were also reported in a 16S rRNA gene survey conducted on filtered waters from NSHQ14 in 2016 but were not detected in communities sampled from the same waters in 2014 and 2015 (5). This may indicate temporally dynamic conditions in the well that fluctuate between those favoring or disfavoring growth of this strain. Genes encoding McrA were also detected in the metagenome from WAB188 (Fig. 3) and were 93 percent identical to those from *Methanobacterium* sp. (Table S5). 16S rRNA gene sequences affiliated with *Methanobacterium* sp. have been previously detected in filtered waters from this well sampled in 2015 but not in 2016 (5). Significant rates of methanogenesis were observed in microcosms from wells WAB105 and WAB104 (Fig. 4B), where *mcrA* was not detected (Fig. 3). 16S rRNA genes affiliated with *Methanobacterium* were previously found to be widely distributed in well waters sampled from the Samail Ophiolite (16 of 20 samples) but were only abundant (>3%) in three samples. Thus, the lack of *mcrA* in

metagenomes from WAB105 and WAB104 presented here may be due to undersampling of rare taxa.

The metagenome from the community inhabiting waters from WAB55 was enriched in genes coding for CODH, in particular those that coded for the “aerobic” Mo-CODH (Fig. 3). The most abundant MAG in WAB55 that was inferred to encode a Mo-CODH protein was most closely related to that encoded by the uncultured *Candidatus* Rokubacteria sp. (89% identity), which has been suggested to be a versatile mixotroph capable of growth under oxic or anoxic conditions (51). This community also exhibited the highest rate of CO assimilation to biomass, but not CO oxidation (Fig. 4C). Previous results suggest that CO primarily served as a source of electrons rather than biomass carbon for organisms residing in a hyperalkaline environment influenced by serpentinization (17). Consistent with this interpretation, rates of CO oxidation exceeded rates of CO assimilation in all microcosms containing waters from the Samail Ophiolite (Fig. 4C). However, CO assimilation was the only rate measured via microcosm assays that correlated significantly with observed cell concentrations in well waters ($p < 0.05$), suggesting that CO assimilation could be a major driver of biomass production *in situ*, especially in the mid-pH contact well, WAB55 (pH 9.2).

We hypothesized that carbon limitation in hyperalkaline wells would lead cells to assimilate a greater fraction of metabolized carbon than cells inhabiting circumneutral waters. To begin to test this hypothesis, we calculated the ratio of rates of $HCOO^-$, HCO_3^-, and CO dissimilation (reduction or oxidation) to assimilation (to biomass) in microcosm assays. A generally negative relationship between the ratio of HCO_3^- and $HCOO^-$ dissimilation to assimilation and pH was observed, with the lowest ratios observed in communities in the contact

and hyperalkaline well waters (Fig. 4D). This suggests that carbon limitation (substrate assimilation) may outweigh energy limitation (substrate dissimilation) for autotrophic populations in higher pH serpentinized waters in Oman. Importantly, high abundance members of hyperalkaline well communities were previously shown to be affiliated with putatively acetogenic organisms belonging to the candidate phylum OP1 that are likely to utilize the Wood-Ljungdahl (WL) pathway for carbon assimilation (5). The WL pathway allows for assimilation of CO, $HCOO^-$, or CO_2 into biomass, so long as reductant is supplied by another component of cellular metabolism such as through H_2 oxidation (52). Homologs of genes encoding the ACS protein were detected in all metagenomes from hyperalkaline waters (Fig. 3). However, since we did not track production of ^{14}C-acetate in the microcosm assays, it is possible that the low ratio of dissimilation to assimilation observed for HCO_3^- and $HCOO^-$ transformation is due to production of acetate. Additionally, we did not track production of ^{14}C-CH_4 from ^{14}C-$HCOO^-$ or ^{14}C-CO, however, *Methanobacterium* spp. can use both $HCOO^-$ and CO as methanogenic substrates (50), and organisms capable of CH_4 production from $HCOO^-$ have previously been shown to inhabit a serpentinizing spring in the Cedars peridotite body, California and the Santa Elena Ophiolite, Costa Rica (8, 47). Thus, it is also possible that the low ratio of dissimilation to assimilation observed for $HCOO^-$ transformation is due to production of CH_4. Additional work is needed to determine the primary processes supporting the energy and carbon metabolism of autotrophs inhabiting hyperalkaline well waters.

A significant inverse relationship was noted between the mean estimated size of MAGs reconstructed from communities inhabiting well waters in the Samail Ophiolite and the pH of those waters (Fig. 5B). This observation is consistent with genomic streamlining as a potential

adaptation to energetic stress imposed on cells by the reducing, alkaline, inorganic carbon-limited conditions imposed by increased serpentinization reaction progress. In other nutrient-limited or otherwise stressful environments, organisms have been suggested to encounter selection pressure to minimize the energetic costs associated with genome replication, costs that would be lessened by a reduction in genome size (53). Indeed, members of a microbial community from a hyperalkaline spring in the Cedars were previously shown to comprise organisms with the smallest genomes reported for their respective taxa based on metagenomic inference (37). Likewise, on the other end of the pH spectrum, the genomes of obligate acidophiles, which have been suggested to face chronic energy limitation (54), are relatively small compared with their neutrophilic counterparts (55). This suggests that extremes in pH and potentially also nutrient limitation impose energetic stress on microbial populations, potentially leading to adaptation at the level of genome streamlining.

The average oxidation state of carbon in proteomes inferred from community metagenomes exhibited a significant negative correlation with increased pH of the well waters, with the lowest Z_c observed in NSHQ14C (Fig. 5C). A previous study conducted along an outflow channel of a hot spring also noted an inverse correlation between the Z_c in proteomes inferred from metagenomic data and the oxidation state of the local environment (33). Similarly, the Z_c in proteomes inferred from the genomes of aerobic/facultatively anaerobic taxa (restricted to those involved in N_2 fixation) were significantly higher than those from anaerobic taxa involved in N_2 fixation, an observation that was attributed to the latter inhabiting environments with lower reduction potentials (56). At a mechanistic level, the relationship between the Z_c of inferred proteomes and oxidation state of the local environment has been suggested to reflect

selection to minimize energetic costs during protein synthesis (33). In such a scenario, organisms inhabiting highly reduced environments, such as NSHQ14B and NSHQ14C, would be under selection to synthesize proteins that are comprised of amino acids that themselves are comprised of more reduced carbon which, in turn, would minimize the overall energetic cost of protein synthesis. Indeed, MAGs recovered from NSHQ14B and NSHQ14C here and 16S rRNA genes recovered in a previous analysis of these waters (5) revealed communities dominated by putative acetogens and methanogens, organisms that are adapted to thrive in highly reduced environments (57).

In summary, the observations presented here suggest physiological adaptations to minimize energetic and physiological stress imposed by the highly reducing, carbon-limited conditions in environments impacted by the geological process of serpentinization. These include enrichment of genes (e.g., CODH, MCR, ACS) that allow for use of substrates made available by the process of serpentinization (e.g., CO, HCOO-) and metabolic characteristics to overcome the limited availability of inorganic carbon in these systems. This potentially includes the assimilation of a greater fraction of metabolized carbon from single carbon compounds among communities inhabiting hyperalkaline waters when compared to alkaline waters, a characteristic that may allow cells to overcome carbon limitation associated with the former while supporting their energy metabolism with other substrates (e.g., H_2). Moreover, communities exhibited genomic characteristics that may function to minimize energetic stress imposed by highly reducing, carbon-limited conditions in hyperalkaline waters. This includes a decrease in the genome size of populations (genome streamlining) inhabiting hyperalkaline waters when

compared to alkaline waters as well as a decrease in the Z_c in inferred proteomes, a characteristic that may reduce energetic costs of protein synthesis.

Acknowledgements

This work was supported by a grant from the NASA Astrobiology Institute (NNA15BB02A) to JRS, AST, and ESB. The authors would like to thank Laura Bueter and Eric Ellison for help with sample collection and Juerg Matter for help with equipment acquisition, permitting, and sample export. The authors are also grateful to the Ministry of Regional Municipalities and Water Resources in the Sultanate of Oman for allowing sampling and export of well waters.

Competing Interests

The authors declare that they have no conflict of interest.

Table 1. Locations of the wells that were sampled in 2017 for this study and the bedrock type that hosts them. Bedrock type is as reported in *Rempfert et al., 2017*. A "contact" bedrock type describes wells that are near the contact between gabbro-dominated and peridotite-dominated lithologies. The pH of NSHQ14B (50m depth) and NSHQ14C (85m depth) are separated by a slash. The elevation of each well is listed in meters above sea level.

Well name	**WAB188**	**WAB105**	**WAB104**	**WAB55**	**NSHQ4**	**WAB71**	**NSHQ14B/C**
pH	7.6[1]	8.3[1]	8.5	9.2	10.5[2]	10.6	11.1/11.3
UTM Easting	671,123	644,678	643,099	634,777	670,971	670,322	675,495
UTM Northing	2,529,798	2,536,524	2,541,124	2,506,101	2,531,699	2,533,981	2,529,716
Bedrock type	Contact	Peridotite	Peridotite	Contact	Contact	Peridotite	Peridotite
Fluid Type	Contact	Alkaline Peridotite	Alkaline Peridotite	Contact	Hyperalkaline Peridotite	Hyperalkaline Peridotite	Hyperalkaline Peridotite
Elevation (m)	514	688	842	531	514	608	526

[1]Data collected from wells in 2016 are reported since measurements were not collected during the 2017 field season.

[2]Data collected from wells in 2015 are reported since measurements were not collected during the 2016 or 2017 field seasons.

Table 2. Description of field measurements of well waters collected in 2017. Water level and pump depth level refer to the number of meters below the top of the well casing that water was encountered and where water was pumped from, respectively. A (–) indicates that data was not collected for waters from the specified well. All "alkaline" and "hyperalkaline" wells are hosted by peridotite bedrock.

Well	**WAB188**	**WAB105**	**WAB104**	**WAB55**	**NSHQ4**	**WAB71**	**NSHQ14B (50m)**	**NSHQ14C (85m)**
Fluid Type	Contact	Alkaline	Alkaline	Contact	Hyper-alkaline	Hyper-alkaline	Hyper-alkaline	Hyperalkaline
pH	7.6[1]	8.3[1]	8.5	9.2	10.5[2]	10.6	11.1	11.3
Water Level (m)	9	-	35	8	5	8	12	12
Pump Depth (m)	-	50	70	30	6	50	50	85
Temp. °C	33.0[1]	31.6[1]	33.4[1]	34.7[1]	33.3[2]	34.5[1]	34.4	36.3
Cond. (µs/cm)	926[1]	448[1]	493[1]	1171[1]	1249[2]	1803[1]	493[1]	493[1]
ORP (mV)	214	178[1]	180[1]	110[1]	-342[2]	-86[1]	-415	-253

[1]Data collected from wells in 2016 are reported since measurements were not collected during the 2017 field season.
[2]Data collected from wells in 2015 are reported since measurements were not collected during the 2016 or 2017 field seasons.

Table 3. Description of geochemical measurements conducted on well waters sampled in 2017. Potential sources of measured oxidants, reductants, and single carbon compounds in well waters are reported. Detection limits (DL) are indicated in the far right column.

Well	**WAB188**	**WAB105**	**WAB104**	**WAB55**	**NSHQ4**	**WAB71**	**NSHQ14B (50m)**	**NSHQ14C (85m)**	**DL (μM)**
pH	7.6[1]	8.3[1]	8.5	9.2	10.5[2]	10.6	11.1	11.3	-
Fe^{2+} (μM)	0.4	5.0	2.0	2.5	0.8	0.2	0.1	2.0	0.006
SO_4^{2-} (μM)	1130	292	477	875	683	42	131	2	1.04
NO_2^- (μM)	6	*DL*	*DL*	8	*DL*	14	17	16	2.17
NO_3^- (μM)	118	135	123	143	3.0	2.5	*DL*	*DL*	1.61
H_2 (μM)	0.92	*DL*	*DL*	*DL*	*DL*	0.51	21	164	0.45
CH_4 (μM)	1.69	0.02	0.02	0.10	155	12.6	34.6	12.6	0.015
DIC (mM)	3.0	3.5	3.5	2.9	0.04	0.12	0.05	0.13	0.098

[1]Data collected from wells in 2016 are reported since measurements were not collected during the 2017 field season.

[2]Data collected from wells in 2015 are reported since measurements were not collected during the 2016 or 2017 field seasons.

Abbreviation: DL, detection limit in μM

Supplemental Table 1. Metagenome assembly statistics for 2015 samples. Eight metagenome assemblies were produced from DNA extracted from filtered biomass collected from eight subsurface wells in 2015.

	WAB103	NSHQ3B	WAB188	WAB55	NSHQ4	WAB56	WAB71	NSHQ14 (50m)
Size (Mbp)	6.71	3.36	14.67	12.48	5.46	6.47	23.56	11.32
Contigs >500 bp	8,445	3,875	8,349	13,014	6,251	5,261	15,964	3,693
Contigs >10 kbp	1	0	184	0	0	0	11	208
Largest contig (bp)	23,649	6,070	83,349	10,388	7,755	18,065	64,983	144,968
N50 (bp)	742	850	2,724	978	855	1,534	2,052	6,788
Protein-coding genes	6,151	3,539	14,949	14,219	5,436	6,694	23,519	11,216

Supplemental Table 2. Metagenome assembly statistics for 2017 samples. Eight metagenome assemblies were produced from DNA extracted from filtered biomass collected from seven subsurface wells in 2017.

	WAB104	WAB105	WAB188	WAB55	NSHQ04	WAB71	NSHQ14B (50m)	NSHQ14C (85m)
Size (Mbp)	128.95	60.57	233.69	137.23	151.80	87.17	129.50	72.70
Contigs >500 bp	54,250	23,170	67,947	51,969	54,133	36,106	40,614	23,055
Contigs >10 kbp	989	434	3838	1352	1651	633	1711	986
Largest contig (bp)	351,116	364,202	341,956	122,697	167,295	107,801	205,427	148,789
N50 (bp)	2,534	2,926	5,567	3,118	3,421	2,694	4,249	4,262
Protein-coding genes	136,597	63,112	235,265	143,326	151,456	90,312	131,167	73,525

Supplemental Table 3. Planktonic cell densities (cells mL^{-1}) in subsurface well water samples from the Samail Ophiolite. The average (Avg) and standard deviations (SD) associated with reported cell densities were calculated for three replicate subsamples that were each enumerated in a minimum of 10 fields of view.

	WAB105	WAB104	WAB55	WAB71	NSHQ14C (85m)
Cells mL^{-1} (Avg)	3.77×10^5	4.03×10^5	7.28×10^5	2.58×10^5	1.16×10^5
Cells mL^{-1} (SD)	1.51×10^5	1.21×10^5	1.38×10^5	9.07×10^4	4.37×10^4

Supplemental Table 4. Maximum potential rates of biological assimilation and dissimilation (oxidation/reduction) of select one carbon compounds by planktonic microbial communities in well water samples collected from the Samail Ophiolite. Maximum potential rates of biological substrate transformation were determined via microcosm assays using well waters collected from the Samail Ophiolite, with rates of abiological assays subtracted from biological assays. The average maximum rates of substrate transformation observed in triplicate abiological controls were subtracted from triplicate biological assays (Avg), and their combined standard deviations (SD) are presented. *P*-values were determined between biological assays and abiological controls via Student's t-test assuming unequal variance for each condition.

	WAB105	WAB104	WAB55	WAB71	NSHQ14
Formate ($HCOO^-$) Oxidation to carbon dioxide (CO_2)					
Avg Maximum Rate (pmol mL^{-1} day^{-1})	13138	5171	1321	810	309
SD	2143	3173	580	221	129
P-value	0.01	0.21	0.04	0.03	0.07
$HCOO^-$ Assimilation to Biomass					
Avg Max Rate (pmol mL^{-1} day^{-1})	143	79	148	220	230
SD	43	18	66	22	97
P-value	0.02	0.01	0.07	<0.01	0.08
Carbon Monoxide (CO) Oxidation to CO_2					
Avg Max Rate (pmol mL^{-1} day^{-1})	148	179	134	57	62
SD	43	72	48	23	12
P-value	0.02	0.07	0.05	0.07	<0.01
CO Assimilation to Biomass					
Avg. Max Rate (pmol mL^{-1} day^{-1})	4	5	57	6	2
SD	1	2	8	1	2
P-value	0.04	0.04	<0.01	<0.01	0.09
Bicarbonate (HCO_3^-) Reduction to Methane (CH_4)					
Avg Max Rate (pmol mL^{-1} day^{-1})	1057	2267	157	26	18
SD	273	543	91	15	6
P-value	0.03	0.03	0.13	0.13	0.04
HCO_3^- Assimilation to Biomass					
Avg Max Rate (pmol mL^{-1} day^{-1})	28	69	29	56	70
SD	8	32	18	19	62
P-value	0.04	0.09	0.12	0.01	0.21

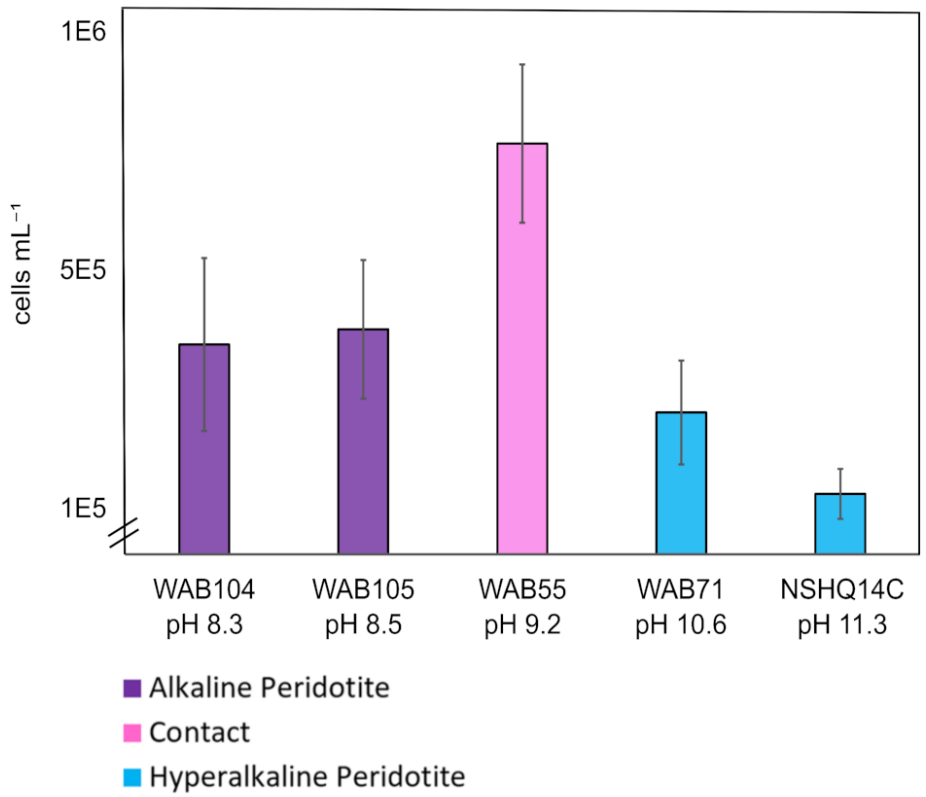

Figure 1. Planktonic cell concentration (cells mL^{-1}) in subsurface waters sampled from wells in the Samail Ophiolite. The planktonic cell concentration in water sampled from each subsurface well is represented by a bar whose color corresponds to the legend at the bottom of the figure describing well water type. Subsurface well waters were filtered onto 0.22 µm membranes and cells were enumerated via epifluorescence microscopy (Table S3). Error bars reflect the standard deviation of three replicate subsamples with a minimum of 10 fields of enumeration.

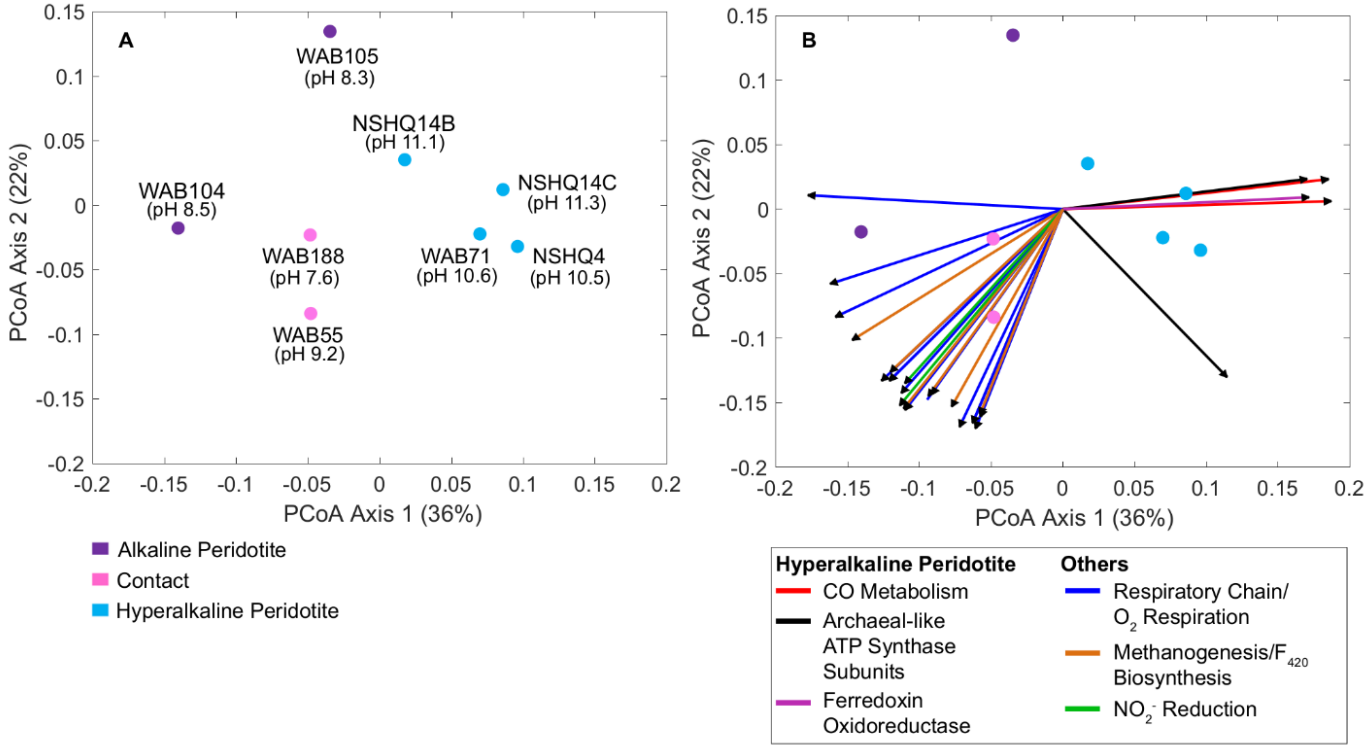

Figure 2. Similarity in protein-coding genes among eight metagenomes generated from communities sampled from well waters within the Samail ophiolite (A) correlated with protein-coding gene functions involved in energy metabolism (B). Each metagenome is represented by a filled circle that is colored by water type, as displayed in the legend below the plot. The percent variation explained by each axis is given in parentheses in each axis label (as indicated by relative eigenvalues). Ordination of the metagenomes is based on dissimilarity in protein-coding gene homolog families that were annotated using the KEGG database as being involved in 'Metabolism.' Panel B displays the same ordination as shown in (A), overlaid with vectors representing KEGG orthology groups that were significantly ($p < 0.05$) associated with the overall differences in the functional composition of metagenomes. The vectors are colored according to broad metabolism categories displayed in the legend below the plot.

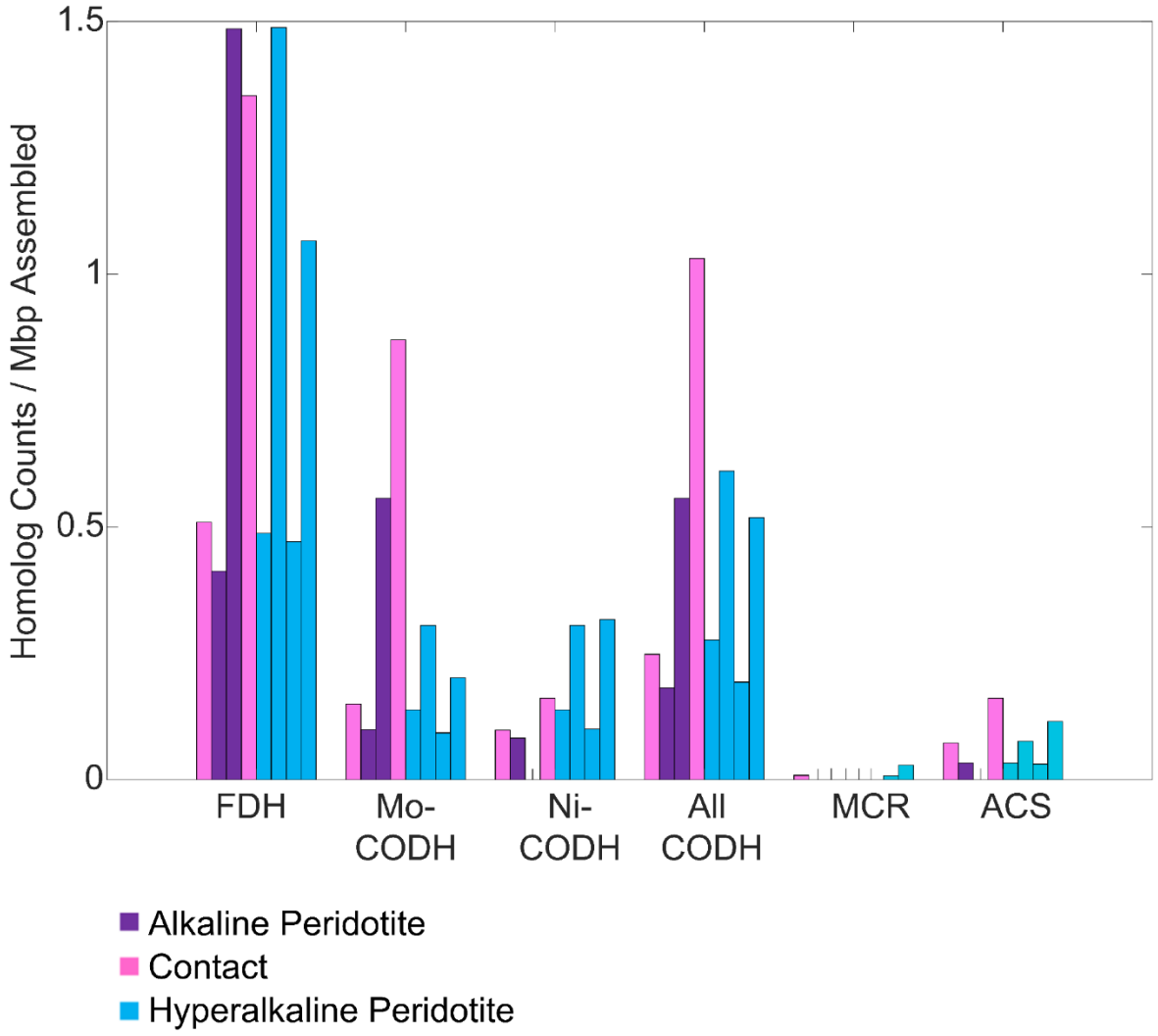

Figure 3. Enrichment of select functional genes associated with target one or two carbon metabolisms in metagenomes. Each bar represents one metagenome, ordered from left to right by increasing pH of the well waters that hosted these communities: WAB188, WAB105, WAB104, WAB55, NSHQ04, WAB71, NSHQ14B (50m depth), NSHQ14C (85m depth). Functional genes that were not detected in individual well metagenomes are indicated by tick marks where bars would otherwise be present. Abbreviations: FDH, formate dehydrogenase; Mo-CODH, molybdenum-containing carbon monoxide dehydrogenase; Ni-CODH, Ni-containing CODH; MCR, methyl coenzyme M reductase; ACS, acetyl coenzyme A synthase.

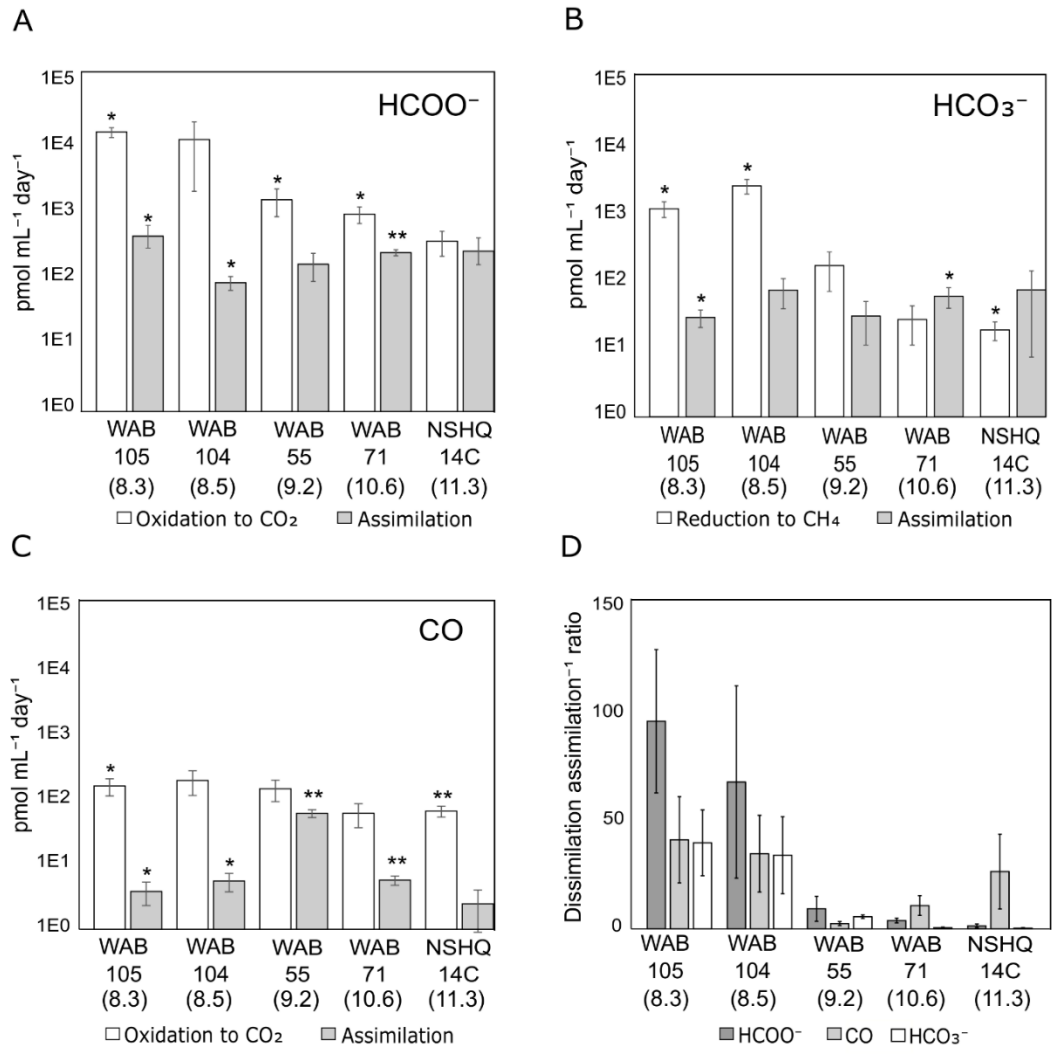

Figure 4. Maximum potential rates of biological assimilation and dissimilation (oxidation or reduction) of select one carbon compounds by planktonic microbial communities in subsurface well waters collected from the Samail Ophiolite. Maximum potential rates of biological formate ($HCOO^-$) oxidation to carbon dioxide (CO_2) and assimilation of $HCOO^-$ to biomass (A), bicarbonate (HCO_3^-) reduction to methane (CH_4) and HCO_3^- assimilation to biomass (B), carbon monoxide (CO) oxidation to CO_2 and CO assimilation to biomass (C), and the ratio of the rate of substrate dissimilation (reduction or oxidation) to assimilation (to biomass) (D). The pH of each well is displayed in parentheses below the well name. Rates of substrate transformation were determined via microcosm assays using radiolabeled carbon tracers. Rates of substrate transformation in abiological controls were subtracted from biological assays to determine rates that are attributable to biology. Statistical significance of differences between biological assays and abiological controls were assessed via Student's t-test assuming unequal variance for each condition (*$p < 0.05$, **$p < 0.01$). Error bars reflect the standard deviation of measurements of three replicate biological assays and three replicate abiological assays for each condition.

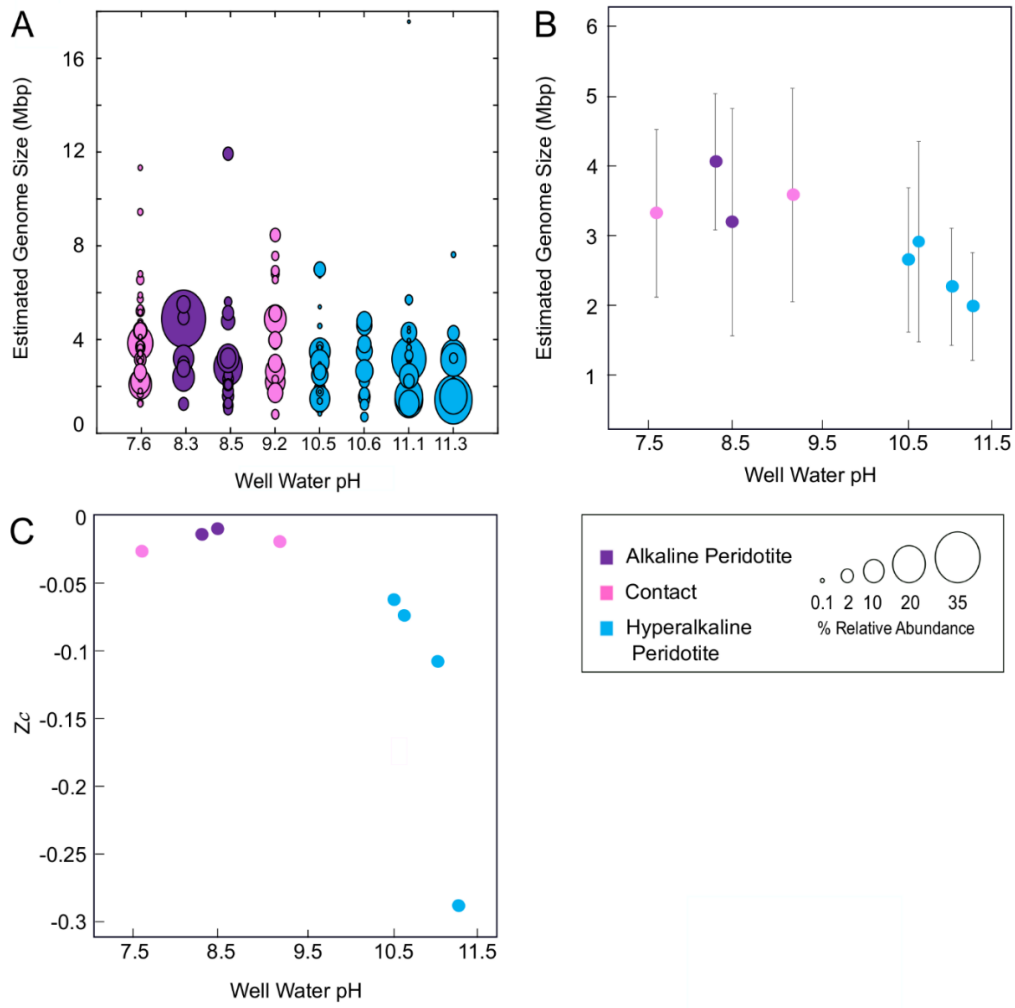

Figure 5. Features of metagenomes reflecting possible adaptations to hyperalkaline conditions. Plot depicting the distribution of estimated genome sizes (in Mbp) of metagenome assembled genomes (MAGs) (**A**). MAGs are represented by circles ordered from left to right by increasing pH of the waters that hosted these communities. The size of each circle corresponds to the estimated relative abundance of each MAG, as indicated in the legend on the bottom right of the figure. Plot of median estimated genome sizes (in Mbp) of metagenome assembled genomes (MAGs) as a function of pH (**B**). Each point depicts the median estimated MAG size (in Mbp) for each well. Error bars depict the standard deviation of the estimated sizes of all MAGs with at least 40% estimated completeness within each metagenome. Plot of the weighted average oxidation state of carbon (Z_c) in inferred proteomes of eight metagenomes as a function of pH (**C**). Each point represents the weighted Z_c value calculated for each metagenome based upon the Z_c per amino acid in the inferred protein sequences encoded by each metagenome. Z_c values were then normalized to protein length and read coverage of the gene encoding each specified protein and finally to the number of base pairs sequenced per metagenome.

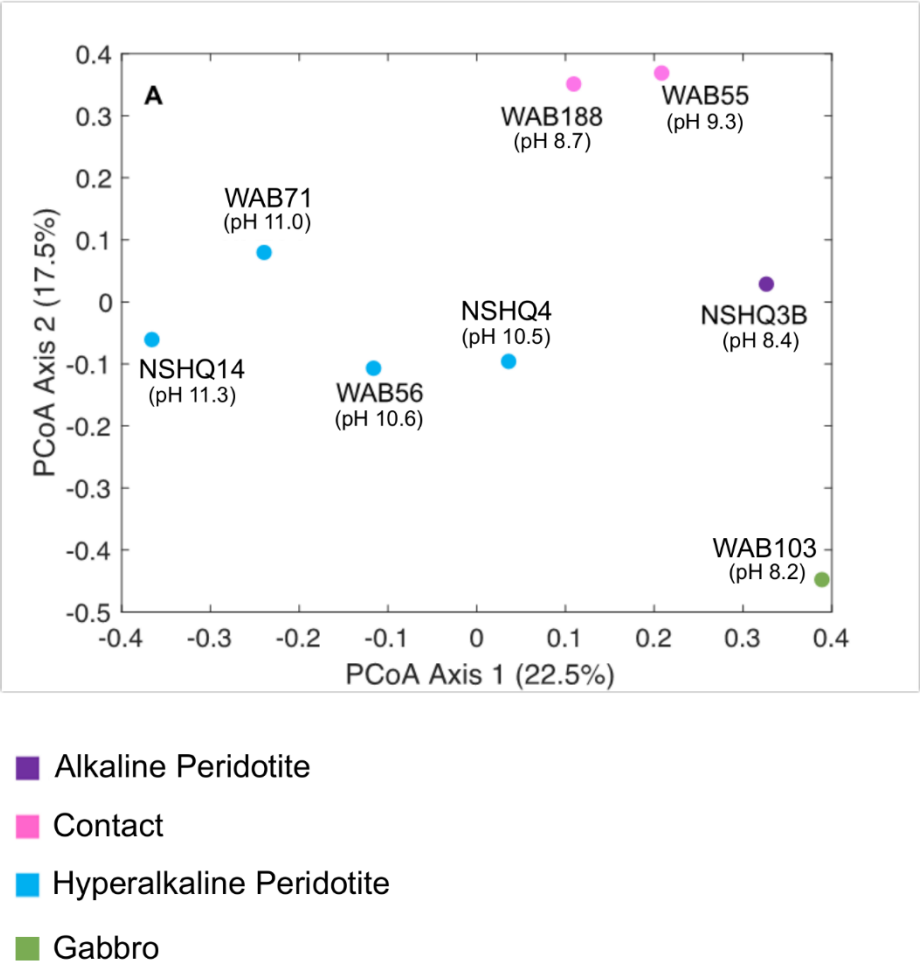

Supplemental Figure 1. Eight metagenome assemblies were produced from eight subsurface wells using the same DNA fraction as was used for 16S rRNA gene sequencing in *Rempfert et al., 2017* (46). The pH of the water hosting each community at the time of sampling is listed below the well name, as reported in *Rempfert et al.*, 2017 (46). Metagenome assembly and analysis of 2015 metagenomes is the same as for 2017 metagenomes, except 2015 metagenomes were quality filtered and trimmed of adapters using Trimmomatic v.0.36 and the following parameter settings: LEADING:3 TRAILING:3 SLIDINGWINDOW:4:15 MINLEN:50 (47). Ordination of the 2015 metagenomes is based on dissimilarity in all protein-coding gene homolog families rather than just those annotated as being involved in 'Metabolism.' Comparison of ordinations with all protein coding gene homolog families of the 2017 metagenomes and those annotated as being involved in 'Metabolism' yielded nearly identical results (data not shown).

References

1. Sousa FL, Martin WF. Biochemical fossils of the ancient transition from geoenergetics to bioenergetics in prokaryotic one carbon compound metabolism. Biochim Biophys Acta 2014; 1837: 964-981.

2. Schulte M, Blake D, Hoehler T, McCollom T. Serpentinization and its implications for life on the early Earth and Mars. Astrobiology 2006; 6: 364-376.

3. McCollom TM, Seewald JS. Abiotic synthesis of organic compounds in deep-sea hydrothermal environments. Chem Rev 2007; 107: 382-401.

4. Seewald JS, Zolotov MY, McCollom T. Experimental investigation of single carbon compounds under hydrothermal conditions. Geochim Cosmochim Ac 2006; 70: 446-460.

5. Rempfert KR, Miller HM, Bompard N, Nothaft D, Matter JM, Kelemen P et al. Geological and geochemical controls on subsurface microbial life in the Samail Ophiolite, Oman. Front Microbiol 2017; 8.

6. Kelemen PB, Matter J, Streit EE, Rudge JF, Curry WB, Blusztajn J. Rates and mechanisms of mineral carbonation in peridotite: natural processes and recipes for enhanced, in situ CO2 capture and storage. Annu Rev Earth Pl Sc 2011; 39: 545-576.

7. Clark ID, Fontes JC. Paleoclimatic Reconstruction in northern Oman based on carbonates from hyperalkaline groundwaters. Quaternary Res 1990; 33: 320-336.

8. Crespo-Medina M, Twing KI, Sanchez-Murillo R, Brazelton WJ, McCollom TM, Schrenk MO. Methane dynamics in a tropical serpentinizing environment: the Santa Elena Ophiolite, Costa Rica. Front Microbiol 2017; 8.

9. Twing KI, Brazelton WJ, Kubo MD, Hyer AJ, Cardace D, Hoehler TM et al. Serpentinization-influenced groundwater harbors extremely low diversity microbial communities adapted to high pH. Front Microbiol 2017; 8: 308.

10. Brazelton WJ, Morrill PL, Szponar N, Schrenk MO. Bacterial communities associated with subsurface geochemical processes in continental serpentinite springs. Appl Environ Microbiol 2013; 79: 3906-3916.

11. Lang SQ, Fruh-Green GL, Bernasconi SM, Lilley MD, Proskurowski G, Mehay S et al. Microbial utilization of abiogenic carbon and hydrogen in a serpentinite-hosted system. Geochim Cosmochim Ac 2012; 92: 82-99.

12. Schrenk MO, Kelley DS, Bolton SA, Baross JA. Low archaeal diversity linked to subseafloor geochemical processes at the Lost City Hydrothermal Field, Mid-Atlantic Ridge. Environ Microbiol 2004; 6: 1086-1095.

13. Brazelton WJ, Thornton CN, Hyer A, Twing KI, Longino AA, Lang SQ et al. Metagenomic identification of active methanogens and methanotrophs in serpentinite springs of the Voltri Massif, Italy. PeerJ 2017; 5: e2945.

14. Morrill PL, Kuenen JG, Johnson OJ, Suzuki S, Rietze A, Sessions AL et al. Geochemistry and geobiology of a present-day serpentinization site in California: The Cedars. Geochim Cosmochim Ac 2013; 109: 222-240.

15. Tiago I, Chung AP, Verissimo A. Bacterial diversity in a nonsaline alkaline environment: heterotrophic aerobic populations. Appl Environ Microbiol 2004; 70: 7378-7387.

16. Brazelton WJ, Nelson B, Schrenk MO. Metagenomic evidence for H2 oxidation and H2 production by serpentinite-hosted subsurface microbial communities. Front Microbiol 2012; 3.

17. Morrill PL, Brazelton WJ, Kohl L, Rietze A, Miles SM, Kavanagh H et al. Investigations of potential microbial methanogenic and carbon monoxide utilization pathways in ultra-basic reducing springs associated with present-day continental serpentinization: the Tablelands, NL, CAN. Front Microbiol 2014; 5: 613.

18. Woycheese KM, Meyer-Dombard DR, Cardace D, Argayosa AM, Arcilla CA. Out of the dark: transitional subsurface-to-surface microbial diversity in a terrestrial serpentinizing seep (Manleluag, Pangasinan, the Philippines). Front Microbiol 2015; 6: 44.

19. Neubeck A, Sun L, Muller B, Ivarsson M, Hosgormez H, Ozcan D et al. Microbial community structure in a serpentine-hosted abiotic gas seepage at the Chimaera Ophiolite, Turkey. Appl Environ Microbiol 2017; 83.

20. Lang SQ, Fruh-Green GL, Bernasconi SM, Brazelton WJ, Schrenk MO, McGonigle JM. Deeply-sourced formate fuels sulfate reducers but not methanogens at Lost City hydrothermal field. Sci Rep 2018; 8: 755.

21. Nicolas A, Boudier E, Ildefonse B, Ball E. Accretion of Oman and United Arab Emirates ophiolite - discussion of a new structural map. Mar Geophys Res 2000; 21: 147-179.

22. Miller HM, Matter JM, Kelemen P, Ellison ET, Conrad ME, Fierer N et al. Modern water/rock reactions in Oman hyperalkaline peridotite aquifers and implications for microbial habitability. Geochim Cosmochim Ac 2016; 179: 217-241.

23. Okland I, Huang S, Dahle H, Thorseth IH, Pedersen RB. Low temperature alteration of serpentinized ultramafic rock and implications for microbial life. Chem Geol 2012; 318: 75-87.

24. Kampbell D, Wilson J, McInnes D. Determining dissolved hydrogen, methane, and vinyl chloride concentrations in aqueous solution on a nanomolar scale with the bubble strip method. Proceedings of the 1998 Conference on Hazardous Waste Research 1998: 176-190.

25. Fu L, Niu B, Zhu Z, Wu S, Li W. CD-HIT: accelerated for clustering the next-generation sequencing data. J Bioinform 2012; 28: 3150-3152.

26. Colman DR, Poudel S, Hamilton TL, Havig JR, Selensky MJ, Shock EL et al. Geobiological feedbacks and the evolution of thermoacidophiles. ISME J 2018; 12: 225-236.

27. Kanehisa M. Enzyme annotation and metabolic reconstruction using KEGG. Protein Function Prediction: Methods and Protocols 2017; 1611: 135-145.

28. Moriya Y, Itoh M, Okuda S, Yoshizawa AC, Kanehisa M. KAAS: an automatic genome annotation and pathway reconstruction server. Nucleic Acids Res 2007; 35: W182-W185.

29. Team RC. R: a language and environment for statistical computing. Version 3.0. 1. R Foundation for Statistical Computing. Vienna, Austria 2013.

30. Oksanen J, Blanchet FG, Kindt R, Legendre P, O'hara R, Simpson GL et al. vegan: community ecology package. R package version 2.3 edn 2015.

31. Markowitz VM, Chen IMA, Palaniappan K, Chu K, Szeto E, Grechkin Y et al. IMG: the integrated microbial genomes database and comparative analysis system. Nucleic Acids Res 2012; 40: D115-D122.

32. Parks DH, Imelfort M, Skennerton CT, Hugenholtz P, Tyson GW. CheckM: assessing the quality of microbial genomes recovered from isolates, single cells, and metagenomes. Genome Res 2015; 25: 1043-1055.

33. Dick JM, Shock EL. Calculation of the relative chemical stabilities of proteins as a function of temperature and redox chemistry in a hot spring. PLoS One 2011; 6: e22782.

34. Urschel MR, Kubo MD, Hoehler TM, Peters JW, Boyd ES. Carbon source preference in chemosynthetic hot spring communities. Appl Environ Microbiol 2015; 81: 3834-3847.

35. Schrenk MO, Brazelton WJ, Lang SQ. Serpentinization, carbon, and deep life. Rev Mineral Geochem 2013; 75: 575-606.

36. Suzuki S, Ishii S, Wu A, Cheung A, Tenney A, Wanger G et al. Microbial diversity in The Cedars, an ultrabasic, ultrareducing, and low salinity serpentinizing ecosystem. PNAS 2013; 110: 15336-15341.

37. Suzuki S, Ishii S, Hoshino T, Rietze A, Tenney A, Morrill PL et al. Unusual metabolic diversity of hyperalkaliphilic microbial communities associated with subterranean serpentinization at The Cedars. ISME J 2017; 11: 2584-2598.

38. Canovas PA, Hoehler T, Shock EL. Geochemical bioenergetics during low-temperature serpentinization: An example from the Samail ophiolite, Sultanate of Oman. J Geophys Res-Biogeo 2017; 122: 1821-1847.

39. Colman DR, Lindsay M. R., and E.S. Boyd. Mixing of meteoric and geothermal fluids supports hyperdiverse chemosynthetic hydrothermal communities. Nat Commun 2019; 10: 681.

40. Adam PS, Borrel G, Gribaldo S. Evolutionary history of carbon monoxide dehydrogenase/acetyl-CoA synthase, one of the oldest enzymatic complexes. PNAS 2018; 115: E1166-1173.

41. Jeoung JH, Fesseler J, Goetzl S, Dobbek H. Carbon monoxide. toxic gas and fuel for anaerobes and aerobes: carbon monoxide dehydrogenases. Met Ions Life Sci 2014; 14: 37-69.

42. Can M, Armstrong FA, Ragsdale SW. Structure, function, and mechanism of the nickel metalloenzymes, CO dehydrogenase, and acetyl-CoA synthase. Chem Rev 2014; 114: 4149-4174.

43. Nielsen MB, Kjeldsen KU, Ingvorsen K. Desulfitibacter alkalitolerans gen. nov., sp. nov., an anaerobic, alkalitolerant, sulfite-reducing bacterium isolated from a district heating plant. Int J Syst Evol Microbiol 2006; 56: 2831-2836.

44. McCollom TM, Seewald JS. A reassessment of the potential for reduction of dissolved CO_2 to hydrocarbons during serpentinization of olivine. Geochim Cosmochim Ac 2001; 65: 3769-3778.

45. Miller HM, Mayhew LE, Ellison ET, Kelemen P, Kubo M, Templeton AS. Low temperature hydrogen production during experimental hydration of partially-serpentinized dunite. Geochim Cosmochim Ac 2017; 209: 161-183.

46. Brazelton WJ, Schrenk MO, Kelley DS, Baross JA. Methane- and sulfur-metabolizing microbial communities dominate the Lost City hydrothermal field ecosystem. Appl Environ Microbiol 2006; 72: 6257-6270.

47. Kohl L, Cumming E, Cox A, Rietze A, Morrissey L, Lang SQ et al. Exploring the metabolic potential of microbial communities in ultra-basic, reducing springs at The Cedars, CA, USA: Experimental evidence of microbial methanogenesis and heterotrophic acetogenesis. J Geophys Res-Biogeo 2016; 121: 1203-1220.

48. Postec A, Quemeneur M, Bes M, Mei N, Benaissa F, Payri C et al. Microbial diversity in a submarine carbonate edifice from the serpentinizing hydrothermal system of the Prony Bay (New Caledonia) over a 6-year period. Front Microbiol 2015; 6.

49. Ermler U, Grabarse W, Shima S, Goubeaud M, Thauer RK. Crystal structure of methyl coenzyme M reductase: The key enzyme of biological methane formation. Science 1997; 278: 1457-1462.

50. Boone DR. Methanobacterium. Bergey's Manual of Systematics of Archaea and Bacteria 2015. Bergey's Manual Trust: New York, NY.

51. Becraft ED, Woyke T, Jarett J, Ivanova N, Godoy-Vitorino F, Poulton N et al. Rokubacteria: genomic giants among the uncultured bacterial phyla. Front in Microbiol 2017; 8: 2264.

52. Takami H, Noguchi H, Takaki Y, Uchiyama I, Toyoda A, Nishi S et al. A deeply branching thermophilic bacterium with an ancient acetyl-CoA pathway dominates a subsurface ecosystem. PLoS One 2012; 7.

53. Giovannoni SJ, Thrash JC, Temperton B. Implications of streamlining theory for microbial ecology. ISME J 2014; 8: 1553-1565.

54. Valentine DL. Adaptations to energy stress dictate the ecology and evolution of the Archaea. Nat Rev Microbiol 2007; 5: 316-323.

55. Baker-Austin C, Dopson M. Life in acid: pH homeostasis in acidophiles. Trends Microbiol 2007; 15: 165-171.

56. Poudel S, Colman DR, Fixen KR, Ledbetter RN, Zheng YN, Pence N et al. Electron transfer to nitrogenase in different genomic and metabolic backgrounds. J Bacteriol 2018; 200: 00757-00717.

57. Thauer RK, Jungermann K, Decker K. Energy-conservation in chemotropic anaerobic bacteria. Bacteriol Rev 1977; 41: 100-180.

CHAPTER THREE

DIVERSIFICATION OF METHANOGENS INTO HYPERALKALINE SERPENTINIZING ENVIRONMENTS THROUGH ADAPTATIONS TO MINIMIZE OXIDANT LIMITATION

Contribution of Authors and Co-Authors

Manuscript in Chapter 3

Author: Elizabeth M. Fones
Contributions: Designed and conducted the experiments. Performed bioinformatics analyses. Contributed to the writing the manuscript.

Co-Author: Daniel R. Colman
Contributions: Contributed to bioinformatics analyses and writing the manuscript.

Co-Author: Emily A. Kraus
Contributions: Contributed to collecting samples, conducting experiments, and writing the manuscript.

Co-Author: Ramunas Stepanauskas
Contributions: Contributed to cell sorting and amplification, sequencing, and assembly of single amplified genomes. Contributed to editing of manuscript.

Co-Author: Alexis S. Templeton
Contributions: Contributed to sample collection and writing the manuscript.

Co-Author: John R. Spear
Contributions: Contributed to sample collection and writing the manuscript.

Co-Author: Eric S. Boyd
Contributions: Contributed to experimental design, sample collection, and writing the manuscript.

Manuscript Information Page

Elizabeth M. Fones, Daniel R. Colman, Emily A. Kraus, Ramunas Stepanauskas, Alexis S. Templeton, John R. Spear, and Eric S. Boyd

The International Society for Microbial Ecology Journal

Status of Manuscript:

____ Prepared for submission to a peer-reviewed journal

____ Officially submitted to a peer-reviewed journal

____ Accepted by a peer-reviewed journal

__x__Published in a peer-reviewed journal

Nature Publishing Group

Issue date: April 2021, doi: 10.1038/s41396-020-00838-1

Diversification of methanogens into hyperalkaline serpentinizing environments through adaptations to minimize oxidant limitation

Elizabeth M. Fones[1], Daniel R. Colman[1], Emily A. Kraus[2], Ramunas Stepanauskas[3], Alexis S. Templeton[4], John R. Spear[2], and Eric S. Boyd[1*]

[1]*Department of Microbiology and Immunology, Montana State University, Bozeman, MT 59717*
[2]*Department of Civil and Environmental Engineering, Colorado School of Mines, Golden, CO 80401*
[3]*Bigelow Laboratory for Ocean Sciences, East Boothbay, ME 04544*
[4]*Department of Geological Sciences, University of Colorado, Boulder, CO 80309*

***** Author of Correspondence: Eric S. Boyd (*eboyd@montana.edu*)

Department of Microbiology & Immunology

Montana State University

PO Box 173520

Bozeman, MT 59717

Phone: (406) 994-7046

Fax: (406) 994-4926

Metagenome assembled genomes (MAGs) and single amplified genomes (SAGs) affiliated with two distinct *Methanobacterium* lineages were recovered from subsurface fracture waters of the Samail Ophiolite, Sultanate of Oman. Lineage Type I was abundant in waters with circumneutral pH, whereas lineage Type II was abundant in hydrogen rich, hyperalkaline waters. Type I encoded proteins to couple hydrogen oxidation to CO_2 reduction, typical of hydrogenotrophic methanogens. Surprisingly, Type II, which branched from the Type I lineage, lacked homologs of two key oxidative [NiFe]-hydrogenases. These functions were presumably replaced by formate dehydrogenases that oxidize formate to yield reductant and cytoplasmic CO_2 via a pathway that was unique among characterized Methanobacteria, allowing cells to overcome CO_2/oxidant limitation in high pH waters. This prediction was supported by microcosm-based radiotracer experiments that showed significant biological methane generation from formate, but not bicarbonate, in waters where the Type II lineage was detected in highest relative abundance. Phylogenetic analyses and variability in gene content suggested that recent and ongoing diversification of the Type II lineage was enabled by gene transfer, loss, and transposition. These data indicate that selection imposed by CO_2/oxidant availability drove recent methanogen diversification into hyperalkaline waters that are heavily impacted by serpentinization.

Hydrogen (H_2) links the geosphere to the biosphere and has likely done so since early in Earth's history (24, 42, 48, 49). H_2 can be generated through hydration and oxidation of ferromagnesian minerals (e.g., olivine) in mafic and ultramafic rocks during serpentinization (3), a geochemical process that has been proposed to have supported life on early Earth (1, 2). High concentrations of H_2, in turn, can abiotically reduce dissolved inorganic carbon (DIC) to generate reduced carbon substrates including carbon monoxide (CO), formate ($HCOO^-$), and methane (CH_4) (4, 5), additional potent reductants capable of fueling microbial metabolism (6, 10, 11, 17-21, 50, 51). However, the process of serpentinization also generates hyperalkaline waters that are highly reduced and limited in DIC and other oxidants capable of supporting autotrophs, including methanogens and acetogens (6, 52, 53). As such, the process of serpentinization can create competing benefits (replete reductant supply) and challenges (limited DIC and oxidant supply) for autotrophic subsurface microbial life, both today and early in Earth's history.

Microbial communities that inhabit hyperalkaline waters in serpentinizing environments tend to be less diverse and less abundant than those inhabiting waters with circumneutral pH (6, 10, 14, 15, 22, 51), consistent with the polyextremophilic and DIC/oxidant limited conditions commonly found at pH > 10. More specifically, the decrease in diversity among communities that inhabit hyperalkaline waters tends to be associated with a shift toward a predominance of strict anaerobes, a finding that is in line with the highly reduced nature of these fluids (6, 22). Among the anaerobes commonly detected in hyperalkaline serpentinized waters are methanogens affiliated with the autotrophic and hydrogenotrophic genus, *Methanobacterium* (6, 14, 19, 23, 50, 51, 54).

Hydrogenotrophic methanogens are often advocated as having the most ancient of extant metabolisms (24-26). There are numerous rationales for the primacy of hydrogenotrophic methanogens. First, CH_4 in fluid inclusions in ancient rocks dated to 3.46 Ga are isotopically light, consistent with active methanogenesis at this time (55), and phylogenetic data suggest that these cells were likely dependent on H_2 as the electron donor (24, 48). Second, the ability of hydrogenotrophic methanogens to use CO_2 as the sole carbon source and electron acceptor may have alleviated a major barrier for early autotrophic life. CO_2 is presumed to have been readily available on early Earth whereas organic carbon and other potential oxidants (e.g., oxygen, nitrate, and sulfate) are likely to have been far more limiting (29). However, modern serpentinizing environments exhibit extremely low concentrations of DIC (6, 14, 19, 23, 50, 51), and it is not yet understood how methanogens or other autotrophs could have overcome this limitation.

CH_4 in hyperalkaline, highly serpentinized waters typically exhibits isotopically heavy carbon ($\delta^{13}C\text{-}CH_4 > -40‰$) (23, 50, 56, 57), a finding that has been suggested to result from abiotic processes or biological methanogenesis under extreme DIC limitation (23, 58, 59). Support for the latter interpretation includes experimental evidence demonstrating that biological methanogenesis under carbon-limited conditions can result in relatively high $\delta^{13}C\text{-}CH_4$ values (60) and the presence of lipid biomarkers associated with methanogenic archaea recovered from globally distributed serpentinizing environments that exhibit high ^{13}C values (61, 62). These observations point to near-complete (quantitative) consumption of bioavailable DIC by methanogens in these environments. Furthermore, cells in hyperalkaline waters in serpentinizing systems tend to preferentially assimilate carbon substrates for biomass synthesis rather than

dissimilate them for energy production when compared to cells from waters with circumneutral pH (51). This is consistent with cells, including autotrophic methanogens, experiencing DIC limitation in hyperalkaline waters (51, 63). Here, we apply metagenomics and single cell genomics (SCG) to examine how autotrophic methanogens overcome DIC/oxidant limitation imposed by highly reducing, high pH conditions in the Samail Ophiolite, Sultanate of Oman, the largest ophiolite and one that is undergoing active low temperature serpentinization (23, 52, 64-68). Microcosm assays utilizing radioisotopically labeled substrates are used to evaluate hypotheses generated from metabolic reconstructions inferred from genomic data. Finally, phylogenomic and SCG approaches are used to describe the diversification of methanogens in hyperalkaline waters resulting from serpentinization and to identify the mechanisms involved in their apparent speciation.

Materials and Methods

Sample collection.

A Grundfos SQ 2-85 submersible pump was used to collect water samples in February 2017 from seven previously drilled wells in the Samail Ophiolite, Sultanate of Oman, as previously described (6, 51). Briefly, waters were collected at least 20 m below the water table in each well, including two depths at well NSHQ14: 50 m (NSHQ14B) and 85 m (NSHQ14C). After pumping ~100 L of water through the tubing and filter housing, biomass was collected using in-line 0.2 μm Millipore polycarbonate filters in 47 mm Pall polycarbonate filter housings, as described previously (51). Filters and their contents were transferred to sterile screw top vials and were immediately flash frozen in the field with liquid nitrogen. Water samples for single cell genomics (SCG) were collected from NSHQ14C only. Filter-sterilized (0.2 μm) glycerol (5%

final concentration) and TE buffer (1x) were added to samples as cryoprotectants, after which the samples were flash frozen in liquid nitrogen and stored at -80°C until further analysis.

A Grundfos SQ 2-85 submersible pump was again used to collect water samples for methanogenic activity assays from well WAB188 at a depth of 50 m on March 6, 2020. A Double Packer Standard System (SolExperts, France) was deployed in well NSHQ14 to attempt to isolate shallow versus deep waters in the well. However, attempts to isolate deep waters were unsuccessful as there was insufficient flow to pump water to the surface when the top packer was inflated (at both 30 m and at 18 m depths). Sufficient flow was achieved when the bottom packer was inflated at a depth of 30 m with the top packer left uninflated, isolating waters from an interval extending between the depth of the water table (9 m) to 30 m on February 28, 2020. After pumping ~100 liters of water through the sampling manifold and tubing at each site, water samples for methanogenic activity assays were collected by direct injection from the sampling manifold into N_2-purged, autoclave-sterilized, butyl-stopped glass serum vials. Samples were maintained at ambient temperature during transport to the laboratory and were then placed at 4°C for storage. Water temperature and pH were measured in the field in 2020 with a Hach (Loveland, CO) HQ40D Portable Multi Meter.

Site Description.

The classification scheme used here to describe major water types (hyperalkaline peridotite, contact, and alkaline peridotite) in the Samail Ophiolite is as reported previously (6, 51). Increasing pH is generally interpreted to reflect the extent of serpentinization reaction progress and the degree of fluid mixing in each well (6). DIC was replete (3.0 to 3.5 mM) and H_2 was limited (undetectable to 0.92 μM) in circumneutral waters (pH 7.6 to 8.5) from wells

WAB188, WAB105, and WAB104 at the time of sampling in 2017 (**Table 1**) (51). In contrast, DIC was limited (0.05 to 0.13 mM) and H_2 was replete (21 to 164 μM) in hyperalkaline waters (pH 11.1 to 11.3) from well NSHQ14 in 2017. Formate ($HCOO^-$), another potential reductant generated during serpentinization, has been measured at concentrations ranging from 1.0 to 1.7 μM in these wells (6). Further details of the geochemistry of waters sampled from the Samail Ophiolite are reported elsewhere (6, 51).

DNA extraction and shotgun metagenomic sequencing.

DNA was extracted for metagenomic sequencing as previously described (51). Briefly, DNA was extracted from filtered biomass using a Zymo (Irvine, CA) Research Xpedition Soil/Fecal DNA MiniPrep Extraction kit according to manufacturer instructions. Sequencing libraries were prepared in triplicate using the Nextera XT kit (Illumina Inc., San Diego, CA) and sequenced on the Illumina HiSeq 2500 Rapid Run platform (2 × 250 bp).

Metagenomic assembly and binning of metagenome assembled genomes (MAGs).

Raw sequence reads were quality filtered, trimmed of adapters, and assembled as described previously (51). Contigs were binned into draft MAGs based on tetranucleotide frequencies and coverage profiles using the MetaBAT software package (v. 0.26.3) (69). Contigs with ≥ 98% nucleotide identity to the *Methanobacterium* Type I MAG from WAB188 were classified as Type I and contigs with ≥ 98% nucleotide identity to the *Methanobacterium* Type II MAG from NSHQ14C were classified as Type II. The number of reads affiliated with *Methanobacterium* Type I or II MAGs as a percentage of the total reads in each metagenome were used to calculate estimated relative abundances of each population.

Single cell genomics (SCG).

Individual microbial cells were separated by fluorescence-activated cell sorting, lysed by a combination of freeze-thawing and KOH, and their genomes were amplified by WGA-X and subject to low-coverage sequencing (LoCoS) and assembly at the Bigelow Laboratory Single Cell Genomics Center, as described previously (70). MAG and single amplified genome (SAG) data have been submitted to GenBank under the BioProject number *PRJNA631088*.

Phylogenomic analyses.

Phylogenomic reconstruction of target MAGs (i.e., *Methanobacterium* spp. described below) recovered from the Samail Ophiolite and representative reference Methanobacteria genomes were performed using a concatenation of 103 aligned, single-copy, phylogenetic marker genes, as previously described (71). Briefly, all genomes classified within the 'Methanobacteria' class were retrieved from the Department of Energy-Integrated Microbial Genome (IMG) and National Center for Biotechnology Information (NCBI) GenBank databases. Marker genes were identified from the genome set using Amphora2 (72), individually aligned using Clustal Omega (v.1.2.4) (73), and concatenated. The concatenated alignment was subject to Maximum Likelihood phylogenetic reconstruction in IQ-TREE (v.1.6.11) (74) after identifying the optimal amino acid substitution model (LG+F+R10) via the Bayesian Information Criterion, as implemented in modelfinder (75).

Metabolic reconstructions of MAGs and SAGs.

Gene prediction and annotation for MAGs and SAGs were performed with Prodigal v.2.6.3 (76) as implemented in Prokka v.1.11 (77) specifying default parameters. Following preliminary predictions and annotations for MAGs, gene functions were further examined using

the Kyoto Encyclopedia of Genes and Genomes (KEGG) function database (78) with the KEGG Automatic Annotation Server (KAAS) (79). Genomes were also queried via BLASTp (80) for specific gene functions, as guided by gene contents of closely related genomes. BLASTp searches were conducted using bait sequences specific for active site subunits for each protein or protein complexes. Positive matches for protein homologs in MAGs and SAGs were considered as those with a BLASTp E-value of $< 1 \times 10^{-6}$, >30% amino acid sequence similarity, and > 60% of the length of the query sequence. The complete WAB188, NSHQ14B, and NSHQ14C metagenome assemblies were queried for genes encoding homologs of key proteins initially absent from the MAGs (i.e., H_2-dependent methenyltetrahydromethanopterin dehydrogenase, Hmd, F_{420}-dependent methylenetetrahydromethanopterin dehydrogenase, Mtd, and the formate and formate/nitrate transporters, FdhC, FocA, and YfdC, in both Type I and Type II MAGs; the ion-translocating [NiFe]-hydrogenase complex, Mrp-Mbh, in the Type I MAG; the Group 3 F_{420}-reducing [NiFe]-hydrogenase, Frh, and Group 3c bifurcating [NiFe]-hydrogenase, Mvh, in Type II MAGs, described below) via BLASTp. Single amplified genomes affiliated with *Methanobacterium* were also queried for proteins missing from the MAGs via BLASTp. Unbinned contigs containing these homologs were manually assigned to MAGs based on consensus with contig coverage profiles and average GC content, as determined using CheckM (81).

Homologs of [NiFe]-hydrogenase were identified by BLASTp using query sequences for active site subunits. Briefly, candidate [NiFe]-hydrogenase catalytic subunits were compiled and combined with references for specific hydrogenase groups, as defined previously (82). The combined dataset was aligned with Clustal Omega, evaluated manually for the presence of

conserved N- and C-terminal CxxC motifs (83), and subjected to Maximum Likelihood phylogenetic analysis, as described above. The putative directionality and redox partner coupling, as determined initially from phylogenetic analyses above, were further evaluated by comparing amino acid conservation in the L1 and L2 motifs to previously characterized hydrogenases (82). These functional assignments were further assessed by examining the genes co-localized with the genes encoding hydrogenase catalytic subunits for key partner proteins (e.g., F_{420} binding proteins), as determined with the Conserved Domain Database (84) and BLASTp analysis against the NCBI non-redundant database.

Comparison of MAGs and SAGs.

The average nucleotide identities (ANIs) among SAGs and MAGs were calculated using the MUMmer (v4.0.0beta2) average_nucleotide_identity.py script in python (85). SAGs (B04, E10, J15, M05, P19, O02, and O05) that were found to have insufficient hits to calculate pairwise ANIs with at least one other genome were removed from this analysis. ANIs among the SAGs and the NSHQ14 MAGs were used to construct a dissimilarity matrix that was translated into a Euclidean distance matrix and used to construct a dendrogram using the hclust function in R specifying the “single linkage” agglomeration method (86).

To evaluate the similarity of proteins encoded among the MAGs and SAGs, the percent identities between each encoded protein homolog were first determined. Homologs were defined as those with ≥ 30% identity to protein coding genes in the NSHQ14C MAG (used as a reference genome), as identified by BLASTp searches of the proteins encoded by each SAG. The amino acid identities of proteins encoded by the SAGs relative to proteins encoded in the NSHQ14C

MAG were then averaged to calculate an overall average amino acid identity (AAI) for each SAG.

Orthologous protein groups among the SAGs were first defined as those proteins encoded in SAGs that were most closely related to a single protein from the reference genome (NSHQ14C Type II MAG), as determined by BLASTp. Among the most commonly identified SAG orthologs that exhibited differences in pairwise amino acid identity were transposases. Transposase orthologs were further classified using ACLAME v.0.4 (87) and were then subjected to alignment with Clustal Omega and maximum-likelihood phylogenetic reconstruction with PhyML v.3.0 via the Bayesian Information Criterion as implemented in the Smart Model Selection in PhyML (88, 89). The synteny of genes flanking transposases was assessed by aligning contigs encoding transposases using progressiveMauve (90), and alignments were visualized using Gene Graphics (91). To evaluate the possibility that divergent orthologous proteins contributed to apparent diversification of SAGs, Mantel tests describing correlations between protein ortholog amino acid dissimilarities and whole genome ANI dissimilarities were performed for the ten most abundant orthologous proteins identified in SAGs that differ from those in the NSHQ14 Type II MAG. Mantel tests were performed using the mantel function of the vegan: community ecology package in R specifying 100 permutations using the Pearson correlation method (92).

Methanogenesis rate potentials.

Potential rates of biological transformation of HCO_3^- and $HCOO^-$ to CH_4 were measured via microcosm-based activity assays containing ^{14}C-radiolabeled substates as previously described (51). Briefly, well water samples stored at 4°C were homogenized and 10mL aliquots

were transferred from storage vials to 26mL N_2-purged, autoclave-sterilized, butyl-stoppered experimental vials (4 biological replicates and 4 abiotic controls per condition) using a sterile, N_2-purged needle and syringe. Abiotic controls were sterilized by autoclaving twice, with incubation at room temperature overnight between autoclave cycles to allow for germination of spores. One mM (final concentration) of $HCOO^-$ or HCO_3^- that included 5 μCi ^{14}C-$HCOO^-$ or ^{14}C-HCO_3^- (American Radiolabeled Chemicals, St. Louis, MO), respectively, was then added to each vial. H_2 gas was added in excess of atmospheric pressure to each vial to account for 20% of headspace volume. Following incubation for one, two, four, six, and eight weeks at *in situ* temperature (34°C), 3 mL filtered (0.2 μm) N_2 was added to each vial using an N_2-purged sterile needle and syringe to maintain positive headspace pressure, and 3 mL headspace gas was removed using a needle and syringe equipped with a stopcock. The 3mL headspace gas from each microcosm vial was then injected into a specially fabricated scintillation vial containing a butyl rubber septum and CH_4 was trapped with 10 mL Cytoscint ES scintillation cocktail, as described previously (51). The radioactivity, measured in counts per minute, associated with ^{14}C-CH_4 from each of the samples was measured on a PerkinElmer Tri Carb 2900TR Liquid Scintillation Analyzer (PerkinElmer, Waltham, MA), converted to disintegrations per minute using a quench curve, normalized to account for total substrate added (radiolabeled and unlabeled) and total headspace gas volume, and used to calculate the rates of substrate transformation. ^{14}C-CH_4 values in abiotic controls were subtracted from ^{14}C-CH_4 values in biological replicates to arrive at the amount of ^{14}C-CH_4 produced that could be attributed to biology. Statistical significance of differences between biological assays and abiotic controls were assessed via Student's *t*-test assuming unequal variance for each condition.

Results and Discussion

Reconstructed genomes from metagenomic sequences were used to develop metabolic models for methanogen populations inhabiting waters that span a range of geochemical conditions due to differences in serpentinization reaction progress. Two phylogenetically distinct lineages affiliated with *Methanobacterium* were the sole methanogens recovered from subsurface well waters from the Samail Ophiolite (Fig. 1). One MAG (Type I) represented an abundant microbial lineage in a well with circumneutral water (WAB188: pH 7.6), whereas another MAG (Type II) represented a lineage that was abundant in a well with hyperalkaline water, including samples collected at both 50 m (NSHQ14B: pH 11.1) and 85 m depths (NSHQ14C: pH 11.3) (Fig. 1A). MAGs affiliated with the Type II lineage from NSHQ14B and from NSHQ14C exhibited > 99.99% identity to each other on an average nucleotide level (data not shown). Due to the extremely high similarity between these two MAGs, one MAG (*Methanobacterium* Type II from NSHQ14C) was selected as the reference genome for the Type II lineage. Contigs affiliated with both Type I and Type II lineages were also detected at low abundances in most of the other wells, which is consistent with the previous finding that 16S rRNA genes affiliated with *Methanobacterium* were widely distributed at varying abundances among subsurface well waters collected from the Samail Ophiolite (e.g., previously detected in 16 of 20 samples in relative abundances of <3% to 28.0% of total 16S rRNA gene transcripts) (6). Accordingly, sequences closely affiliated with *Methanobacterium* have been detected in a range of other serpentinites and often in high abundance (14, 19, 50, 54), suggesting that this genus is a ubiquitous member of globally distributed serpentinite communities.

All *Methanobacterium* MAGs exhibited high levels of estimated completeness and low contamination (Table S1), and were classified as high-quality draft genomes (93). The Type I *Methanobacterium* MAG was larger (1.904 Mbp) than the NSHQ14C *Methanobacterium* Type II MAG (1.511 Mbp) and encoded more proteins (2,052 versus 1,806), despite both MAGs exhibiting the same estimated levels of completeness (98.4%) (Table S1). This finding is consistent with previous results that revealed an inverse relationship between the average estimated genome size and the pH of subsurface well waters in the Samail Ophiolite (51). This observation is also consistent with data from the serpentinization impacted environment termed The Cedars (California, USA), where members of a microbial community from a hyperalkaline spring (pH ~12) harbored the smallest genomes reported for their respective taxa (94). Microorganisms residing in highly serpentinized waters presumably exhibit streamlined genomes to minimize energetic costs and nutrient demands associated with their replication and repair under extreme conditions, as has been suggested previously (51, 95).

Phylogenomic reconstruction of Oman methanogen MAGs in relation to other *Methanobacterium* genomes suggested that the taxa corresponding to Type I and II MAGs diverged relatively recently within the *Methanobacterium* lineage (Fig. 1B). The Type I and II MAGs were most closely related to each other, and unexpectedly, the Type II MAG appeared to correspond to a taxon that was descended from the Type I taxon, as described below. The Type I MAG encoded homologs of two key [NiFe]-hydrogenases, Group 3c bifurcating [NiFe]-hydrogenase (Mvh) and Group 3 F_{420}-reducing [NiFe]-hydrogenase (Frh) (discussed below) (Fig. 1B; Fig. S1), which are common to other Methanobacteria. However, homologs of these genes were not detected in any of the Type II genomes, including both Type II MAGs and all single

amplified genomes (SAGs, described below). Furthermore, the large subunits of Group 3 [NiFe]-hydrogenases encoded by the Type I MAG were used to query the entire assemblies of both NSHQ14 metagenomes with no positive matches identified. Together, these data indicated gene loss in the Type II lineage. In contrast, among available Methanobacteria genomes, only the Type II lineage encoded a homolog of the ion-translocating [NiFe]-hydrogenase complex, Mrp-Mbh, indicating gene acquisition (Fig. 1B; Fig. S2). The large subunit of the Mrp-Mbh [NiFe]-hydrogenase encoded by the Type II MAGs was not detected in the WAB188 metagenomic assembly. Phylogenetic analysis of the large subunit of the Mrp-Mbh [NiFe]-hydrogenase encoded by the Type II MAGs revealed it to be nested among bacterial Group 4d [NiFe]-hydrogenase homologs, suggesting acquisition via horizontal gene transfer from an ancestor of the Firmicutes or Thermotogae (Table S2; Fig S2). Members of the Firmicutes are commonly identified in subsurface waters of the Samail Ophiolite (6) and other serpentinizing systems (14, 19, 54), leading to the possibility that the genes encoding Mrp-Mbh could have been acquired in a similar environment type. As such, the divergence between Type I and Type II MAGs appears to have occurred relatively recently, a conclusion that is supported by short estimated branch lengths separating these lineages (Fig. 1B).

Metabolic reconstructions of *Methanobacterium* Type I and II MAGs indicated that both organisms encoded methanogenesis pathways, albeit with several key differences as mentioned briefly above (Fig. 2). The Type I MAG encoded all requisite genes for hydrogenotrophic methanogenesis in Methanobacteria (96) (Fig. 2A), including Group 4 energy-converting [NiFe]-hydrogenase (Eha/Ehb), Frh, and the Mvh-heterodisulfide reductase complex (Mvh-Hdr) (Fig. S1; Fig. S2). Homologs of H_2-dependent methenyltetrahydromethanopterin dehydrogenase

(Hmd) and F_{420}-dependent methylenetetrahydromethanopterin dehydrogenase (Mtd), which can function independently or in tandem to catalyze a critical step in hydrogenotrophic methanogenesis (97, 98), were initially not detected in either the Type I or Type II MAG. However, contigs containing homologs of Mtd with 89% identities to a previously described *Methanobacterium* sp. per BLASTp were later identified in unbinned contigs of the WAB188 metagenome and both NSHQ14 metagenomes and were assigned to the Type I and Type II MAGs, respectively (Table S3).

The Type II MAG encoded Eha (Fig. S2; Fig. S3) but surprisingly did not encode Frh (Fig. 1B; Table S4), the latter of which couples the oxidation of H_2 to the reduction of coenzyme F_{420} (82, 99). The Type II MAG also did not encode Mvh (Fig. 1B; Table S4), which couples with Hdr to bifurcate electrons from H_2 to simultaneously reduce low potential ferredoxin (Fd) and the heterodisulfide bond between coenzyme M and coenzyme B (CoM-S-S-CoB) (82). Mvh-Hdr and Frh are [NiFe]-hydrogenases characteristically encoded in the genomes of all other members of the Methanobacteria (Fig. 1B; Table S4) and are common features associated with all hydrogenotrophic (Class I) methanogens (96). Importantly, genetic experiments indicated that neither Mvh nor Frh homologs are required during methanogenic growth with formate (100, 101). For example, in *Methanococcus maripaludis* Vhu (alternative name for Mvh) and Frh deletion strains, these functions are thought to be replaced by a formate dehydrogenase (Fdh)-Hdr complex and a F_{420}-reducing Fdh, respectively (100-104). FdhAB and VhuD proteins have been suggested to form a complex with HdrABC that allows for bifurcation of electrons from formate and their coupled reduction of heterodisulfide and Fd (102, 105). In support of this, the alpha subunit of Fdh from *M. maripaludis* co-purified with the beta subunit of Fdh, the delta

subunit of Vhu, and all subunits (i.e., ABC) of Hdr (102, 105). Additionally, the tungsten-containing formylmethanofuran dehydrogenase (Fwd), which catalyzes the reduction of CO_2 and covalent attachment of methanofuran (MFR) in the first step of methanogenesis, was found to co-purify with FdhAB, HdrABC, and VhuD in *M. maripaludis* when grown under formatotrophic, but not hydrogenotrophic, conditions (102). This may help to explain how *M. maripaludis*, and potentially other hydrogenotrophic methanogens, prevent the loss of cytoplasmic CO_2 for use in methanogenesis and biomass generation during formate-dependent growth.

The biochemical and phenotypic observations of Frh and Vhu deletion strains of *M. maripaludis* provide a framework to rationalize how the Type II cells from the Samail Ophiolite, which lack Frh and Mvh, might catalyze methanogenesis. The Type II MAG encoded Fdh (*fdhAB*) and this was co-localized in the genome with *mvhD* and *hdrBC* (Fig. 3). While the structure of F_{420}-reducing Fdh has not yet been resolved (103), Fdh purified from *Methanobacterium formicicum* reduced coenzyme F_{420} (106, 107), and the beta subunit (FdhB) was predicted to have an F_{420}-binding domain similar to that of the Frh beta subunit (FrhB) (108). The residues involved in F_{420} coordination by FrhB in *Methanothermobacter marburgensis* (positions 163, 165-167, and 208-211) (108) were conserved in FdhB proteins from both *M. formicicum* and the Type II *Methanobacterium* MAG with two exceptions (Fig. S4). The two positions that were not conserved in *M. formicicum* and the Type II MAG, however, harbor substitutions to amino acids of the same polarity and charge (S to N and V to W) and were consistent between both FdhB proteins. The mechanism of formate transport into the cell remains somewhat unclear as *Methanobacterium* Type I and Type II MAGs both lacked

homologs of the canonical formate transporters FdhC, YfdC, and FocA. Each *Methanobacterium*-affiliated SAG and the entire metagenomic assemblies from WAB188, NSHQ14B, and NSHQ14C were queried for these possible formate transporters with no positive matches identified. However, the Type II MAG encoded a homolog (38.8% identity, 95% query coverage) of the formate:oxalate antiporter, OxlT (Table S2), which was lacking from the Type I MAG and may function in transporting formate into the Type II cells. These data collectively suggest that the Type II *Methanobacterium* may drive methanogenesis via a pathway that is unique among characterized Methanobacteria, wherein formate is required as electron donor and with H_2 serving as a source of additional reductant (Fig. 2B).

Consistent with previous work suggesting an essential anaplerotic role for Eha during formatotrophic methanogenesis (100), both the Type I and II MAGs encoded homologs of this enzyme complex (Fig. S2; Fig. S3). The Type II MAGs, but not Type I MAG or other members of the Methanobacteria (Fig. 1B), also encoded a [NiFe]-hydrogenase that is homologous to the membrane-bound Mrp-Mbh complex in *Pyrococcus furiosus* (Fig. S5) (109). Mrp-Mbh in *P. furiosis* comprises 14 subunits, including a Na^+/H^+ antiporter domain (Mrp) and a [NiFe]-hydrogenase domain (Mbh) (109). In *P. furiosus,* the Mrp-Mbh complex catalyzes the reversible oxidation of Fd coupled with H_2 production, with excess potential used to pump Na^+ or H^+ outside of the cell. In this case, oxidation of Fd would generate an electrochemical gradient that could be used to drive ATP synthesis. Alternatively, Fd reduction could be coupled to H_2 oxidation, with the shortage of potential compensated for by releasing Na^+ or H^+ into the cell. Consequently, the Type II *Methanobacterium* cells could use this complex to: 1) generate reduced Fd and 2) neutralize cytoplasmic pH (if the coupling ion is H^+). Indeed, Mrp was first

characterized in the alkaliphile *Bacillus halodurans*, where it was found to be critical for pH homeostasis under alkaline conditions (110). The reversibility of the enzyme system may allow for these functions to shift with changing cellular demands.

Why would *Methanobacterium* Type II have evolved to drive methanogenesis with formate rather than H_2 as primary reductant in an environment such as NSHQ14, where H_2 concentrations (21 to 2900 μM) were over 1-3 orders of magnitude higher than formate (1.7 μM) (Table 1) (6, 23, 51)? The standard state reduction potentials of hydrogen and formate are similar (-414 and -430, respectively) (43), although the non-standard state potential of H_2 is likely to be lower than that of formate in environments where the concentration of H_2 exceeds formate. It is also possible that the differential mobility of formate and H_2 in aqueous solutions could favor formate utilization (111). Alternatively, we propose adaptation to extreme CO_2 limitation in highly serpentinized waters as a likely explanation. Although H_2 was replete in the environment inhabited by Type II *Methanobacterium* cells, use of H_2 as sole electron donor for methanogenesis necessitates coupling with CO_2 as both electron acceptor and source of carbon (96). However, dissolved CO_2 is extremely limited in highly serpentinized waters due to prior reactions that precipitated DIC as mineral carbonates. Furthermore, DIC speciates primarily as bicarbonate or carbonate ions under high pH conditions such as those present in NSHQ14 (4). Although methanogens may convert bicarbonate to CO_2 for use in methanogenesis or biomass generation, this reaction ($HCO_3^- + H^+ \rightarrow CO_2 + H_2O$) consumes protons, which are limiting at high pH. Formatotrophic methanogenesis may help circumvent carbon acquisition problems because the oxidation of formate yields intracellular CO_2 which could be subsequently reduced to CH_4 (Fig. 2B) or biomass via the Wood-Ljungdahl pathway (Table S2). Additionally, a putative

acetogen lacking all known hydrogenases and apparently using CO to drive acetogenesis was detected in the CO_2-limited, serpentinization-impacted groundwater of The Cedars, California (112). This suggests that replacement of hydrogen-based reductant by single-carbon reduced substrates (i.e., formate or CO) may be a common strategy to circumvent CO_2 limitation among organisms encoding the Wood-Ljungdahl pathway of carbon fixation in serpentinizing environments.

The source of formate in waters of the Samail Ophiolite has not yet been resolved, however, consumption of CO_2 and H_2, coinciding with generation of nearly 100 μM formate, has been observed during low-temperature abiotic reactions between water and rocks from the Samail Ophiolite (64). A positive correlation (Pearson R = 0.72, $p < 0.05$) existed between formate concentrations and pH in subsurface waters from the Samail Ophiolite sampled in 2015 (6) (formate was not measured in 2017), which is potentially consistent with the hypothesis that formate can be generated abiotically as a result of equilibration of CO_2 with H_2 produced during serpentinization reactions (4, 5, 113, 114). Additionally, formate formed via past reactions could potentially be stored in the rock (e.g., in fluid inclusions) (115). Regardless of the source of formate in the system, it is possible that methanogens and other formatotrophic populations actively maintain formate at a low (~ 1 μM) steady state concentration (Table 1).

To begin to test these predictions, well waters were sampled again from WAB188 and NSHQ14 in February and March, 2020, for use in quantifying rates of ^{14}C-CH_4 generation from ^{14}C-radiolabeled substrates (^{14}C-$HCOO^-$ and ^{14}C-HCO_3^-). Temperature and pH values were similar between waters sampled from each well in 2017 and 2020 (Table 1). Microcosms containing waters from WAB188 that were amended with either H_2 + bicarbonate (including

5μCi ^{14}C-HCO_3^-) and with H_2 + formate (including 5μCi ^{14}C-$HCOO^-$) generated significantly more CH_4 than killed controls, and CH_4 generation attributable to biological processes increased over time (Fig. 4, Table S5). No significant differences were observed between the amount of biologically-generated CH_4 in WAB188 microcosms amended with H_2 + bicarbonate versus H_2 + formate at each time point. This is potentially consistent with the hypothesis that *Methanobacterium* Type I, which was detected in high abundance in well WAB188 among 2017 metagenomes, functions as a canonical Class I methanogen (similar to other members of the Methanobacteria) which can commonly use H_2 + CO_2 or formate as methanogenic substates (96).

In contrast, significantly higher quantities of CH_4 were generated in NSHQ14 microcosms amended with H_2 + formate (including 5μCi ^{14}C-$HCOO^-$) than in killed controls, and biologically-generated CH_4 increased over time (Fig. 4, Table S5). However, no CH_4 generation attributable to biology was observed in NSHQ14 microcosms amended with H_2 + bicarbonate (including 5μCi ^{14}C-HCO_3^-). This potentially supports the genomic prediction that *Methanobacterium* Type II, which was detected in high abundance in NSHQ14 among 2017 metagenomes, can couple H_2 with formate but not DIC to drive methanogenesis via a pathway that is unique among characterized Methanobacteria. Further, the rates of methanogenesis were lower in NSHQ14 microcosms as compared with WAB188 microcosms, which is potentially consistent with the previous finding that rates of utilization of select single-carbon compounds were generally lower in hyperalkaline waters than alkaline waters, possibly due to extreme conditions imposed by high pH waters (51).

The short branch length separating the Type I and Type II MAGs and differences in their methanogenesis pathways due to gene loss/acquisition suggests that the Type II cells were

derived from Type I cells. This prompted the generation of single amplified genomes (SAGs) to further evaluate whether this phenomenon was prevalent among individual cells and to uncover evidence for continued strain-level diversification in this lineage. A total of 71 SAGs were assembled from NSHQ14C, 69 of which were affiliated with *Methanobacterium* (Table S6). One of the other SAGs was affiliated with the methanotrophic bacterial genus, *Methyloccocus*, and the other was too incomplete to classify taxonomically. The low genome recovery from SAGs (71 out of 317 single cells) is possibly attributable to the low efficiency of lysing cells that are adapted to hyperalkaline waters using potassium hydroxide.

Among the 69 *Methanobacterium* affiliated SAGs, the pairwise average nucleotide identities (ANIs) indicated an average difference of only ~1 bp per kbp between them and the NSHQ14C Type II MAG (average ANI of 99.90%) (Fig. 5A). For comparison, the Type I MAG shared 91.11% and 90.59% ANI with the Type II MAGs from NSHQ14B and NSHQ14C, respectively. Proteins involved in cellular metabolism (e.g., HdrABC, FdhB, MvhD, and the large subunits of both Eha and Mrp-Mbh [NiFe]-hydrogenases) were all found to exhibit identical nucleotide sequences among the Type II SAGs and MAGs. Similarly, FdhA exhibited identical nucleotide sequences among all Type II SAGs and MAGs, except for a single SAG (B06) that was found to exhibit a single non-synonymous nucleotide polymorphism resulting in a change from an aspartate to a glutamate. Both aspartate and glutamate have negatively charged side chains, indicating that this change likely conserved protein function, which is consistent with the presumed critical importance of FdhA in the metabolism of Type II cells (Fig. 3B). Consistent with the Type II MAGs, homologs of Mvh and Frh [NiFe]-hydrogenases were not found in any of the *Methanobacterium* affiliated SAGs. Together, these observations indicate

that the core metabolism inferred for the Type II cells is likely a prevalent feature associated with this population.

In contrast, a number of orthologous proteins were identified in SAGs that differed markedly from those encoded by the NSHQ14C Type II MAG. Notably, among the ten orthologs that had the highest representation in SAGs and that differed from the NSHQ14C MAG, five were transposases (Table 2). This finding is in line with the previous detection of abundant transposases in a biofilm metagenome recovered from the Lost City serpentinizing system (116). Mantel tests of matrices describing the ANI among SAGs (Table S7) and the amino acid dissimilarity of the ten orthologs (Table 2) were used to identify orthologs that likely contributed to apparent diversification in the SAGs (Fig. 5). Among the ten orthologs considered, the dissimilarities in eight proteins were not significantly correlated with ANI. However, the dissimilarity of a protein belonging to the Peptidase C39 family and an ISNCY ("insertion sequence not classified yet") transposase were significantly and positively correlated with the dissimilarity in ANI, suggesting that they may contribute to the apparent recent diversification of these cells.

The genes flanking the ten divergent orthologs were examined to identify evidence of recent transposition and/or horizontal gene transfer events in the form of different genomic locations in the SAGs. The unclassified transposase with the greatest number of SAG homolog variants that, based on the results of a Mantel test (Table 2), is not suggested to have significantly contributed to the recent vertical diversification of SAGs, was flanked by a randomized assortment of genes (data not shown). This is consistent with its recent and likely random integration into the genomes of Type II cells. In contrast, genes flanking the ISNCY

family transposase that is suggested to have significantly contributed to recent diversification of these cells were largely syntenic among closely related orthologs but not among those encoding more divergent orthologs (Fig. 6). Additionally, variability of gene order and gene content among the SAGs and MAGs suggested rearrangement of genes flanking this transposase. These observations suggest that multiple transposition events likely led to this variable genomic arrangement, thereby revealing a mechanism that could have contributed to the recent diversification of Type II cells.

Intriguingly, SAGs K19, G13, E08, and B06 all encoded closely related ISNCY transposases upstream of a CRISPR-associated Cas4 protein (Fig. 6). This Cas4 protein was not encoded by the Type II NSHQ14B or NSHQ14C MAGs, with the most similar protein in the MAGs only exhibiting < 30% identity. Moreover, this protein was only encoded by these four SAGs and one other (D03) where it was located on a contig that encoded multiple putative transposases (data not shown). Surprisingly, however, the contigs encoding Cas4 and the ISNCY transposase did not code for other Cas proteins or other genetic elements (i.e., CRISPRs and spacer sequences) that act in tandem with Cas4 (117) to confer adaptive immunity against invading viruses and plasmids in Bacteria and Archaea (118). However, Cas4 is not always directly colocalized with other elements of CRISPR arrays (119) and, importantly, the ends of contigs represent portions of the genome where reads do not sufficiently overlap to generate contiguous sequences. Therefore, it is possible that transposases (especially ISNCY type) catalyzed the integration of functional CRISPR-Cas systems that may confer a subset of the population with adaptive immunity from foreign genetic material.

The findings herein are potentially in line with previous studies of organisms that are closely related to one another, wherein microbial genomes have been conceptualized as containing two distinct components, core and variable, collectively termed the pan-genome (120, 121). The core genome is composed of genes that are common to all strains, whereas the variable genome consists of genes that differ between strains, for example resulting from gain via horizontal gene transfer or loss. For example, 7 *Sulfolobus islandicus* genomes recovered from globally distributed locations that diverged recently in evolutionary time (~910,000 years ago) shared a core genome including housekeeping genes, but also encoded variable genomic regions containing small inversions and rearrangements, many of which were also associated with CRISPR-Cas genes (120). Like the *Methanobacterium* populations from 85m depth in NSHQ14, other subsurface communities include population level genomic diversity that was proposed to have been generated via the activity of mobile elements (122-124).

Similar to the ISNCY transposase, genes flanking a protein belonging to the C39 peptidase family that is suggested to have contributed to recent diversification of Type II *Methanobacterium* cells (Table 2) were largely syntenic among closely related proteins but not among those encoding more divergent orthologs, and rearrangement of genes co-localized with this peptidase were also observed (Fig. S7). These rearrangements may have been catalyzed by a transposase that was detected downstream of the peptidase in at least one of these SAGs (I11). The diversification of peptidase C39 and its potential integration into cellular genomes by transposase activity may have implications for cellular fitness as these proteins function in bacteriocin (antimicrobial peptide) processing (125). Thus, it is possible that Type II *Methanobacterium* cells employ bacteriocidin-type antimicrobials to increase their competitive

advantage for limiting nutrients (e.g., formate) over other co-inhabiting species, potentially helping to explain their prevalence in hyperalkaline waters.

Conclusions:

Reconstruction of two *Methanobacterium* genomes from metagenomic sequences obtained from subsurface waters exhibiting contrasting geochemical characteristics of the Samail Ophiolite, Sultanate of Oman, provided an opportunity to conduct comparative genomic and evolutionary investigations into adaptations that enable putative hydrogenotrophic methanogens to overcome DIC limitation associated with hyperalkaline conditions. Metabolic reconstruction of a Type I *Methanobacterium* MAG that was abundant in circumneutral, DIC replete waters revealed canonical hydrogenotrophic methanogenesis pathways. However, Type II *Methanobacterium* MAGs from extensively serpentinized, DIC limited waters lacked homologs of key [NiFe]-hydrogenases, Mvh and Frh, that supply reductant from H_2 oxidation for methanogenesis. Metabolic reconstructions indicated that these functionalities were replaced by formate dehydrogenases that supply reductant from formate oxidation and that yield intracellular CO_2 to allow for methanogenesis to proceed under otherwise DIC limited conditions. The genomic prediction that *Methanobacterium* Type II can couple H_2 with formate but not DIC to drive methanogenesis via a pathway that is unique among characterized Methanobacteria was supported by microcosm-based radiotracer experiments revealing significant biological methane production from H_2 + formate but not H_2 + bicarbonate. The combination of phylogenetic and gene distribution data relative to other Methanobacteria indicated that the Type II lineage was derived from the Type I lineage, suggesting that the replacement of H_2-based reductant by formate-based reductant is a derived trait. In turn, this suggested that the directionality of the

diversification of *Methanobacterium* inhabiting the Samail Ophiolite was from circumneutral into hyperalkaline environments, the latter of which is likely to be limiting in DIC, but where formate could be supplied by serpentinization reactions. Thus, diversification may have taken place in a system where serpentinization was generating large amounts of formate which could act as a selective pressure to evolve the suite of physiological traits allowing for its use in key methanogenesis reactions.

The recent diversification of *Methanobacterium* into hyperalkaline environments appeared to have been facilitated, in part, by lateral gene transfer of a [NiFe]-hydrogenase complex from a bacterium, perhaps affiliated with an ancestor of Firmicutes. Single cell genomes of Type II *Methanobacterium* revealed evidence of gene rearrangement, possibly through transposition. Collectively, these results point to the importance of gene loss, gain, and transposition in the adaptation of methanogens to hyperalkaline conditions and provide strong, albeit indirect, evidence that cells are active and adapted to the polyextremophilic subsurface environment of the serpentinizing Samail Ophiolite.

Data Availability.

The data that support the findings of this study are available on The ISME Journal's website and from the corresponding author on request. The metagenomes analyzed in this study have been deposited to the MG-RAST metagenomics analysis server, https://www.mg-rast.org/linkin.cgi?project=mgp85625.

Acknowledgements.

This work was supported by a grant from the NASA Astrobiology Institute (NNA15BB02A) to JRS, AST, and ESB, and by NSF grants OCE-1335810 and OIA-1826734 to RS. We thank staff of the Single Cell Genomics Center at the Bigelow Laboratory for Ocean Sciences for generating the single cell genomics data. The authors are grateful to Juerg Matter for help with equipment acquisition, permitting, and sample export and to the Ministry of Regional Municipalities and Water Resources in the Sultanate of Oman for allowing sampling and export of well waters.

Conflict of Interest.

The authors declare that they have no conflict of interest.

Table 1. Geochemical measurements for well waters sampled in 2017 and 2020.

Well	**WAB188**		**NSHQ14**		
Year	2017	2020	2017	2017	2020
Water table depth (m)	9	8.5	12	12	9
Sampled depth (m)	78	50	50	85	9-30
pH	7.6[a]	7.5	11.1	11.3	11.3
Temperature (°C)	33.0[a]	34.7	34.4	36.3	35.7
H_2 (µM)	0.92	-	21	164	-
DIC (mM)	3.0	-	0.05	0.13	-
Formate (µM)	1.0[b]	-	1.7[b*]	1.7[b*]	-
CH_4 (mM)	1.69	-	34.6	12.6	-

Values measured in 2017 were previously reported in Fones et al., 2019.
[a]Data collected from wells in 2016 that were previously reported in Rempfert et al., 2017 are displayed since measurements were not collected during the 2017 field season.
[b]Data collected from wells in 2015 that were previously reported in Rempfert et al., 2017 are displayed since measurements were not collected during the 2017 field season.
[*]The formate concentration was measured in only one depth interval (20m) in NSHQ14 in 2015, as previously reported in Rempfert et al., 2017.
- Denotes data that is not available from the 2020 field season.

Table 2. The ten most abundant orthologous proteins identified in single amplified genomes (SAGs) that differ from those in the NSHQ14C Type II metagenome assembled genome (MAG).

Variant protein ortholog annotation (SAGs vs. NSHQ14C MAG)	# of SAGs encoding orthologs with <100% identity to the NSHQ14C MAG	Amino acid identities (SAGs vs. NSHQ14C MAG)	Closest taxonomic affiliation of the most divergent ortholog	Mantel correlation (R) and significance (*p*) among protein ortholog amino acid dissimilarities and whole genome ANI dissimilarities
Transposase	21	96.8-98.4%	*Methanosarcina mazei*	R = -0.01, *p* =0.44
GDP-mannose 4,6 dehydratase	17	73.9-100%	*Methanobacterium congolense*	R = 0.07, *p* = 0.07
DDE-type integrase/ transposase/recombinase	17	97.2-100%	*Methanobacterium formicicum*	R = 0.09, *p* = 0.21
Peptidase C39	16	76.5-100%	*Methanothermus fervidus*	R = 0.19, *p* = 0.02
Transposase (IS5 family)	16	96.6-100%	*Methanoculleus taiwanensis*	R = 0.04, *p* = 0.23
ISNCY family transposase	15	91.6–100%	*Methanobacterium subterraneum*	R = 0.37, *p* = 0.01
Histidine kinase	13	99.7-100%	*Methanobacterium formicicum*	R = 0.22, *p* = 0.07
Transposase (IS630 family)	12	97.4-100%	*Methanobacterium subterraneum*	R = -0.08 *p* = 0.84
MFS transporter	12	99.8-100%	*Methanobacterium paludis*	R = 0.01 *p* = 0.43
Exosome complex protein Rrp4	7	99.6-100%	*Methanobacterium congolense*	R = 0.01 *p* = 0.50

Supplementary Table 1. Assembly statistics for *Methanobacterium* Type I and II metagenome

	Methanobacterium Type I	*Methanobacterium* Type II
Bins	WAB188.10	NSHQ14B.3 / NSHQ14C.4
Size (Mbp)	1.904	1.496 / 1.511
Completeness (%)	98.4	98.4 / 98.4
Contamination (%)	0	0 / 0
Contigs	126	141 / 141
Largest contig (bp)	69,880	57,643 / 57,403
N50 (bp)	22,304	15,814 / 15,975
G+C content (%)	35.1 ± 1.39	35.2 ± 1.82 / 35.2 ± 1.85
Protein coding genes	2,052	1,787 / 1,806
Average contig coverage	41.56 ± 9.46	428.41 ± 127.88 / 501.76 ± 169.69

assembled genomes (MAGs).

Supplementary Table 3. Protein affiliations, coverage profiles, and GC content values used to assign unbinned contigs encoding F_{420}-dependent methylenetetrahydromethanopterin dehydrogenase (Mtd) to Type I and Type II MAGs.

	Genome encoding most closely related protein per BLASTp	**Contig coverage**	**GC content (%)**	**Genome designation**
WAB188 contig encoding Mtd homolog	*Methanobacterium* sp.	61.48	38.1	WAB188 *Methanobacterium* Type I MAG
NSHQ14B contig encoding Mtd homolog	*Methanobacterium* sp.	433.47	36.4	NSHQ14B *Methanobacterium* Type II MAG
NSHQ14C contig encoding Mtd homolog	*Methanobacterium* sp.	504.88	36.5	NSHQ14C *Methanobacterium* Type II MAG

Supplementary Table 5. Potential rates of biological methanogenesis from formate and bicarbonate by planktonic microbial communities in well water samples collected from the Samail Ophiolite in 2020. Potential rates of biological substrate transformation were determined via microcosm assays using well waters collected from the Samail Ophiolite in 2020. The average rates of methane generation observed in four replicate abiological controls were subtracted from values in four replicate biological assays (Avg) and their combined standard deviations (SD) are presented at five timepoints over an 8-week time course series. *P*-values were determined between biological assays and abiological controls at each timepoint via Student's t-test assuming unequal variance for each condition.

	1 week	2 weeks	4 weeks	6 weeks	8 weeks
Methane generation in microcosms supplied with H_2 + formate					
WAB188 Avg (pmol CH_4 mL^{-1})	5144	9731	11472	25978	32815
SD	383	2115	2981	6354	6945
p-value	<0.01	<0.01	<0.01	<0.01	<0.01
NSHQ14 Avg (pmol CH_4 mL^{-1})	0	0	325	2411	4551
SD	-	-	195	1336	2632
p-value	-	-	0.02	0.02	0.02
Methane generation in microcosms supplied with H_2 + bicarbonate					
WAB188 Avg (pmol CH_4 mL^{-1})	3892	13624	21388	35158	47564
SD	5093	9084	7765	11331	9483
p-value	0.13	0.03	<0.01	<0.01	<0.01
NSHQ14 Avg (pmol CH_4 mL^{-1})	0	0	0	0	0
SD	-	-	-	-	-
p-value	-	-	-	-	-

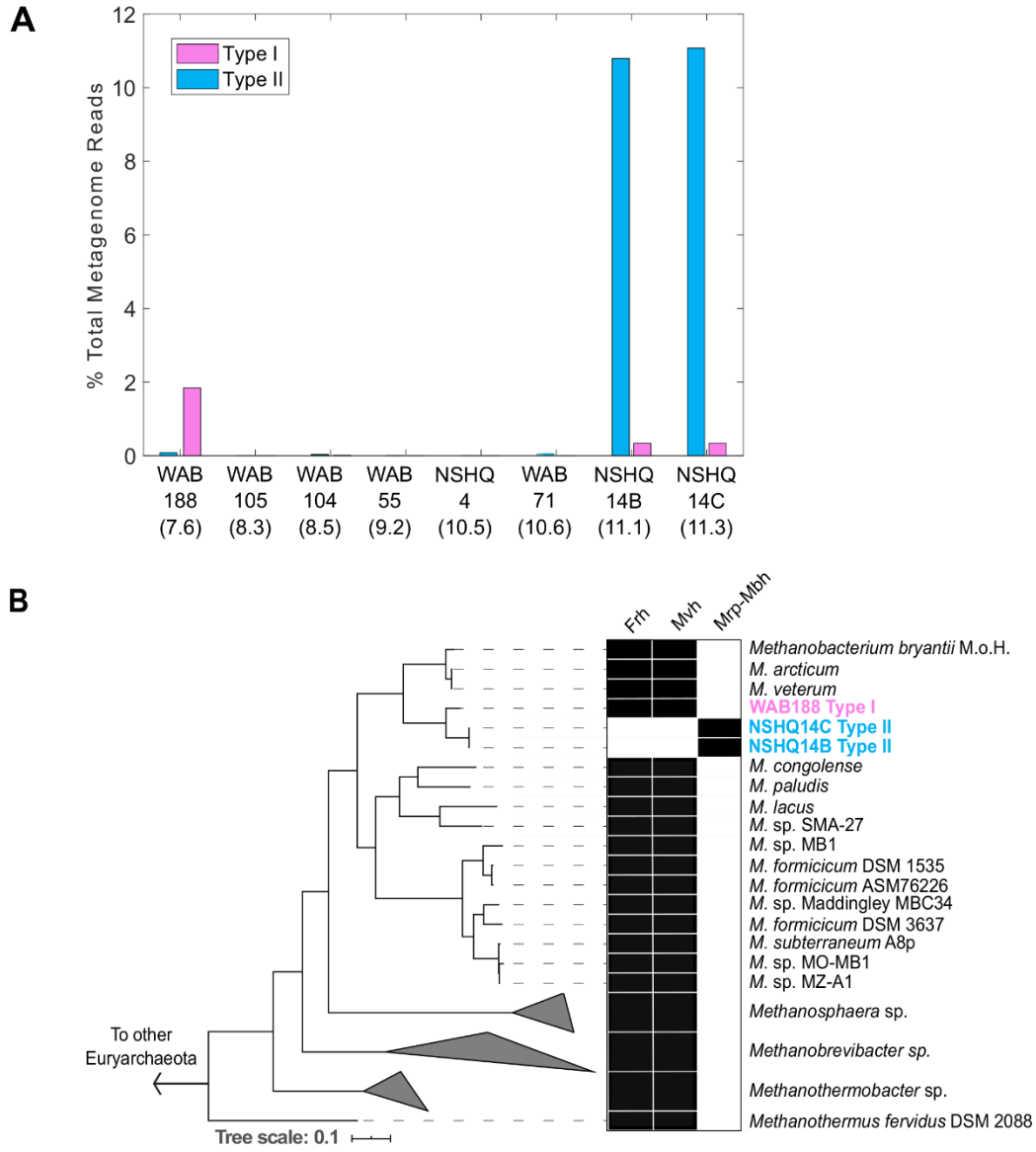

Figure 1. The estimated relative abundances of *Methanobacterium* MAGs in communities from subsurface fracture waters collected from wells intersecting the Samail Ophiolite in 2017 (A) and phylogenomic reconstruction of Oman methanogen metagenome assembled genomes (MAGs) in relation to representative *Methanobacterium* genomes (B).

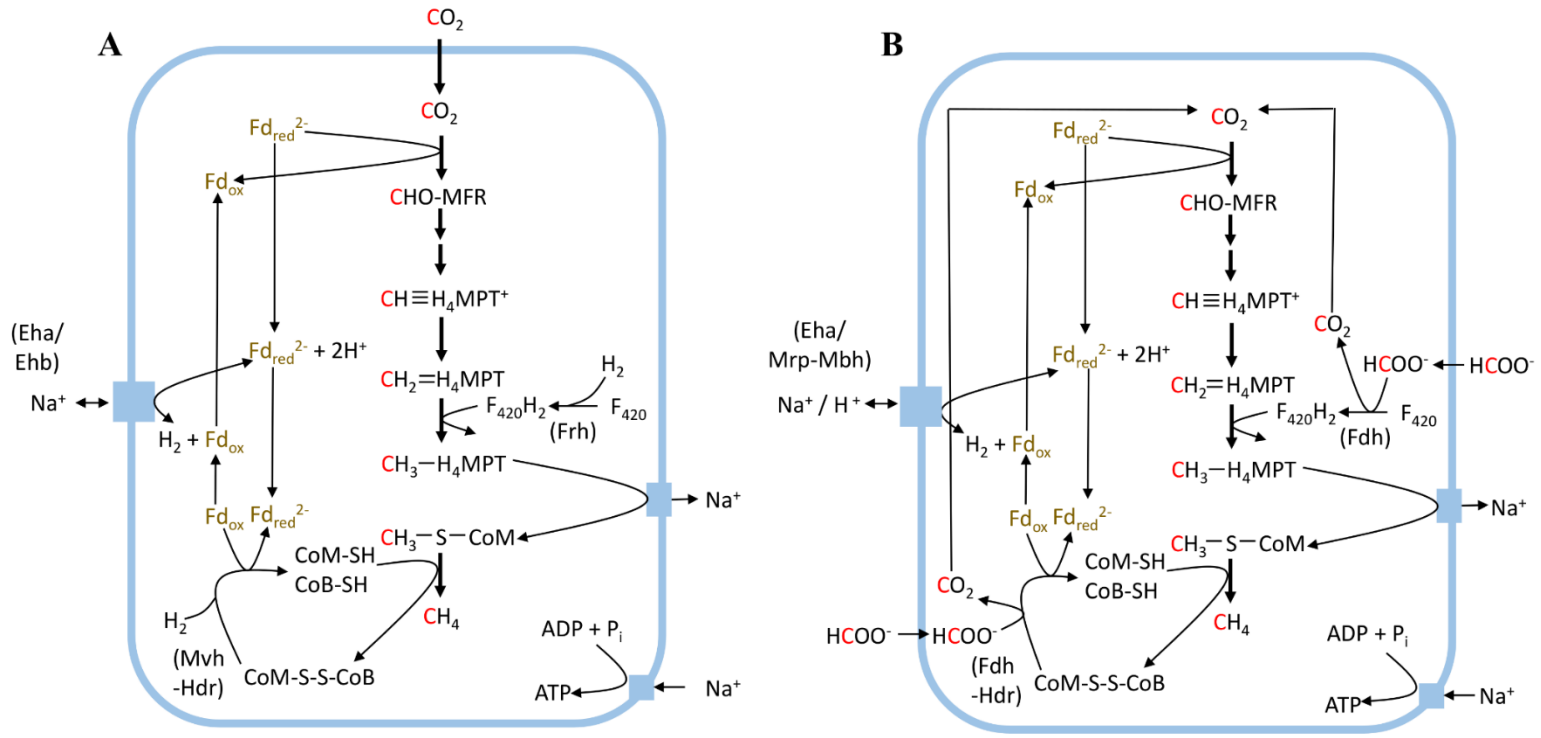

Figure 2. Proposed hydrogenotrophic and formatotrophic methanogenesis pathways in *Methanobacterium* Type I (A) and Type II (B) populations, respectively, from the Samail Ophiolite, Oman.

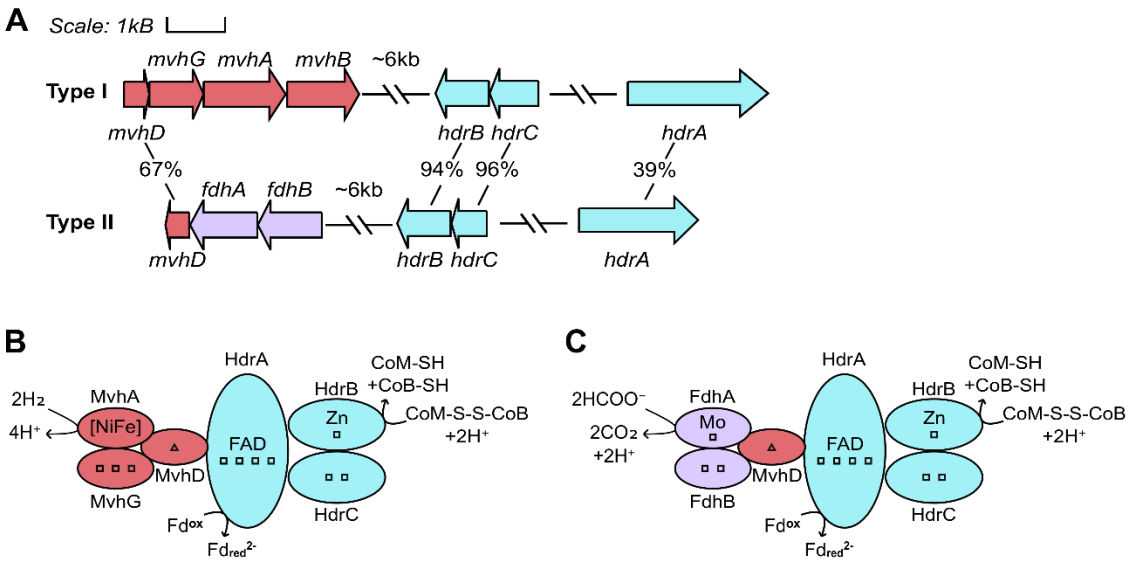

Figure 3. Genes inferred to be co-localized with those coding for methyl viologen-reducing (Group 3c) [NiFe]-hydrogenase (Mvh) and formate dehydrogenase (Fdh) in Type I and II MAGs (A) and the putative protein complexes they form to bifurcate electrons from H_2 (B) or formate (C), respectively, to simultaneously reduce ferredoxin and heterodisulfide.

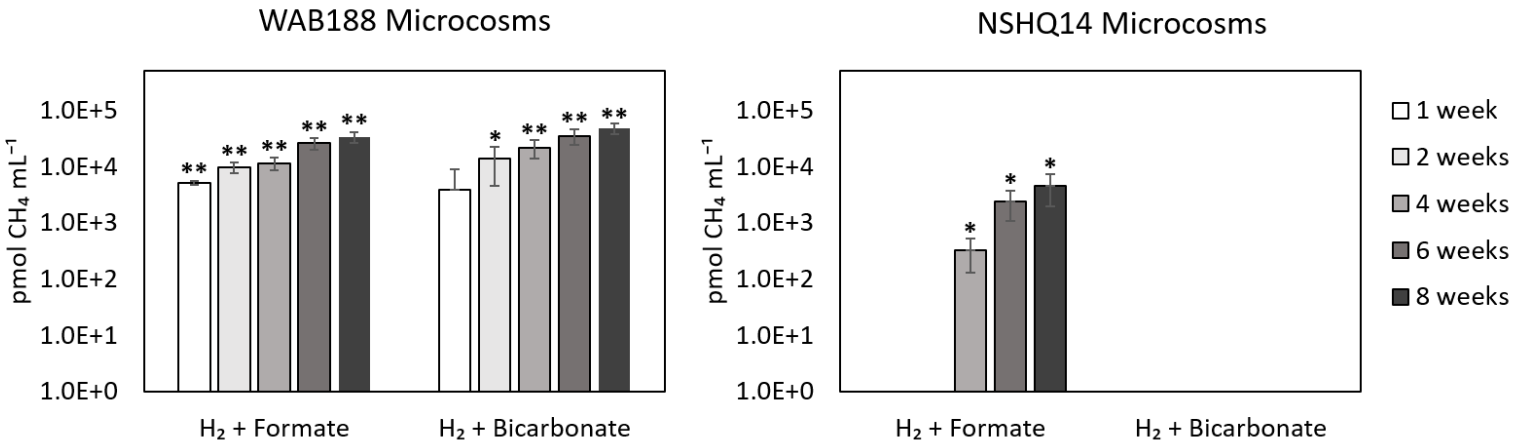

Figure 4. Potential rates of biological methanogenesis from formate and bicarbonate by planktonic microbial communities in well water samples collected from the Samail Ophiolite in 2020.

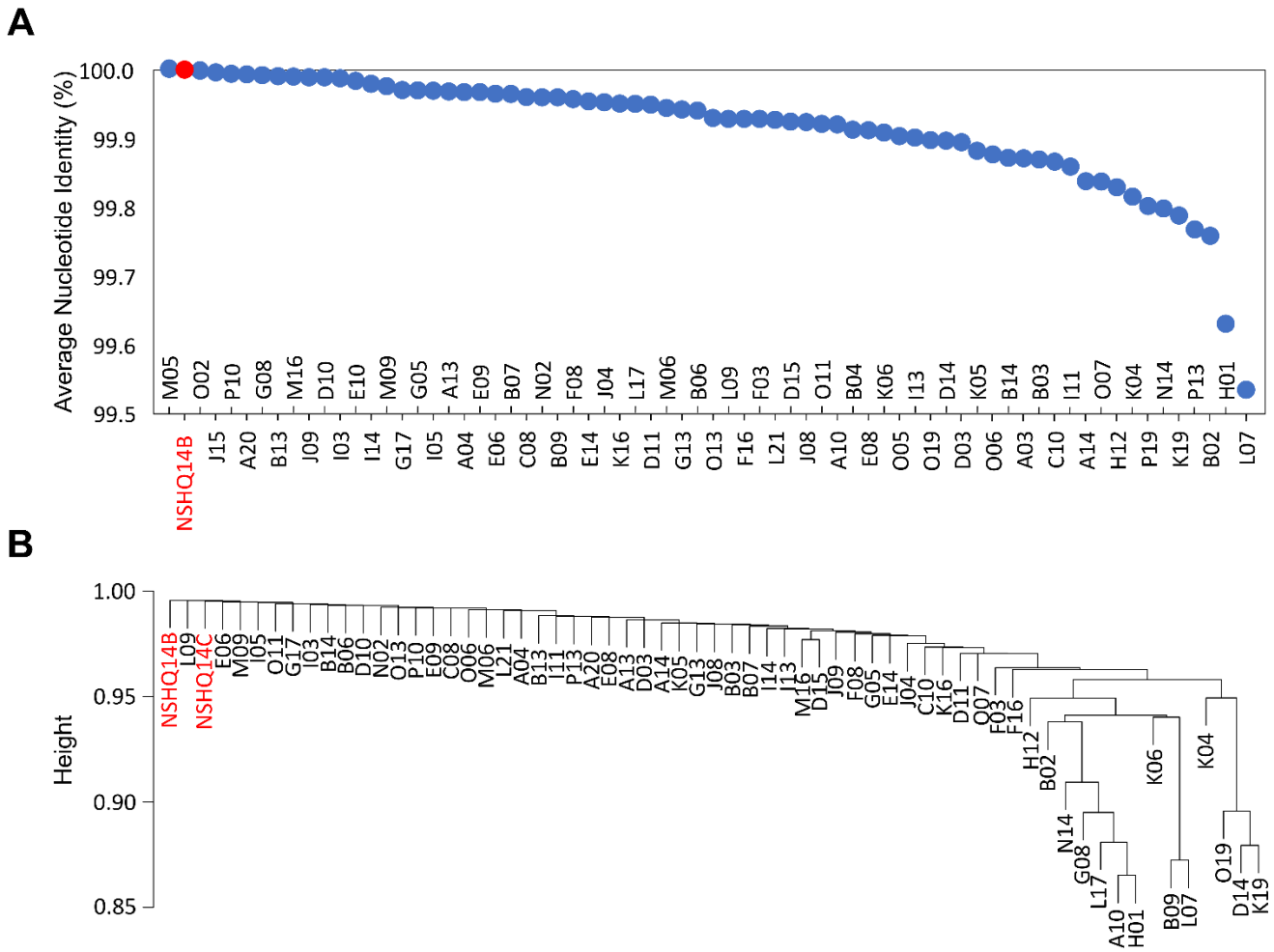

Figure 5. Average nucleotide identities (ANIs) between *Methanobacterium* single amplified genomes (SAGs) and Type II metagenome assembled genomes (MAGs).

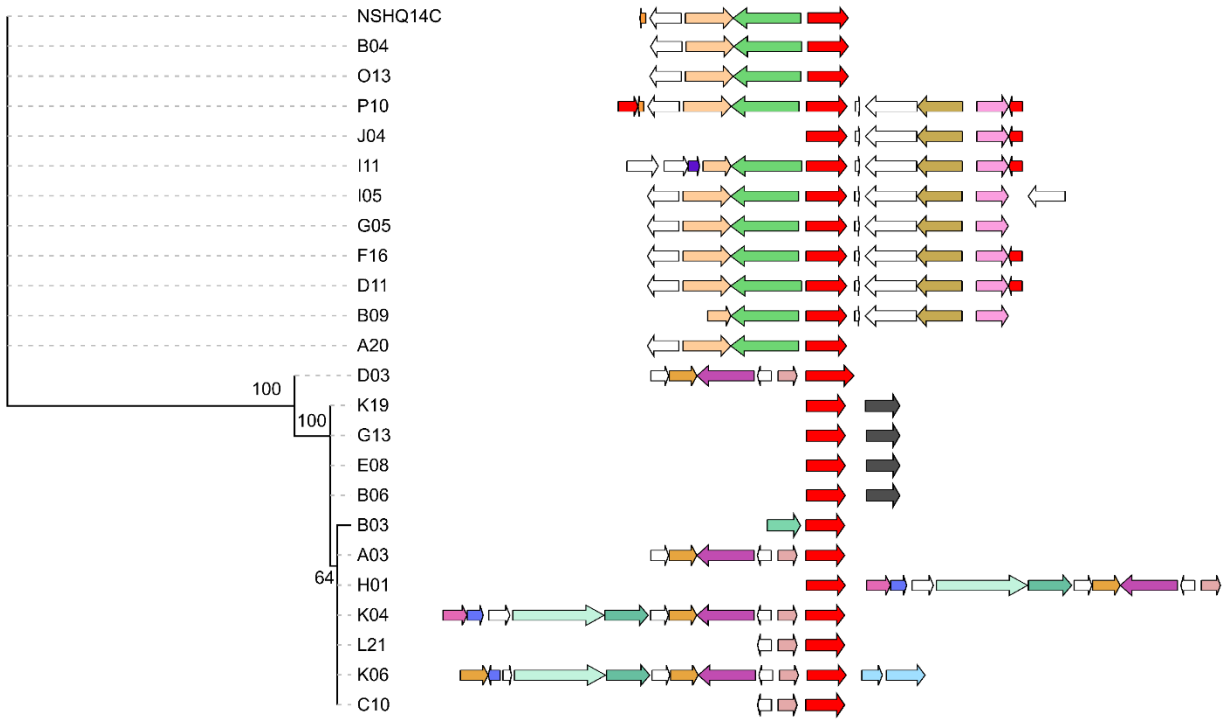

Figure 6. ISNCY transposase protein phylogeny and genes co-localized with this transposase in the NSHQ14C metagenome assembled genome (MAG) and single cell genomes (SAGs).

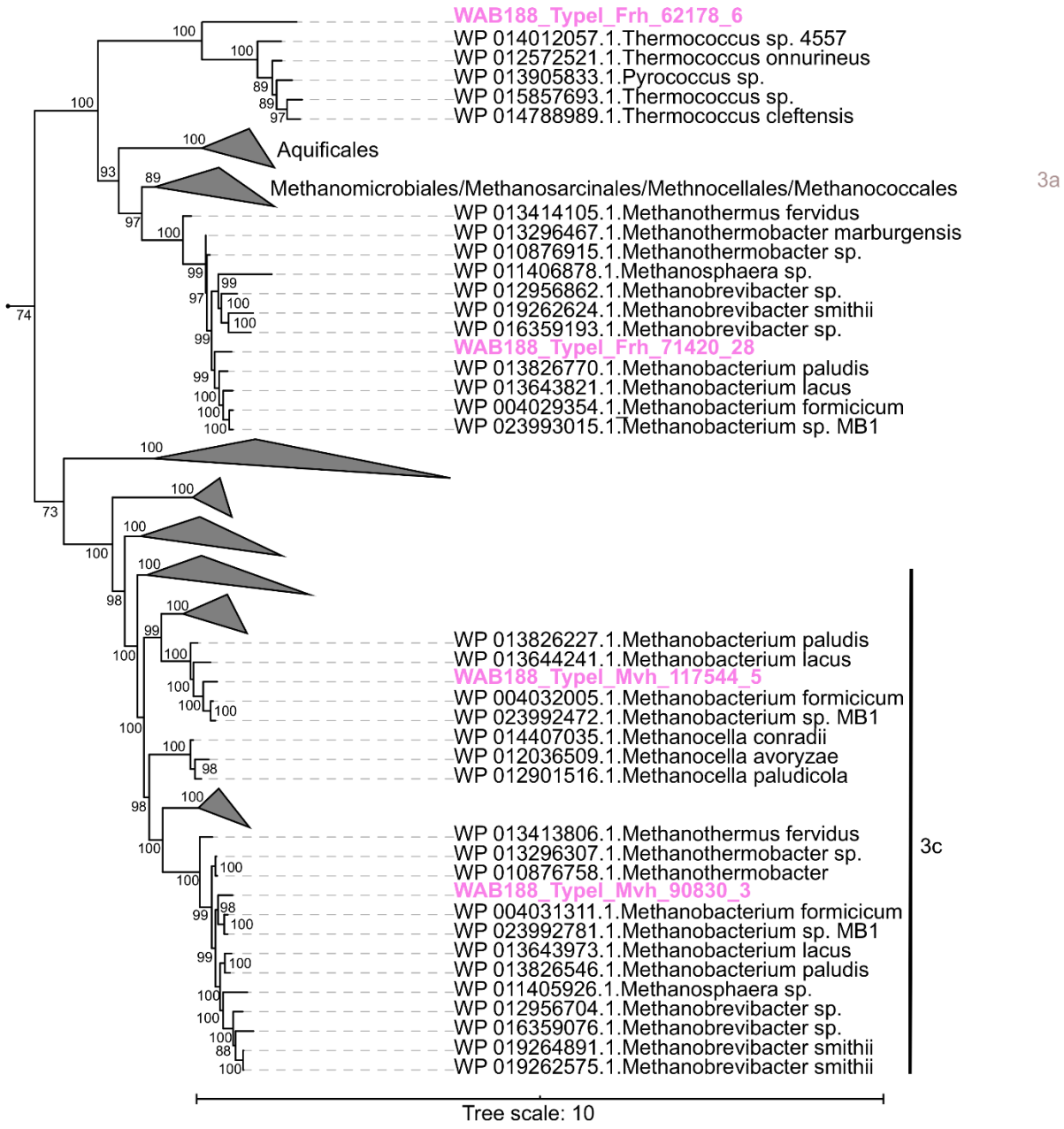

Supplementary Figure 1. Maximum Likelihood phylogenetic reconstruction of the large subunit of F_{420} (Group 3a) and methyl viologen reducing (Group 3c) [NiFe]-hydrogenases encoded in the WAB188 (Type I) MAG. Bootstraps percentages are shown for each node (out of 1,000 replicates). Clade-level triangles indicate the phylogenetic diversity within each group via side lengths that are proportional to the distances between the clade's most closely related and furthest related homologs. Branch length is relative to the scale provided for each tree. Group 3 hydrogenases were not observed in Type II genomes. Group designations follow the previous designations of Greening et al., 2016 (82).

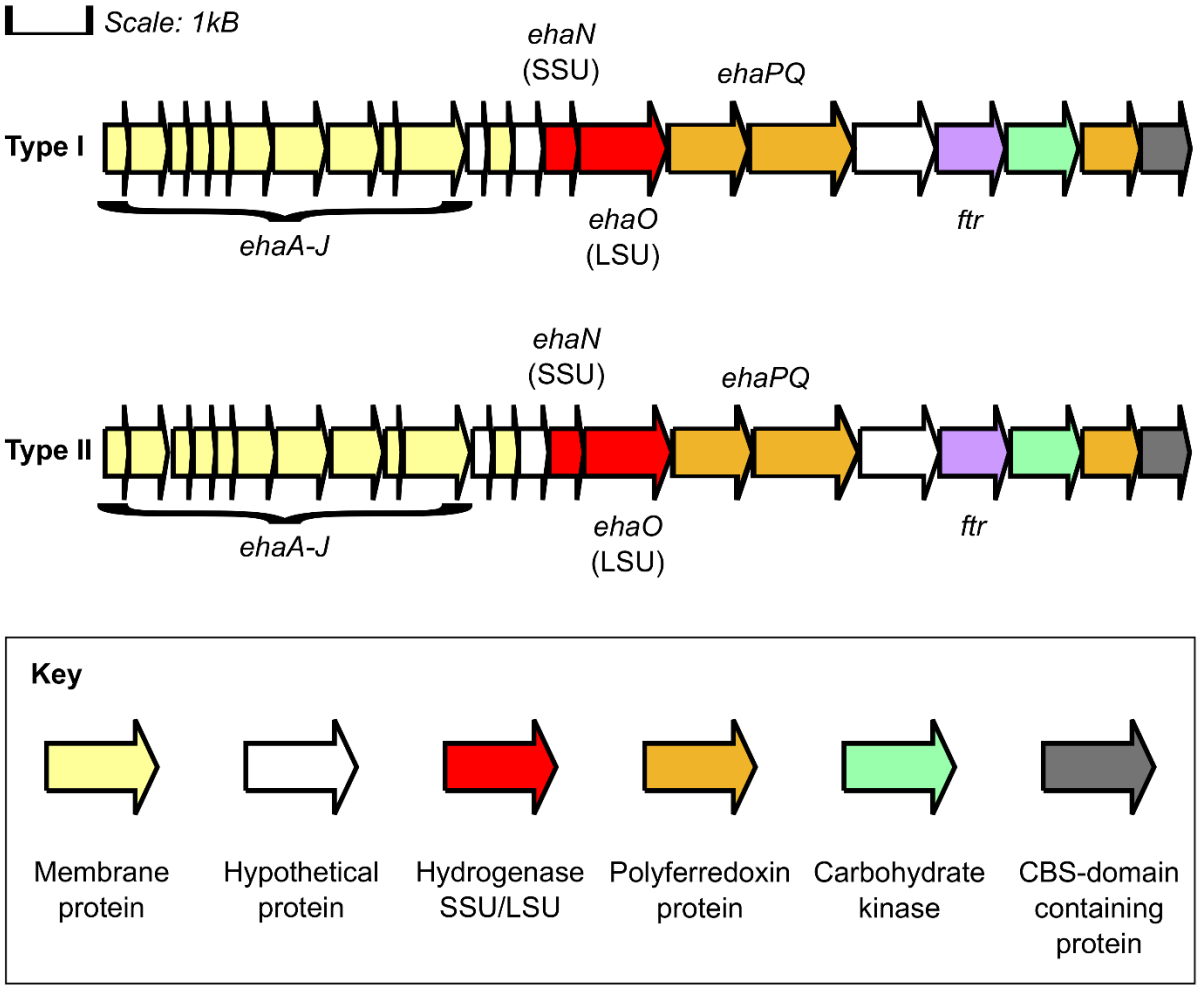

Supplementary Figure 3. Genes flanking the energy conserving Group 4 [NiFe]-hydrogenase, Eha, encoded in WAB188 (Type I) and NSHQ14B/C (Type II) metagenome assembled genomes (MAGs). Gene lengths are relative to the scale provided at the top of the figure. Gene designations are based upon CDD and BLASTp matches in addition to consensus with Tersteegen et al., 1999 (99). Gene colors correspond to functional groupings displayed in the key at the bottom of the figure.

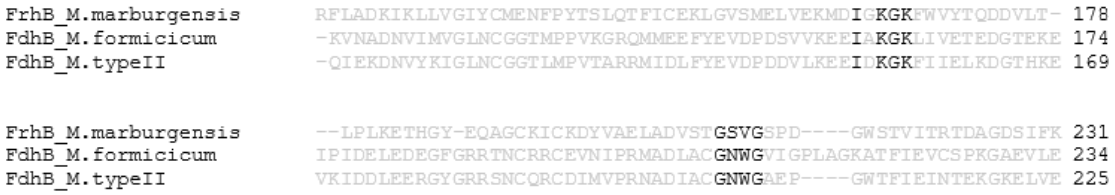

Supplementary Figure 4. Multiple sequence alignment of the Group 3 F_{420}-reducing [NiFe]-hydrogenase beta subunit (FrhB) encoded by *Methanothermobacter marburgensis*, the formate dehydrogenase beta subunit (FdhB) encoded by *Methanobacterium formicicum*, and FdhB encoded in the *Methanobacterium* NSHQ14C Type II metagenome assembled genomes (MAGs). Black text represents amino acid residues involved in F_{420} coordination in FrhB (108) and corresponding residues in FdhB proteins.

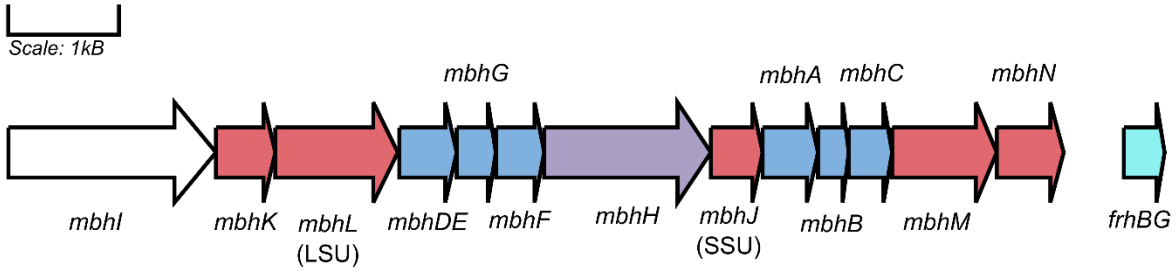

Supplementary Figure 5. Genes flanking the multiple resistance and pH adaptation - membrane bound hydrogenase protein complex (Mrp-Mbh) energy converting (Group 4) [NiFe]-hydrogenases encoded in Type II metagenome assembled genomes (MAGs). The color scheme is based on functional designations outlined by Schut et al., 2012 (109). Red arrows represent genes encoding subunits of the [NiFe]-hydrogenase (Mbh) involved in reversible hydrogen oxidation, blue arrows represent genes putatively involved in ion transport (Mrp), the purple arrow represents *mbhH*, which is putatively a component of both Mbh and Mrp, the white arrow represents *mbhI* which is unique to the Mrp-Mbh complex enzyme class (i.e. not encoded in Mrp or Mbh alone), and the cyan arrow represents the fused homolog of Group 3 F_{420}-reducing [NiFe]-hydrogenase FrhB and FrhG subunits. Gene lengths are relative to the scale provided at the top of the figure.

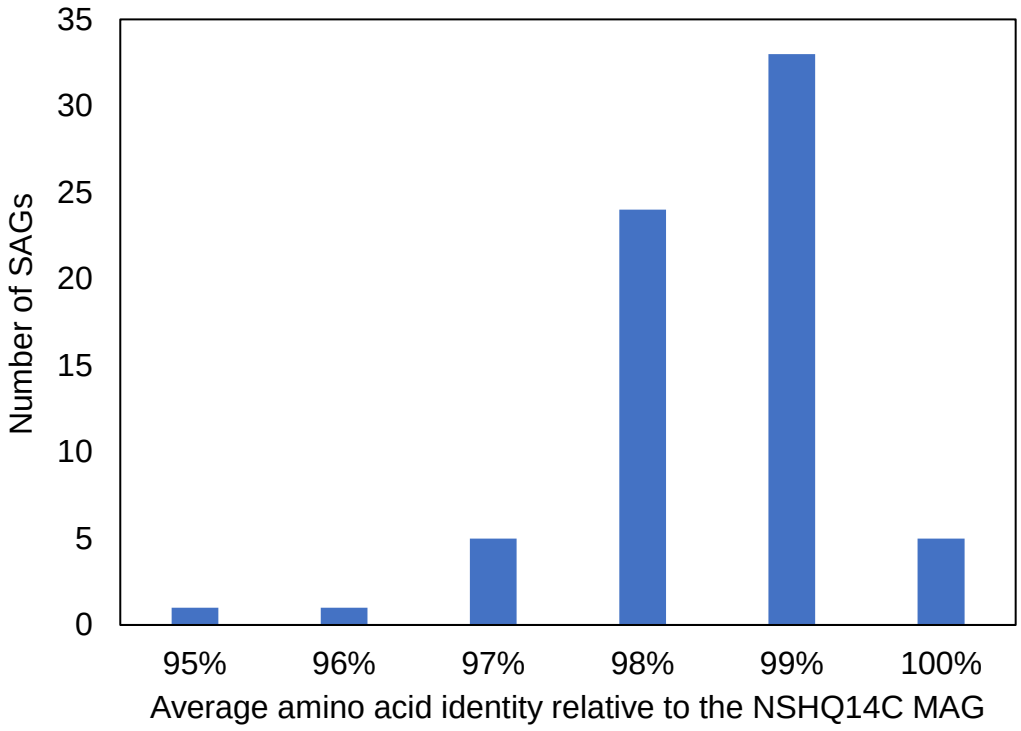

Supplementary Figure 6. Average amino acid identity (AAI) between single amplified genomes (SAGs) and the NSHQ14C (Type II) metagenome assembled genome (MAG). Amino acid identities of protein homologs shared by SAGs and the NSHQ14C Type II MAG were averaged to arrive at an average AAI for each SAG relative to the NSHQ14C Type II MAG.

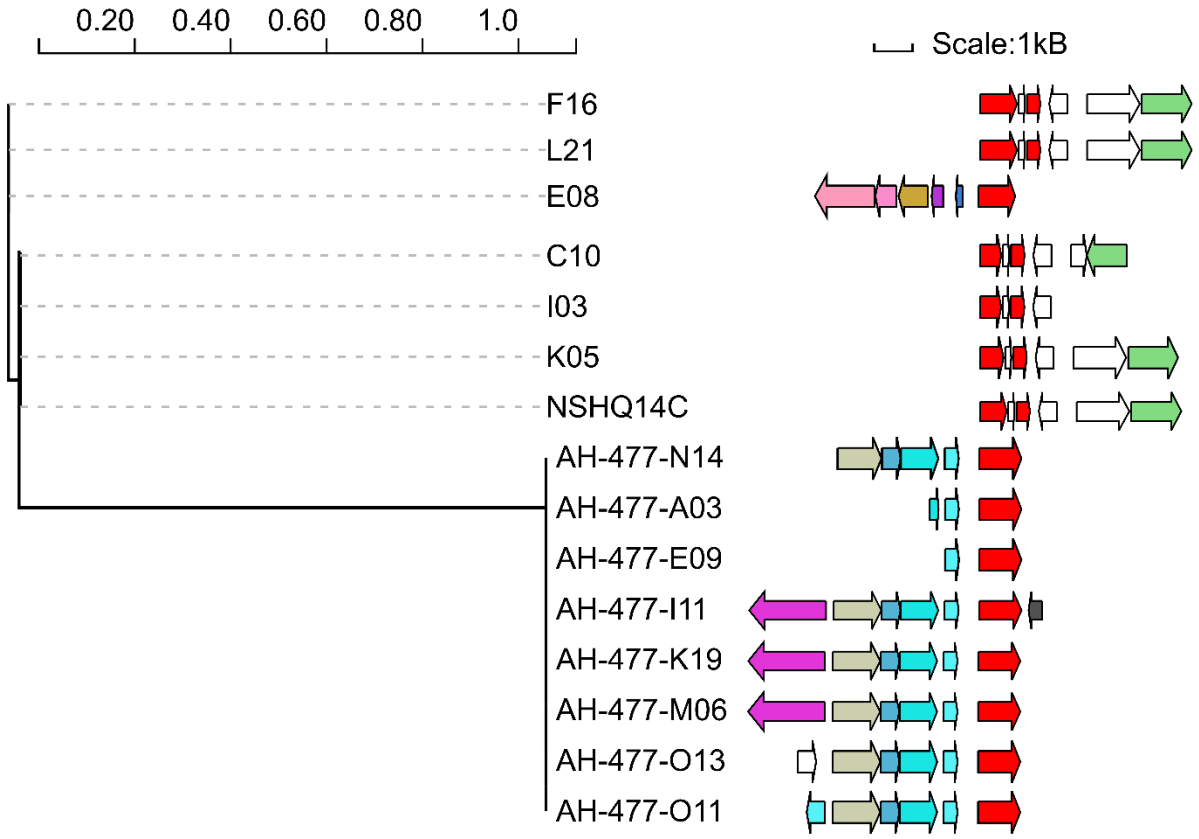

Supplementary Figure 7. Phylogenetic reconstruction of C39 peptidase protein orthologs and their genome arrangements in single amplified genomes (SAGs) and the NSHQ14C Type II metagenome assembled genome (MAG). Branch length is relative to the scale provided at the top of the figure indicating average substitutions per site. The proximal 5 ORFs upstream and downstream of the C39 peptidase are depicted to the right of the terminals. Red arrows represent genes encoding C39 peptidase orthologs, white arrows represent genes encoding hypothetical proteins, black arrows represent genes encoding transposase proteins, and the remaining colored arrows represent genes encoding other functional proteins. Gene lengths are relative to the scale provided at the top of the figure.

References

1. Boyd, E.S., Amenabar, M.J., Poudel, S., and Templeton, A.S. Bioenergetic constraints on the origin of autotrophic metabolism. Philos. T. R. Soc. A 2020; 378: 1471-2962.

2. Boyd, E.S., Schut, G.J., Adams, M.W.W., and Peters, J.W. Hydrogen metabolism and the evolution of biological respiration. Microbe 2014; 9: 361-367.

3. Hoehler, T.M. Biogeochemistry of dihydrogen (H_2). In: Sigel, H., and Sigel, R. (eds). Metal Ions in Biological Systems. Vol 43. (Taylor & Francis Group, Boca Raton, FL, 2005) pp 9-48.

4. Weiss, M.C., Sousa, F.L., Mrnjavac, N., Neukirchen, S., Roettger, M., Nelson-Sathi, S. *et al.* The physiology and habitat of the last universal common ancestor. Nat. Microbiol. 2016; 1: 1-8.

5. McCollom, T.M., Klein, F., Robbins, M., Moskowitz, B., Berquó, T.S., Jöns, N. *et al.* Temperature trends for reaction rates, hydrogen generation, and partitioning of iron during experimental serpentinization of olivine. Geochim. Cosmochim. Acta 2016; 181: 175-200.

6. Schulte, M., Blake, D., Hoehler, T, and McCollom, T. Serpentinization and its implications for life on the early Earth and Mars. Astrobiology 2006; 6: 364-376.

7. Russell, M., Hall, A., and Martin, W. Serpentinization as a source of energy at the origin of life. Geobiology 2010; 8: 355-371.

8. Seewald, J.S., Zolotov, M.Y., and McCollom, T. Experimental investigation of single carbon compounds under hydrothermal conditions. Geochim. Cosmochim. Acta 2006; 70: 446-460.

9. McCollom, T.M. and Seewald, J.S. Abiotic synthesis of organic compounds in deep-sea hydrothermal environments. Chem. Rev. 2007; 107: 382-401.

10. Twing, K.I., Brazelton, W.J., Kubo, M.D.Y., Hyer, A.J., Cardace, D., Hoehler, T.M. *et al.* Serpentinization-influenced groundwater harbors extremely low diversity microbial communities adapted to high pH. Front. Microbiol. 2017; 8: 308.

11. Brazelton, W.J., Nelson, B., and Schrenk, M.O. Metagenomic evidence for H_2 oxidation and H_2 production by serpentinite-hosted subsurface microbial communities. Front. Microbiol. 2012; 2: 268.

12. Morrill, P.L., Brazelton, W.J., Kohl, L., Rietze, A., Miles, S.M., Kavanagh, H. *et al.* Investigations of potential microbial methanogenic and carbon monoxide utilization pathways in ultra-basic reducing springs associated with present-day continental serpentinization: the Tablelands, NL, CAN. Front. Microbiol. 2014; 5: 613.

13. Crespo-Medina, M., Twing, K.I., Sánchez-Murillo, R., Brazelton, W.J., McCollom, T.M., and Schrenk, M.O. Methane dynamics in a tropical serpentinizing environment: The Santa Elena Ophiolite, Costa Rica. Front. Microbiol. 2017; 8: 916.

14. Woycheese, K.M., Meyer-Dombard, D.R., Cardace, D., Argayosa, A.M., and Arcilla, C.A. Out of the dark: transitional subsurface-to-surface microbial diversity in a terrestrial serpentinizing seep (Manleluag, Pangasinan, the Philippines). Front. Microbiol. 2015; 6: 44.

15. Neubeck, A., Sun, L., Müller, B., Ivarsson, M., Hosgörmez, H., Özcan, D. *et al.* Microbial community structure in a serpentine-hosted abiotic gas seepage at the Chimaera Ophiolite, Turkey. Appl. Environ. Microbiol. 2017; 83: p. e03430-16.

16. Lang, S.Q., Früh-Green, G., Bernasconi, S.M., Brazelton, W.J., Schrenk, M.O., and McGonigle, J.M. Deeply-sourced formate fuels sulfate reducers but not methanogens at Lost City hydrothermal field. Sci. Rep. 2018; 8: 1-10.

17. Brazelton, W.J., Morrill, P. L., Szponar, N., and Schrenk, M.O. Bacterial communities associated with subsurface geochemical processes in continental serpentinite springs. Appl. Environ. Microbiol. 2013; 79: 3906-3916.

18. Fones, E.M., Colman, D.R., Kraus, E.A., Nothaft, D.B., Poudel, S., Rempfert, K.R., *et al.* Physiological adaptations to serpentinization in the Samail Ophiolite, Oman. ISME J. 2019; 13: 1750-1762.

19. Rempfert, K.R., Miller, H.M., Bompard, N., Nothaft, D., Matter, J.M., Kelemen, P., *et al.* Geological and geochemical controls on subsurface microbial life in the Samail Ophiolite, Oman. Front. Microbiol. 2017; 8: 56.

20. Kelemen, P.B., Matter, J., Streit, E.E., Rudge, J.F., Curry, W.B., and Blusztajn, J. Rates and mechanisms of mineral carbonation in peridotite: natural processes and recipes for enhanced, in situ CO_2 capture and storage. Annu. Rev. Earth Planet. Sci. 2011; 39: 545-576.

21. Canovas, P.A., Hoehler, T. and Shock, E.L. Geochemical bioenergetics during low-temperature serpentinization: An example from the Samail ophiolite, Sultanate of Oman. J. Geophys. Res.-Biogeo. 2017; 122: 1821-1847.

22. Suzuki, S., Ishii, S., Wu, A., Cheung, A., Tenney, A., Wanger, G. *et al.* Microbial diversity in The Cedars, an ultrabasic, ultrareducing, and low salinity serpentinizing ecosystem. Proc. Natl. Acad. Sci. U.S.A. 2013; 110: 15336-15341.

23. Brazelton, W.J., Thornton, C.N., Hyer, A., Twing, K.I., Longino, A.A., Lang, S.Q. *et al.* Metagenomic identification of active methanogens and methanotrophs in serpentinite springs of the Voltri Massif, Italy. PeerJ. 2017; 5: e2945.

24. Morrill, P.L., Kuenen, J.G., Johnson, O.J., Suzuki, S., Rietze, A., Sessions, A.L., *et al.* Geochemistry and geobiology of a present-day serpentinization site in California: The Cedars. Geochim. Cosmochim. Acta 2013; 109: p. 222-240.

25. Miller, H.M., Matter, J.M., Kelemen, P., Ellison, E.T., Conrad, M.E., Fierer, N. *et al.* Modern water/rock reactions in Oman hyperalkaline peridotite aquifers and implications for microbial habitability. Geochim. Cosmochim. Acta 2016; 179: 217-241.

26. Russell, M.J. and Martin, W. The rocky roots of the acetyl-CoA pathway. Trends Biochem. Sci. 2004; 29: 358-363.

27. Martin, W.F., Weiss, M.C., Neukirchen, S., Nelson-Sathi, S., and Sousa, F.L. Physiology, phylogeny, and LUCA. Microbial Cell 2016; 3: 582-587.

28. Ueno, Y., Yamada, K., Yoshida, N., Maruyama, S., and Isozake, Y. Evidence from fluid inclusions for microbial methanogenesis in the early Archaean era. Nature 2006; 440: 516-519.

29. Moore, E.K., Jelen, B.I., Giovannelli, D., Raanan, H., and Falkowski, P.G. Metal availability and the expanding network of microbial metabolisms in the Archaean eon. Nat. Geosci. 2017; 10: 629-636.

30. Etiope, G., Vadillo, I., Whiticar, M.J, Marques, J.M., Carreira, P.M, Tiago, I. *et al.* Abiotic methane seepage in the Ronda peridotite massif, southern Spain. Geochem. 2016; 66: 101-113.

31. Proskurowski, G., Lilley, M.D., Seewald, J.S., Früh-Green, G., Olson, E.J., Lupton, J.E., *et al.* Abiogenic hydrocarbon production at Lost City hydrothermal field. Science 2008; 319: 604-607.

32. Etiope, G. Methane origin in the Samail ophiolite: Comment on "Modern water/rock reactions in Oman hyperalkaline peridotite aquifers and implications for microbial habitability." Geochim. Cosmochim. Acta 2017; 197: 467-470.

33. Miller, H.M., Matter, J.M., Kelemen, P., Ellison, E.T., Conrad, M.E., Fierer, N. *et al.* Reply to "Methane origin in the Samail ophiolite: Comment on 'Modern water/rock reactions in Oman hyperalkaline peridotite aquifers and implications for microbial habitability.'" Geochim. Cosmochim. Acta 2017; 197: 471-473.

34. Miller, H.M., Chaudhry, N., Conrad, M.E., Markus, B., Kopf, S.H., and Templeton, A.S. Large carbon isotope variability during methanogenesis under alkaline conditions. Geochim. Cosmochim. Acta 2018; 237: 18-31.

35. Bradley, A.S., Hayes, J.M., and Summons, R.E. Extraordinary ^{13}C enrichment of diether lipids at the Lost City Hydrothermal Field indicates a carbon-limited ecosystem. Geochim. Cosmochim. Acta 2009; 73: 102-118.

36. Zwicker, J., Birgel, D., Bach, W., Richoz, S., Smrzka, D., Grasemann, B. *et al.* Evidence for archaeal methanogenesis within veins at the onshore serpentinite-hosted Chimaera seeps, Turkey. Chem. Geol. 2018; 483: 567-580.

37. Kraus, E.A., Stamps, B.W., Rempfert, K.R., Nothaft D.B., Boyd, E.S., Matter, J.M. *et al.* Biological methane cycling in serpentinization-impacted fluids of the Samail ophiolite of Oman. AGU Fall Meeting Abstracts. 2018; (abstract #V13E-0139).

38. Miller, H.M., Mayhew, L.E., Ellison, E.T., Kelemen, P., Kubo, M., and Templeton, A.S. Low temperature hydrogen production during experimental hydration of partially-serpentinized dunite. Geochim. Cosmochim. Acta 2017; 209: 161-183.

39. Neal, C. and Stanger, G. Hydrogen generation from mantle source rocks in Oman. Earth Planet. Sci. Lett. 1983; 66: 315-320.

40. Streit, E., Kelemen P., and Eiler J. Coexisting serpentine and quartz from carbonate-bearing serpentinized peridotite in the Samail Ophiolite, Oman. Contrib. Mineral. Petr. 2012; 164: 821-837.

41. Chavagnac, V., Monnin, C., Ceuleneer, G., Boulart, C., and Hoareau, G. Characterization of hyperalkaline fluids produced by lowtemperature serpentinization of mantle peridotites in the Oman and Ligurian ophiolites. Geochem. Geophys. 2013; 14: 2496-2522.

42. Mervine, E.M., Humphris, S.E., Sims, K.W.W., Kelemen, P.B., and Jenkins, W.J. Carbonation rates of peridotite in the Samail Ophiolite, Sultanate of Oman, constrained through ^{14}C dating and stable isotopes. Geochim. Cosmochim. Acta 2014; 126: 371-397.

43. Kang, D.W.D., Froula, J., Egan, R., and Wang, Z. MetaBAT, an efficient tool for accurately reconstructing single genomes from complex microbial communities. PeerJ 2015; 3: e1165.

44. Stepanauskas, R., Fergusson, E.A., Brown, J., Poulton, N.J., Tupper, B., Labonté, J.M. *et al.* Improved genome recovery and integrated cell-size analyses of individual uncultured microbial cells and viral particles. Nat. Commun. 2017; 8: 84.

45. Colman, D.R., Lindsay, M.R., and Boyd, E.S. Mixing of meteoric and geothermal fluids supports hyperdiverse chemosynthetic hydrothermal communities. Nat. Commun. 2019; 10, 1-13.

46. Wu, M. and Scott, A.J., Phylogenomic analysis of bacterial and archaeal sequences with AMPHORA2. J. Bioinform. 2012; 28: 1033-1034.

47. Sievers, F., Wilm, A., Dineen, D., Gibson, T.J., Karplus, K., Li, W. *et al.* Fast, scalable generation of high quality protein multiple sequence alignments using Clustal Omega. Mol. Syst. Biol. 2011; 7: 539.

48. Nguyen, L.T., Schmidt, H.A., von Haesler, A., and Minh, B.Q. IQ-TREE: a fast and effective stochastic algorithm for estimating maximum-likelihood phylogenies. Mol. Biol. Evol. 2015; 32: 268-274.

49. Kalyaanamoorthy, S., Minh, B.Q., Wong, T.K.F., von Haesler, A., and Jermiin, L.S. ModelFinder: fast model selection for accurate phylogenetic estimates. Nat. Methods 2017; 14: 587.

50. Hyatt, D., Chen, G.L., LoCascio, P.F., Land, M.L., Larimer, F.W., and Hauser, L.J. Prodigal: prokaryotic gene recognition and translation initiation site identification. BMC Bioinformatics 2010; 11: 119.

51. Seemann, T. Prokka: rapid prokaryotic genome annotation. J. Bioinform. 2014; 30: 2068-9.

52. Kanehisa, M. and Goto, S. KEGG: Kyoto Encyclopedia of Genes and Genomes. Nucleic Acids Res. 2000; 28: 27-30.

53. Moriya, Y., Itoh, M., Okuda, S., Yoshizawa, A.C., and Kanehisa, M. KAAS: an automatic genome annotation and pathway reconstruction server. Nucleic Acids Res. 2007; 35: W182-W185.

54. Altschul, S.F., Gish, W., Miller, W., Myers, E.W., and Lipman, D.J. Basic local alignment search tool. J. Mol. Biol. 1990; 215: 403-410.

55. Parks, D.H., Imelfort, M., Skennerton, C.T., Hugenholtz, P., and Tyson, G.W. CheckM: assessing the quality of microbial genomes recovered from isolates, single cells, and metagenomes. Genome Res. 2015; 25: 1043-1055.

56. Greening, C., Biswas, A., Carere, C.R., Jackson, C.J., Taylor, M.C., Stott, M.B. *et al.* Genomic and metagenomic surveys of hydrogenase distribution indicate H_2 is a widely utilised energy source for microbial growth and survival. ISME J. 2016; 10: 761-777.

57. Peters, J.W., Schut, G.J., Boyd, E.S., Mulder, D.W., Shepard, E.M., Broderick, J.B. *et al.* [FeFe]-and [NiFe]-hydrogenase diversity, mechanism, and maturation. BBA-Mol. Cell Res. 2015; 1853: 1350-1369.

58. Marchler-Bauer, A., Bo, Y., Han, L., He, J., Lanczycki, C.J., Lu, S. *et al.* CDD/SPARCLE: functional classification of proteins via subfamily domain architectures. Nucleic Acids Res. 2016; 45: D200-D203.

59. Marçais, G., Delcher, A.L., Phillippy, A.M., Coston, R., Salzberg, S.L., and Zimin, A. MUMmer4: a fast and versatile genome alignment system. PLoS Comput. Biol. 2018; 14: e1005944.

60. R Core Team, R: a language and environment for statistical computing. Version 3.0.1. R Foundation for Statistical Computing. 2013.

61. Leplae, R., Lima-Mendez, G., and Toussaint, A. ACLAME: a CLAssification of Mobile genetic Elements, update 2010. Nucleic Acids Res. 2010; 38: D57-D61.

62. Lefort, V., Longueville, J.-E., and Gascuel, O. SMS: smart model selection in PhyML. Mol. Biol. Evol. 2017; 34: 2422-2424.

63. Guindon, S., Dufayard, J.-F., Lefort, V., Anisimova, M., Hordijk, W., and Gascuel, O. New algorithms and methods to estimate maximum-likelihood phylogenies: assessing the performance of PhyML 3.0. Syst. Biol. 2010; 59: 307-321.

64. Darling, A.E., Mau, B., and Perna, N.T. progressiveMauve: multiple genome alignment with gene gain, loss and rearrangement. PloS One 2010; 5: e11147.

65. Harrison, K.J., Crécy-Lagard, V., and Zallot, R. Gene Graphics: a genomic neighborhood data visualization web application. J. Bioinform. 2018; 34: 1406-1408.

66. Oksanen, J., Blanchet, F.G., Kindt, R., Legendre, P., Minchin, P.R., and O'Hara, R.B. vegan: community ecology package. R Foundation for Statistical Computing. 2015.

67. Bowers, R.M., Kyrpides, N.C, Stepanauskas, R., Harmon-Smith, M., Doud, D., Reddy, T.B.K. *et al.* Minimum information about a single amplified genome (MISAG) and a metagenome-assembled genome (MIMAG) of bacteria and archaea. Nat. Biotechnol. 2017; 25: 725-731.

68. Suzuki, S., Ishii, S., Hoshino, T., Rietze, A., Tenney, A., Morrill, P.L. *et al.* Unusual metabolic diversity of hyperalkaliphilic microbial communities associated with subterranean serpentinization at The Cedars. ISME J. 2017; 11: 2584-2598.

69. Giovannoni, S.J., Thrash, J.C., and Temperton, B. Implications of streamlining theory for microbial ecology. ISME J. 2014; 8: 1553-1565.

70. Thauer, R.K., Kaster, A.K., Seedorf, H., Buckel, W., and Hedderich, R. Methanogenic archaea: ecologically relevant differences in energy conservation. Nat. Rev. Microbiol. 2008; 6: 579-591.

71. Hendrickson, E.L. and Leigh, J.A. Roles of coenzyme F_{420}-reducing hydrogenases and hydrogen-and F_{420}-dependent methylenetetrahydromethanopterin dehydrogenases in reduction of F_{420} and production of hydrogen during methanogenesis. J. Bacteriol. 2008; 190: 4818-4821.

72. Goldman, A.D., Leigh, J.A., and Samudrala, R. Comprehensive computational analysis of Hmd enzymes and paralogs in methanogenic Archaea. BMC Evol. Biol. 2009; 9: 199.

73. Tersteegen, A. and Hedderich, R. Methanobacterium thermoautotrophicum encodes two multisubunit membrane-bound [NiFe] hydrogenases: Transcription of the operons and sequence analysis of the deduced proteins. Eur. J. Biochem. 1999; 264: 930-943.

74. Lie, T.J., Costa, K.C., Lupa, B., Korpole, S., Whitman, W.B., and Leigh, J.A. Essential anaplerotic role for the energy-converting hydrogenase Eha in hydrogenotrophic methanogenesis. Proc. Natl. Acad. Sci. U.S.A. 2012; 109: 15473-15478.

75. Thauer, R.K. The Wolfe cycle comes full circle. Proc. Natl. Acad. Sci. U.S.A. 2012; 109: 15084-15085.

76. Costa, K.C., Wong, P.M., Wang, T., Lie, T.J., Dodsworth, J.A., Swanson, I. *et al*. Protein complexing in a methanogen suggests electron bifurcation and electron delivery from formate to heterodisulfide reductase. Proc. Natl. Acad. Sci. U.S.A. 2010; 107: 11050-11055.

77. Greening, C., Ahmed, F.A., Mohamed, A.E., Lee, B.M., Pandey, G., Warden, A.C. *et al.* Physiology, biochemistry, and applications of F_{420}-and Fo-dependent redox reactions. Microbiol. Mol. Biol. Rev. 2016; 80: 451-493.

78. Yan, Z. and Ferry, J.G. Electron bifurcation and confurcation in methanogenesis and reverse methanogenesis. Front. Microbiol. 2018; 9: 1322.

79. Costa, K.C., Lie, T.J., Xia, Q., and Leigh, J.A. VhuD facilitates electron flow from H_2 or formate to heterodisulfide reductase in Methanococcus maripaludis. J. Bacteriol. 2013; 195: 5160-5165.

80. Schauer, N.L. and Ferry, J.G. Properties of formate dehydrogenase in Methanobacterium formicicum. J. Bacteriol. 1982; 150: 1-7.

81. Schauer, N.L., Ferry, J.G., Honek, J.F., Orme-Johnson, W.H., and Walsh, C. Mechanistic studies of the coenzyme F420-reducing formate dehydrogenase from Methanobacterium formicicum. Biochemistry 1986; 25: 7163-7168.

82. Mills, D.J., Vitt, S., Strauss, M., Shima, S., and Vonck, J. De novo modeling of the F_{420}-reducing [NiFe]-hydrogenase from a methanogenic archaeon by cryo-electron microscopy. Elife 2013; 2: e00218.

83. Schut, G.J., Boyd, E.S., Peters, J.W., and Adams, M.W.W. The modular respiratory complexes involved in hydrogen and sulfur metabolism by heterotrophic hyperthermophilic archaea and their evolutionary implications. FEMS Microbiol. Rev. 2013; 37: 182-203.

84. Hamamoto, T., Hashimoto, M., Hino, M., Kitada, M., Seto, Y., Kudo, T. *et al.* Characterization of a gene responsible for the Na^+/H^+ antiporter system of alkalophilic Bacillus species strain C125. Mol. Microbiol. 1994; 14: 939-946.

85. Buckel, W. and Thauer, R.K. Energy conservation via electron bifurcating ferredoxin reduction and proton/Na^+ translocating ferredoxin oxidation. BBA-Bioenergetics 2013; 1827: 94-113.

86. Boone, D.R., Johnson, R.L., and Liu, Y. Diffusion of the interspecies electron carriers H_2 and formate in methanogenic ecosystems and its implications in the measurement of K_m for H_2 or formate uptake. Appl. Environ. Microbiol. 1989; 55: 1735-1741.

87. McCollom, T.M. and Seewald J.S. Experimental constraints on the hydrothermal reactivity of organic acids and acid anions: I. Formic acid and formate. Geochim. Cosmochim. Acta 2003; 67: 3625-3644.

88. Lang, S.Q., Butterfield, D.A., Schulte, M., Kelley, D.S., and Lilley, M.D. Elevated concentrations of formate, acetate and dissolved organic carbon found at the Lost City hydrothermal field. Geochim. Cosmochim. Acta 2010; 74: 941-952.

89. Zeng, Y. and Liu, J. Short-chain carboxylates in fluid inclusions in minerals. Appl. Geochemistry 2000; 15: 13-25.

90. Suzuki, S., Nealson, K.H., and Ishii, S. Genomic and in-situ transcriptomic characterization of the candidate phylum NPL-UPL2 from highly alkaline highly reducing serpentinized groundwater. Front. Microbiol. 2018; 9: 3141.

91. Brazelton, W.J. and Baross, J.A. Abundant transposases encoded by the metagenome of a hydrothermal chimney biofilm. ISME J. 2009; 3: 1420-1424.

92. Zhang, J., Kasciukovic, T., and White, M.F. The CRISPR associated protein Cas4 Is a 5′ to 3′ DNA exonuclease with an iron-sulfur cluster. PloS One 2012; 7: e47232.

93. Rath, D., Amlinger, L., Rath, A., and Lundgren, M. The CRISPR-Cas immune system: biology, mechanisms and applications. Biochimie 2015; 117: 119-128.

94. Jansen, R., van Embden, J.D.A., Gaastra, W., and Schouls, L.M. Identification of genes that are associated with DNA repeats in prokaryotes. Mol. Microbiol. 2002; 43: 1565-1575.

95. Reno, M.L., Held, N.L., Fields, C.J., Burke, P.V., and Whitaker, R.J. Biogeography of the *Sulfolobus islandicus* pan-genome. Proc. Natl. Acad. Sci. U.S.A. 2009; 106: 8605-8610.

96. Tettelin, H., Masignani, V., Cieslewicz, M.J., Donati, C., Medini, D., Ward, N.L. *et al.* Genome analysis of multiple pathogenic isolates of *Streptococcus agalactiae:* implications for the microbial "pan-genome." Proc. Natl. Acad. Sci. U.S.A. 2005; 102: 13950-13955.

97. Labonté, J.M., Field, E.K., Lau, M., Chivian, D., Van Heerden, E., Wommack, K.E. *et al.* Single cell genomics indicates horizontal gene transfer and viral infections in a deep subsurface Firmicutes population. Front. Microbiol. 2015; 6: 349.

98. Karnachuk, O.V., Frank, Y.A., Lukina, A.P., Kadnikov, V.V., Beletsky, A.V., Mardanov, A.V. *et al.* Domestication of previously uncultivated *Candidatus* Desulforudis audaxviator from a deep aquifer in Siberia sheds light on its physiology and evolution. ISME J. 2019; 13: 1947-1959.

99. Paul, B.G., Burstein, D., Castelle, C.J., Handa, S., Arambula, D., Czornyj, E. *et al.* Retroelement-guided protein diversificiation abounds in vast lineages of Bacteria and Archaea. Nat. Microbiol. 2017; 2: 17045.

100. Dirix, G., Monsieurs, P., Dombrecht, B., Daniels, R., Marchal, K., Vanderleyden, J. *et al.* Peptide signal molecules and bacteriocins in Gram-negative bacteria: a genome-wide in silico screening for peptides containing a double-glycine leader sequence and their cognate transporters. Peptides 2004; 25: 1425-1440.

CHAPTER FOUR

ENDOLITHIC MICROBIAL CARBON CYCLING ACTIVITIES IN SUBSURFACE MAFIC AND ULTRAMAFIC IGNEOUS ROCK

Contribution of Authors and Co-Authors

Manuscript in Chapter 4

Author: Elizabeth M. Fones
Contributions: Collected samples, contributed to experimental design, and conducted the experiments. Contributed to the writing the manuscript.

Co-Author: David W. Mogk
Contributions: Oversaw mineralogical characterization of samples from the Stillwater Mine.

Co-Author: Alexis S. Templeton
Contributions: Designed, led, and carried out sampling protocols of cores for biological analyses from the Samail Ophiolite.

Co-Author: Eric S. Boyd
Contributions: Collected samples, contributed to experimental design, and contributed to the writing the manuscript.

Manuscript Information Page

Elizabeth M. Fones, David W. Mogk, Alexis S. Templeton, and Eric S. Boyd

Status of Manuscript:

__x__ Prepared for submission to a peer-reviewed journal

_____ Officially submitted to a peer-reviewed journal

_____ Accepted by a peer-reviewed journal

_____Published in a peer-reviewed journal

Endolithic microbial carbon cycling activities in subsurface mafic and ultramafic igneous rock

Elizabeth M. Fones[1], David W. Mogk[2], Alexis S. Templeton[3], and Eric S. Boyd[1,*]

[1]*Department of Microbiology, Montana State University, Bozeman, MT 59717*
[2]*Department of Earth Sciences, Montana State University, Bozeman, MT 59717*
3Department of Geological Sciences, University of Colorado, Boulder, CO 80309

[*]Author of correspondence: Eric S. Boyd (*eboyd@montana.edu*)

Department of Microbiology & Immunology

Montana State University

PO Box 173520

Bozeman, MT 59717

Phone: (406) 994-7046

Fax: (406) 994-4926

Subsurface rocks host a substantial portion of the Earth's biosphere. However, most studies of such environments have focused on microbial communities in waters that collect in subsurface wells intersecting rock fractures. As such, little is known of the distribution of cells and their activities in the rocks themselves. Here, microcosm assays were developed and optimized to detect carbon cycling activities of cells residing in pore spaces and microfractures of mafic to ultramafic igneous rocks. Application of an optimized assay to gabbro core from the Stillwater Mine, Montana, USA, revealed maximal methane production from acetate in 2-week incubations near the temperature of the mine. Controls show that these activities are not due to contamination introduced during drilling, exhumation, or laboratory processing of the core. The assay was then applied to two rock cores from the Samail Ophiolite, Sultanate of Oman, which is undergoing low temperature serpentinization. Production of carbon dioxide from acetate and formate and production of methane from formate was detected in a dunite core interfacing waters of pH 9.6 but not a peridotite core interfacing waters of pH 11.4, suggesting the latter may not host a robust population of cells capable of metabolizing these substrates. Collectively, these results show that active microbial communities inhabit subsurface igneous rocks and raise questions about the collective size and contribution of the subsurface biosphere to global nutrient cycles. The development of methods to sensitively detect endolithic life in igneous rocks has implications for life detection on other planetary bodies where similar rock types prevail, such as Mars, Europa, and Enceladus.

Recent estimates suggest that the deep subsurface hosts up to 19% of the Earth's total biomass [1]. Yet, our understanding of life in subsurface environments remains limited, largely due to difficulty of gaining access to samples of cored rocks. A substantial portion of the habitable subsurface, both today and on early Earth, is comprised of mafic and ultramafic igneous rocks [2-4]. Despite their low porosity, mafic and ultramafic igneous rocks are key targets for life detection studies due to their potential to release low potential electron donors capable of fueling robust microbial communities [5-14]. For example, iron(II)-bearing minerals (e.g., olivine) in mafic and ultramafic rocks can readily react with water via the process of serpentinization to generate H_2 [15-19], a source of low potential electrons to fuel microbial metabolism. The H_2 that is generated during serpentinization can also react with dissolved CO_2 to generate reduced carbon substrates such as formate ($HCOO^-$), carbon monoxide (CO), or methane (CH_4) [20, 21], which themselves may support the carbon and energy demands of microorganisms. Serpentinization may have provided substrates that supported the energy metabolisms of early life [22], and mafic and ultramafic rocks are common throughout the solar system [23-26]. This suggests that similar processes could occur on other planetary bodies where ultramafic rocks encounter liquid water. For example, serpentinization is a proposed source of the CH_4 that has been detected in Mars's atmosphere [23], the H_2 detected in plumes emanating from Enceladus's interior [24, 25], and has been predicted to contribute to H_2-flux into Europa's ocean [26, 27]. If serpentinization helped support primitive life on early Earth, it could potentially support primitive life on other planetary bodies.

To date, studies of life in serpentinizing environments have largely focused upon surface springs/subsurface well waters and chimney biofilms collected from terrestrial ophiolites and hydrothermal vents at mid-ocean ridges, respectively. Genomic inference, microcosm-based

experiments, and isotopic analyses have revealed that microorganisms inhabiting waters in serpentinizing environments can utilize abiotic products of serpentinization (e.g., H_2, CO, $HCOO^-$, and CH_4) in their carbon and/or energy metabolisms [5-14]. Morrill et al., 2013, described extremely low (10^2-10^3 cells mL^{-1}) densities of planktonic cells in serpentinite springs of The Cedars (California, USA), but found that glass slides incubated in the springs for 2-3 weeks became colonized by cells with densities ranging from 10^6 to 10^7 cells per cm^2 [28]. This suggests that sessile cells may grow to higher densities than planktonic cells in serpentinizing environments, even when attached to glass that does not provide cells with nutrients or energy substrates.

Rocks undergoing serpentinization would be expected to provide nutrients or energy substrates that might therefore be expected to host a greater abundance of biomass than is present in the waters. Further, most of the habitable volume in serpentinizing environments is comprised of the pore spaces and microfractures of the serpentinized rock itself, which have been understudied thus far with respect to the distribution and activities of cells they may host while effectively controlling for contaminants. The lack of studies focused on the rocks themselves is presumably due to difficulties in identifying discrete locations in rock cores where the activities and thus abundances of endogenous cells are sufficient for downstream characterization. Further confounding such efforts is the difficulty in delineating activities attributable to cells endogenous to the rock core versus those introduced to the core during its drilling, recovery, and handling. Recent efforts to fill this knowledge gap have included enumerating cells in pulverized core samples from serpentinizing environments (e.g., the Samail Ophiolite, Oman, and Atlantis Massif, Mid-Atlantic Ridge) and attempting to distinguish between endemic microbial taxa in serpentinite cores from the Atlantis Massif and possible contaminants [29-31]. Suzuki et al.,

2020, detected microbial cells densely concentrated in Fe-rich smectite on fractures and veins in subseafloor basaltic rock from the South Pacific Gyre [32], and Li et al., 2020, performed an extensive set of analyses on core samples recovered from the Atlantis Bank (southwest Indian Ridge, Indian Ocean) including analyses of cell densities, enzyme activities, lipid biomarkers, marker genes, and an attempt to measure methane production over time in long-term enrichments containing rock core samples [33]. However, control conditions did not account for potential mineral-catalyzed activities or potential contaminants introduced during laboratory processing and the authors acknowledge that the importance of methane metabolism remains unclear in these samples. Templeton et al., 2021, also attempted to determine rates of microbial sulfate reduction in cores from the Samail Ophiolite, Oman, but "abiotic" controls exhibited activities that could not be accounted for which extensively overlapped with activities measured in "live" samples [29]. Thus, the relative contributions of microbial cells to nutrient cycling activities have not been confidently identified in subsurface rock-hosted environments, thereby limiting understanding of the subsurface biosphere.

To improve protocols for measuring microbial carbon cycling activities in order to deepen our understanding of the activities of microbial life in the rock-hosted subsurface, two mafic igneous (gabbro) core samples from the Stillwater Igneous Complex (Nye, Montana, U.S.A.) were used to develop a microcosm approach for detecting the activities of viable cells residing in low-porosity igneous rocks while controlling for potential false positives attributable to drill-site and laboratory contaminants. The Stillwater Complex is a Neoarchaean (~2.7 Ga) layered mafic and ultramafic igneous intrusion [34] with primary olivine and orthopyroxene minerals that have previously undergone substantial alteration to serpentine minerals [35]. The optimized microcosm approach was subsequently applied to rock cores collected during drilling

operations of two new boreholes hosting waters of contrasting geochemical conditions in the Samail Ophiolite, Sultanate of Oman. The Samail Ophiolite is the largest, best-exposed ophiolite in the world, thereby providing an accessible field location for studying cells inhabiting rocks undergoing active, low-temperature serpentinization. Results are discussed in terms of the potential contribution of endolithic cells (cells residing within rocks) in subsurface mafic and ultramafic rocks to global nutrient cycles and implications for guiding life detection strategies on other planetary bodies where similar rock types prevail, such as Mars, Europa, and Enceladus.

Materials and Methods

Sample Collection and Characterization.

Stillwater Igneous Complex, U.S.A. Two gabbro cores (both 3.5 cm diameter by ~20 cm length) from the Stillwater Igneous Complex (Nye, Montana) were kindly provided by the Stillwater Mining Company in June 2017. Cores were transported to the laboratory at ambient temperature and were stored at room temperature prior to analysis. Details of the depth and location of the core were not provided. As such, these sample cores were used to develop methods to optimize measurement of select microbial activities, to assess potential sources of contamination, and to design controls to rule out contamination as the source of measured activities.

The mineralogical composition of the gabbro sample from the Stillwater Complex was determined using X-ray diffraction (XRD), optical petrography, and scanning electron microscopy (SEM) coupled with energy-dispersive X-ray spectrometry (EDS). An approximately 0.5 cm^3 subsample of the gabbro core was removed with a chisel for XRD analysis. The sample chip was ground with a mortar and pestle and passed through a 2 μm sieve prior to analysis on a Scintag X1 Diffraction System. Mineral phases were identified using Jade

9.0 software (KS Analytical Systems - http://ksanalytical.com/jade-9/). Mineral assemblages were calculated based on Rietveld refinement using TOPAS software with crystal structures from the American Mineralogist Crystal Database (AMCSD). Pearson VII peak were used for all refinements.

Standard polished thin sections were prepared from gabbro core samples by Spectrum Petrographics (Vancouver, WA) and analyzed for mineral identification using standard optical minerology procedures. Photomicrographs were taken with a Leica DM EP Polarizing Microscope (Meyer Instruments, Houston, TX) in plane-polarized and cross-polarized light at 25x and 100x total magnification. Thin sections were coated with iridium and imaged with a JSM-6100 Scanning Electron Microscope (JEOL USA, Peabody, MA) using Backscattered Electron Imaging (BEI). Elemental point analyses were performed using EDS.

Samail Ophiolite, Oman. Intact whole round core sections were recovered during wireline diamond coring operations from boreholes BA3A (coordinates: 22°51.970' N, 58°42.634' E) and BA4A (coordinates: 22°53.101' N, 58°41.703' E) in the Samail Ophiolite, Sultanate of Oman, in January and February of 2018, respectively, as described previously [29, 36]. Briefly, core sections to be used for biological analyses were immediately rinsed with 18.2 MΩcm water upon sample recovery. The core was then placed on a combusted aluminum foil liner where it remained for all stages of sample preparation except when it was placed on a core scanner that had been pre-cleaned with bleach and ethanol. After core scanning, the core surface was further cleaned with an ethanol wipe. A subsection was then removed from a larger core section using a diamond blade saw lubricated with 18.2 MΩcm water. This subsection was moved into a mobile laboratory on site in combusted foil. Inside the mobile laboratory, discrete 5 cm core sections were separated for biological activity assays and mineralogical analyses using

an ethanol-washed hammer, chisel, and tongs while resting on combusted foil. Sub-cores designated for activity assays or mineralogy were transferred into a vinyl anaerobic chamber (Coy Laboratory Products, Grass Lake, MI), washed twice with N_2-purged 18.2 MΩcm water, wrapped in foil, sealed into mylar bags flushed with N_2 together with an O_2-scrubbing sachet (BD GasPak 260001: Becton, Dickinson and Company, Franklin Lakes, NJ), and stored at 4°C until further analysis. The subsection of cores used to measure microbial activities were from 80 m (BA3A) and from 50 m (BA4A), as described in more detail below. The mineralogical composition of BA3A and BA4A have been reported previously [16, 29, 36] and are briefly summarized below. Following completion of drilling in 2018, pH and Eh were measured using a down-borehole logger. These values were reported previously [29, 36] and are briefly summarized below.

In February and March of 2020, two years after the BA3A and BA4A cores were drilled, a Grundfos SQ 2–85 submersible pump was lowered into the wells to sample waters following methods described previously [5, 6]. These waters were used for activity assays and as "medium" for microcosm-based activity assays (described below). Waters were collected from 75 m (BA3A) and from 50 m (BA4A), corresponding to the depths of the core sections (BA3A 80 m and BA4A 50 m, respectively) that were selected for measurement of microbial activities. After pumping ~100 liters of water through the tubing and sampling manifold, site waters were collected directly from the sampling manifold into N_2-purged, butyl-stoppered, borosilicate glass serum vials that had been pre-sterilized by autoclaving. The temperature and pH of waters were measured in the field as described previously [6, 37]. Water samples were transported at ambient temperature and stored at 4°C upon arrival in the laboratory.

<u>Development and Optimization of Assays to Measure Microbial Activities in Gabbro Cores from the Stillwater Complex.</u>

Overview. Experiments were designed to maximize detection of the potential activities of microorganisms residing within rock cores while accounting for abiotic reactivity or contamination during core drilling, recovery, and handling. The overall experimental design (described in detail in the sections that follow) first involved decontaminating core surfaces and surface-accessible fractures by coating the core exteriors with 70% ethanol and briefly exposing them to flame. Next, "decontaminated" cores were subjected to jaw crushing to generate coarse rock fragments. Coarse rock fragments were then milled via a series of ball milling speeds and times to optimize measurement of target microbial activities. Activities were measured using ^{14}C-radiolabeled tracers in microcosms containing rocks and a fluid medium.

Effect of Surface Decontamination on Cell Viability. A method was developed and tested for its efficacy in decontaminating the surface of gabbro core (and surface-accessible fractures and pores) from the Stillwater Complex that may have been exposed to drilling fluid and associated microbial contaminants during its exhumation and handling. Two replicate gabbro core subsamples were removed from the larger core section via autoclaved hammer and chisel in an ethanol washed- and UV-irradiated laminar flow hood. These subsamples were wrapped in aluminum foil and subjected to a dry autoclave cycle (30 min, 22 psi, 123°C), incubated at room temperature (~22°C) overnight, and then a second autoclave cycle. The two gabbro core subsamples were subsequently coated in a dense (~10^8 cells mL^{-1}) liquid culture of late-log phase *Geobacillus stearothermophilus* cells (ATCC 7953) to simulate high levels of contamination for a period of 60 min. This organism was chosen because it is known to form spores [38] thereby allowing for an assessment of contamination by both active cells and possibly by germinating spores. One of the core subsamples was then coated with 70% ethanol for a period of three min.

and then the core was exposed to flame. The other core subsample was not subjected to this decontamination procedure.

Surface decontaminated and non-surface decontaminated cores were separately subjected to coarse pulverization (to variably sized fragments up to ~2 mm) with a pre-decontaminated (sprayed with 100% ethanol and then flamed) LC-8 Mini-Jaw Crusher (Gilson Co., Lewis Center, OH) in an ethanol sprayed- and UV-treated laminar flow hood. One half of a gram of the coarsely pulverized core from each treatment was then mixed with 0.5 mL molecular grade sterile water to create slurries. The slurries were subjected to a dilution series using molecular grade sterile water and subsamples of each dilution were plated on nutrient agar. Plates were incubated at 38°C for 12 hours and viable colony forming units (CFUs) were quantified.

Effect of Milling on Cell Viability. An experiment was designed to identify a milling speed and milling time that maximized the survival of viable cells and still generated a homogenous, fine rock powder. Double autoclave-sterilized gabbro core samples were coarsely ground (~ <2 mm fragments) with a jaw crusher, as described above. Coarsely ground gabbro fragments were coated in a dense (~10^9 cells mL^{-1}) liquid culture of mid-log phase *Escherichia coli* K12 (ATCC 23740) for 10 min. *E. coli* cells were used since they are easily lysed and would presumably be highly sensitive to mechanical disruption of their membrane, resulting in loss of viability. Coarsely-ground gabbro fragments coated with *E. coli* were milled with a Pulverisette 6 (Fritsch, Pittsboro, NC) ball mill equipped with a gas-tight tungsten carbide milling bowl and balls that had been previously decontaminated by treatment with 70% ethanol and exposure to ultraviolet light for 30 min. Prior to milling, the milling bowl was pre-cooled at 4°C for 30 min. to minimize the generation of high temperatures that could decrease cell viability. The gas phase during milling was air since *E. coli* is not sensitive to oxygen. Milling was performed at three

sets of speeds and times (100 RPM for 10 min., 170 RPM for 4 min., and 200 RPM for 2 min.). Viable CFUs in each sample were quantified by dilution series and plating on Lennox Broth (LB) agar, as described above, following incubation for 12 hrs at 35°C. The milling condition that maintained the most viable cells (100 RPM for 10 min.) was used in subsequent experiments.

Effect of Milling on Activity. An experiment was conducted to examine the effect of milling (and by extension surface area) on detectable microbial activities. It was hypothesized that milling rock samples to a homogenous fine powder before adding them to a fluid medium would increase microbial activities by limiting diffusional constraints associated with substrate acquisition or product release. Coarsely ground gabbro subsamples that had been pre-crushed using a jaw crusher (~ <2 mm fragments) under aerobic conditions (see above) were immediately transferred to butyl-stoppered glass serum vials that had been autoclave-sterilized and N_2-purged to minimize exposure of cells to oxygen. Approximately 50 g of coarse rock fragments were then transferred to pre-cooled, ethanol- and UV-sterilized, gas-tight Pulverisette 6 milling bowl in an anaerobic chamber and subsequently milled at 100 RPM for 10 min. A second subsample (approximately 50 g – same as above) did not undergo milling.

Both sets of samples were transferred to an anaerobic chamber (Coy Laboratory Products, Grass Lake, MI) and 0.5 g subsamples of each were weighed on ethanol-treated foil and transferred via ethanol-treated spatula to triplicate 24 mL serum bottles that contained 10 mL of autoclaved M9 minimal medium (sans glucose) that had been sparged with N_2 gas passed over heated (200°C) and reduced copper shavings. The medium was amended with Wolfe's trace vitamins and SL-10 elements and the bottles were capped with butyl rubber stoppers. The vials were removed from the chamber and the headspace purged with N_2. Finally, 1 mM sodium

acetate (CH_3COONa) that included 5 μCi $^{14}CH_3COONa$ (American Radiolabeled Chemicals, St. Louis, MO) was added to each vial. This label was chosen since only CH_4 production from acetate was being monitored and because it is the methyl group of acetate that is reduced to CH_4. Production of CH_4 from acetate (acetoclastic methanogenesis) was chosen as the target activity since this process should be sensitive to O_2, allowing us to evaluate whether procedures used to handle the Stillwater Complex core samples were sufficient to preserve and detect the anaerobic activities to be targeted for measurement in Oman rock cores. Secondly, this is a microbial process that might be expected in this type of rock type based on the recovery of DNA sequences affiliated with acetoclastic methanogens in waters from other mafic and ultramafic rock-hosted sites [10, 39-41]. Additionally, acetate is a central metabolite for many cells, and tracking methane generation from acetate may include acetate oxidation (e.g., to CO_2) performed by one cell type and reduction of this product to methane by another cell type. This approach may increase the measurable rate of methane production in microcosms as compared with measuring inorganic carbon reduction to methane alone.

Triplicate "abiotic control" vials were prepared as described above, except that rock powders were autoclaved twice (~12 hrs apart) under N_2 headspace prior to addition of sterile medium and acetate to account for potential abiotic conversion of acetate to CH_4. Triplicate "processing control" vials containing rock core that had been autoclaved twice prior to pulverizing, milling, weighing, and adding to medium vials were also prepared to account for any microbial contaminants introduced during laboratory processing. Triplicate biotic vials and triplicate abiotic control vials for each condition were incubated at 4°C, 15°C, 25°C, and 35°C for 14 days. Triplicate "processing controls" were incubated at 15°C for 14 days.

Following incubation, a subsample of the headspace gas was collected via syringe and needle equipped with a stopcock and transferred to a specially fabricated scintillation vial containing a butyl rubber septum. CH_4 was trapped with 10 mL Cytoscint ES scintillation cocktail, as described previously [5]. The radioactivity (measured in counts per minute) associated with ^{14}C-CH_4 was quantified via liquid scintillation counting (LSC). Total rates of CH_4 production were calculated by normalizing gas subsample volume to total headspace gas volume, normalizing counts per minute to disintegrations per minute via a quench curve, multiplying measured rates of $^{14}CH_4$ production by the molar ratio of $^{14}CH_4COO^-$ to CH_4COO^- (radiolabeled and unlabeled) added to each vial, and normalizing to grams dry weight rock added to each vial.

Quantification of Biological Activities in Core Sections from the Samail Ophiolite.

Core samples from BA3A (50m) and BA4A (80m) were each split roughly in half using an autoclaved and flamed hammer and chisel in a laminar flow hood that had been pre-cleaned with ethanol and treated with UV light. One half of each core sample was autoclaved twice (with incubation at room temperature overnight between autoclave cycles to allow for germination of spores) to serve as a processing control, as described above. The other half of the core sample was passed through a pre-sterilized jaw crusher, as described above. This pulverized rock was separated using an autoclave and flame-sterilized spatula into two N_2-purged borosilicate glass butyl-stoppered vials that had been pre-sterilized by autoclaving. Both vials were immediately purged with filtered (0.1 μm pore size) N_2 that had been passed over heated (200°C) and H_2-reduced copper shavings, as described above. One vial containing pulverized rock under a N_2-headspace was then autoclaved twice (with incubation at room temperature (~22°C) overnight

between autoclave cycles) to serve as an abiotic control. The other vial containing pulverized rock served as a live (biotic) sample that did not undergo sterilization.

Preliminary data indicates that milling gabbro powders from the Stillwater Mine decreased cell viability (Supplementary Fig. 1) but also increased the ability to detect activity (Supplementary Fig. 2). Thus, we opted to not mill the pulverized rock from BA3A and BA4A since we suspected low biomass in these cores (described below). Instead, microcosm vials were inoculated with a slurry of small particles generated during jaw crushing of the rock. Slurries were generated using sterilized site waters collected in 2020 (described above) that had been passed through N_2-purged syringe filters (0.1 μm pore size) via a N_2-purged sterile needle and syringe. Filtered waters were autoclaved twice with incubation at room temperature (~22°C) overnight between autoclave cycles to allow for germination of spores. The same volume of suspended particles was injected via syringe and 18-gauge needle, thereby restricting the particles that were used to <0.84 mm (the inner diameter of the needle).

Acetate. Five mL of this homogenized slurry was transferred via sterile syringe and 18-gauge needle along with 5 mL of sterilized site waters (three replicates per condition) to N_2-purged 26 mL butyl-stoppered borosilicate glass serum vials that had been pre-sterilized by autoclaving. Triplicate 5 mL slurry samples were dried overnight to quantify the grams dry weight rock added to each vial. One mM (final concentration) of acetate that included 5 μCi [1,2-^{14}C] sodium acetate ($^{14}CH_3{}^{14}COONa$) was added to each vial. The dually labeled acetate was chosen since both CO_2 and CH_4 production were monitored in this experiment. Following incubation for 2 weeks at 34°C, CH_4 was trapped with 10 mL Cytoscint ES scintillation cocktail, as described above. Samples were then acidified via addition of 200 μL of 12N HCl to volatilize dissolved inorganic carbon. The headspace gas was subsampled and CO_2 was trapped using

Carbo-Sorb E (PerkinElmer, Waltham, MA) using methods described previously [42]. This value was used to calculate total CO_2 generated from acetate per gram of rock added to each microcosm via the conversions described above.

Rates of acetate metabolism among cells inhabiting subsurface waters of the Samail Ophiolite have not been previously measured. To measure rates of acetate metabolism in the waters for comparison to the activities of endolithic cells in the rocks, 10 mL of site waters from BA4A (50 m) and BA3A (75 m) were injected into triplicate N_2-purged 26 mL butyl-stoppered borosilicate glass vials that had been pre-sterilized by autoclaving. One mM (final concentration) acetate that included 5 μCi [1,2-^{14}C] sodium acetate ($^{14}CH_3{}^{14}COONa$) was added to each vial as described above. Microcosms were incubated in parallel with the rock core incubations described above, and CO_2 and CH_4 were quantified as above.

Formate. The same slurries described above were used to inoculate microcosm vials to measure rates of formate metabolism among microorganisms inhabiting BA3A and BA4A rocks, since a previous study highlighted the role of formate in allowing autotrophic methanogen cells to overcome inorganic carbon limitation in waters of high pH in the Samail Ophiolite [6]. Microcosm vials were prepared as above except 1 mM (final concentration) of $HCOO^-$ that included 5 μCi ^{14}C-$HCOO^-$ (American Radiolabeled Chemicals, St. Louis, MO) was added to each microcosm vial instead of acetate. H_2 gas was added to a concentration of 20% of headspace volume, with the balance as nitrogen. Following incubation for 1, 2, 4, 8, and 12 weeks at *in situ* temperature (34°C), 4 mL filtered (0.2 μm) N_2 was added to each vial using an N_2-purged sterile needle and syringe to maintain positive headspace pressure, and 4 mL headspace gas was removed using a needle and syringe equipped with a stopcock. The 4 mL volume was then separated into two, 2 mL aliquots for use in quantifying CO_2 and CH_4

production, as described above. The radioactivity, measured in counts per minute, associated with ^{14}C-CO_2 and ^{14}C-CH_4 in the headspace of the samples was measured as above and used to calculate the rates of formate transformation per gram dry weight rock added to each vial. After incubation for 12 weeks, samples were acidified via addition of 200 µL of 12N HCl to volatilize dissolved inorganic carbon. The headspace gas was again subsampled, and CO_2 was trapped using Carbo-Sorb E, as described above. This value was used to calculate total CO_2 generated per gram of rock added to each microcosm via the conversions described above. The rates of formate metabolism among cells inhabiting subsurface waters ranging in pH values from approximately 7.5 to greater than 11 in the Samail Ophiolite have been measured previously [11, 12], and therefore were not measured again in this study to compare with the activities measured in the rocks.

DNA extractions from Samail Ophiolite microcosms.

Replicate microcosms were prepared as above except they were amended with 1 mM (final concentration) of either formate or acetate without the addition of ^{14}C-radiolabeled substrates. These non-radiolabeled microcosms were incubated in parallel with the microcosms containing ^{14}C at 34°C. At the end of the incubation periods (2 weeks for microcosms containing acetate and 12 weeks for the microcosms containing formate), the rock particles and cells in the non-radiolabeled microcosms were concentrated via centrifugation. Concentrated material was subjected to DNA extraction using the FastDNA Spin Kit for Soil (MP Biomedicals, Irvine, CA) according to manufacturer instructions with the addition of 100 µl skim milk (500 mg L^{-1}) that had previously been sterilized via autoclaving, filtration, and UV-light treatment. DNA yield in extraction products were quantified using a Qubit 2.0 fluorometer (Invitrogen, Carlsbad, CA). PCR amplifications of archaeal and bacterial small subunit rRNA genes were performed in

triplicate reactions using the 515F/806R primer pair at an annealing temperature of 50°C using methods described previously [43]. The result of PCR was confirmed by gel electrophoresis.

Results and Discussion

Development and Optimization of Assays to Measure Endolithic Microbial Activity.

The objective of this study was to develop a method to sensitively detect microbial activities in rock cores sampled from the Samail Ophiolite, Oman, a site of active low-temperature serpentinization [15, 16, 19, 41, 42], while controlling for the effects of contaminating cells. A gabbro rock core from the Stillwater Mine was selected for the development and optimization of a protocol to achieve this objective as it was readily available and mineralogically similar to core samples obtained from the Samail Ophiolite (i.e., a mafic rock exhibiting evidence of hydrous alteration). Further, unlike the limited quantity of core (approximately 9 cm diameter x 5 cm length per depth interval) available for use from the Samail Ophiolite, the quantity of gabbro cores provided by the Stillwater Mine (approximately 3.5 cm diameter x 40 cm total length) were sufficient to perform multiple experimental iterations as described herein. The gabbro core collected from the Stillwater Mine consisted primarily of andesine (~59.7 wt%), augite (~33.2 wt%), and talc (~7.2 wt%) and included talc veins crosscutting primary orthopyroxene (Fig. 1).

To evaluate the efficacy of an ethanol/flame decontamination protocol in removing viable cells introduced to the sample exterior (and easily penetrable interior) during drilling and subsequent handling, Stillwater gabbro core samples were intentionally contaminated with a dense (~10^8 CFU mL^{-1}) culture of *G. stearothermophilus* in the late-logarithmic phase of growth for one hr. *G. stearothermophilus* is a robust, gram-positive, sporulating thermophile that is

commonly used in sterilization studies [45]. No viable CFUs were observed in the sample that had been decontaminated prior to pulverization (Fig. 2), indicating that these protocols are likely sufficient to remove viable contaminating cells from core exteriors and the easily penetrable interior when exposed to contaminants (e.g., drilling mud) for similar periods of time during drilling and exhumation. Furthermore, approximately 10^3 CFU sample^{-1} remained viable following pulverization without first undergoing decontamination, indicating that pulverization itself does not destroy all (presumably surface exposed) viable cells. A 1 mL aliquot of culture was used to coat the gabbro core section. However, most of the added culture (10^8 CFU) was not absorbed by the core sample and therefore the difference between the number of cells in the original culture (10^8 CFU) and in the pulverized sample (10^3 CFU) should not be interpreted as the number of viable cells destroyed by jaw crushing.

Second, the viability of *E. coli* cells following milling of coarsely-ground gabbro core at three different milling speeds and times was assessed to determine milling conditions that generated a fine, homogenous powder but was least destructive to cells. Immediately following pulverization, gabbro samples were coated in a dense (~10^9 CFU mL^{-1}) broth culture of *E. coli* cells in the mid-logarithmic phase of growth and subjected to milling at three speeds using a ball mill (described above). The slowest milling speed (100 rpm for 10 min.) was found to maximize cell viability (Supplementary Fig. 1) and was therefore used in subsequent optimization experiments.

Third, the hypothesis that milling rock samples to a homogenous fine powder before adding them to a fluid medium increases detectable microbial activities, likely by limiting diffusional constraints associated with microbial access to nutrients, was evaluated. Rates of $^{14}CH_3COO^-$ disproportionation to $^{14}CH_4$ were measured in milled and un-milled gabbro samples.

Accumulation of $^{14}CH_4$ was observed in the headspace of biotic microcosms containing gabbro rock that had been amended with ^{14}C-acetate; $^{14}CH_4$ did not accumulate in abiotic controls containing gabbro rock and ^{14}C-acetate. This indicates the presence of either viable acetoclastic methanogens or a co-culture of cells wherein one cell type oxidizes acetate (e.g., to CO_2) and a hydrogenotrophic methanogen reduces the labeled CO_2 to CH_4 (Supplementary Fig. 2). This is potentially consistent with the common detection of methanogens in subsurface environments [47], including waters from mafic and ultramafic rock-hosted environments [37, 48-50].

Multiple control conditions ensured that CH_4 production from acetate could be attributed to the activities of endemic cells and not abiotic reactivity or contamination introduced during laboratory processing. An abiotic control containing pulverized rock and medium that had been autoclaved prior to addition of $^{14}CH_3COO^-$ accounted for abiotic rates of acetate conversion to CH_4. A processing control in which the rock core was autoclave-sterilized prior to pulverizing, milling, weighing, and adding to sterile medium vials accounted for contamination introduced during the sample preparation process. No $^{14}CH_4$ production was observed in either set of controls. Additionally, higher rates of methanogenesis were observed in the milled samples as compared with the un-milled samples, indicating that milling improves the ability to detect evidence of microbial metabolism under these conditions, likely by removing diffusional constraints associated with substrate acquisition or product release.

Fourth, it was hypothesized that the activity of methanogens in Stillwater gabbro rock cores, if endemic to those rocks, would be higher in microcosms incubated at the temperature of the Stillwater Mine (average yearly temperature is ~15°C [51]). To test this hypothesis, rates of CH_4 production from acetate by microorganisms in gabbro cores were measured using the approach outlined above with samples incubated at 4, 15, 25, and 35°C. Rates of CH_4 production

were highest when incubated at near the temperature of the Stillwater Mine (15°C) (Fig. 3). Biological methanogenesis was not observed at a temperature (35°C) resembling that of the human body (37°C) indicating that the measured activities are highly unlikely to be contaminants associated with humans (e.g., from the skin or gastrointestinal tract) introduced during sample handling.

Site Description and Previous Analyses of Core Sections from the Samail Ophiolite.

After optimizing protocols using gabbro samples from the Stillwater Mine, they were applied to detect the activities of endolithic cells in rock cores sampled from the Samail Ophiolite, Sultanate of Oman. A single core section was recovered from each of the two newly drilled boreholes, BA3A and BA4A, in the Samail Ophiolite as described above. Briefly, the BA4A site is hosted in partially serpentinized dunite and the BA3A site is hosted in partially serpentinized peridotite, both in the mantle section of the Samail Ophiolite, as described in detail in Kelemen et al., 2020 [36]. Core sections were selected for quantification of biological activities from depths in BA4A and BA3A that roughly corresponded to the inflection point between more oxidizing conditions of the surface and more reducing conditions of the subsurface [36]. It was hypothesized that these interfaces between more oxidizing and reducing conditions could provide microorganisms with higher concentrations of oxidants and reductants in disequilibrium when compared with either end-member condition, allowing cells to fuel their metabolisms, as has been suggested previously [5, 52]. This could potentially maximize our ability to detect activities among cells inhabiting the rocks. To this end, the core sections from 50 m depth in BA4A and from 80 m depth in BA3A were selected for biological analyses based upon the downhole Eh data presented in Templeton et al., 2021 [29]. Downhole water Eh values logged in March 2018 were approximately 0 mV near the surface versus -600 mV at

approximately 70 m depth and below in BA4A and -550 mV near the surface versus -700 mV at approximately 200 m depth and below in BA3A [29]. Downhole pH measurements from March 2018 ranged from approximately 9.5 to 10.5 in BA4A and approximately 9.5 to 11.0 in BA3A [36]. BA4A (50 m) waters exhibited an Eh value of approximately -550 mV and pH of approximately 10.0 in 2018 [29, 36]. BA3A (75 m) waters exhibited an Eh value of approximately -650 mV and pH of 10.9 in 2018 [29, 36]. It was hypothesized that viable endolithic microorganisms in rock cores of the Samail Ophiolite, if present, would exhibit lower metabolic rates in rocks interfacing waters of higher pH as compared with rocks interfacing waters exhibiting circumneutral pH. This is due to the polyextremophilic conditions present in these waters, as has been shown previously among microbial communities inhabiting waters sampled from wells in the Samail Ophiolite [5, 6, 37].

Quantitative XRD analyses, as reported previously [16, 29], revealed that the BA4A 50 m sample consisted of approximately 98.9% serpentine, 0.8% andradite, 0.2% pyroxene (diopside), and 0.1% dolomite [16, 29]. The BA3A 80 m sample was not analyzed via quantitative XRD, however, the BA3A 60 m sample consisted of approximately 68.3% serpentine, 11.5% chlorite, 7.1% pyroxene (enstatite), 3.1% forsterite, 3.1% amphibole (tremolite), 2.7% pyroxene (augite), 1.3% pyroxene (diopside), 1.0% amphibole (actinolite), 1.0% brucite, 0.6% andradite, and 0.4% biotite. Further, the BA3A 100 m sample consisted of approximately 96.7% serpentine, 1.3% amphibole (actinolite), 0.6% andradite, 0.5% pyroxene (enstatite), 0.4% chlorite, 0.2% forsterite, 0.2% pyroxene (diopside), and 0.1% dolomite [16, 29]. As reported in Kelemen et al., 2021, bulk density of the BA4A 50 m sample was 2.7 g cm^{-3} with approximately 2% porosity whereas the bulk density of the BA3A 80 m sample was 2.5 g cm^{-3} with approximately 6% porosity [36]. Thus, while the BA3A (80 m) core likely interfaces more reduced and higher pH waters than the

BA4A core (50 m), it has higher porosity and may have a greater amount of habitable space/surface area to support biomass production.

Quantification of biological activities in core sections from the Samail Ophiolite.

Acetate. Rates of acetate oxidation to CO_2 and reduction of acetate (or CO_2 generated from oxidation) to CH_4 were evaluated in microcosm assays containing rocks and sterilized site waters. Microcosm incubations containing pulverized rocks were performed in sterilized (filtered and doubly autoclaved) site waters at 34°C to closely mimic the conditions experienced by the endolithic cells *in situ* (36°C and 35°C for BA3A and BA4A, respectively). The pH of the waters used as "medium" for the assays at the time of sampling (February 2020) was 11.4 and 9.6 for BA3A (75 m) and BA4A (50m), respectively (Table 1). To quantify biological activities attributable to endolithic microorganisms, the average rates of substrate transformation in triplicate processing control microcosms were subtracted from average rates of substrate transformation in triplicate live microcosms. Rates of potential acetate metabolism had never been previously evaluated among cells inhabiting waters of the Samail Ophiolite. To redress this and to compare rates of microbial activities between the waters and the rocks, oxidation of acetate to CO_2 and reduction of acetate (or CO_2 generated from oxidation) to CH_4 were measured in microcosm assays amended with site waters containing planktonic cells collected from BA3A (75 m depth) and BA4A (50 m depth) in 2020.

The average amount of CO_2 produced from acetate in live replicates containing pulverized rocks from BA4A (50 m) was significantly higher ($p < 0.01$) than in processing controls, suggesting that acetate oxidation to CO_2 was performed by cells endemic to the rocks rather than contaminants introduced during laboratory processing (Fig. 4; Supplementary Table 1). CH_4 generation from acetate was not detected in microcosms containing pulverized rock from

BA4A, and neither CH_4 nor CO_2 generation from acetate was detected in microcosms containing pulverized rock from BA3A (Fig. 4; Supplementary Table 1). Significant ($p = 0.01$) biological acetate oxidation to CO_2 was also observed among cells inhabiting BA4A waters (Fig. 4; Supplementary Table 2). To compare rates of microbial activities in pulverized versus in subsurface waters, the average rate of biological acetate oxidation to CO_2 per gram pulverized rock from BA4A was converted to rates per mL of habitable space given a bulk density of 2.7 g per cm^3 and 2% porosity of the BA4A sample at 50 m depth [36]. Following this conversion, the rate of biologically mediated CO_2 generation from acetate per mL was almost three orders of magnitude higher in the pulverized rock from BA4A (50 m depth) as compared with BA4A waters (50 m depth). This is potentially in line with the detection of approximately 1×10^5 cells g^{-1} in veins/fractures of core from BA4A (50 m depth) [29], which converts to approximately 1.4×10^7 cells mL^{-1} habitable space, or about 2 orders of magnitude higher cell densities than have previously been measured in Samail Ophiolite waters (~10^5 cells mL^{-1}) [11]. A small amount of biological CH_4 from acetate (or from CO_2 generated via oxidation) was detected among cells inhabiting BA4A waters (Fig. 4; Supplementary Table 2), however, this value was not significantly higher than abiotic controls ($p = 0.12$), which is potentially consistent with the prediction that the dominant methanogens in the subsurface waters of the Samail Ophiolite are dependent upon $HCOO^-$ or CO_2, rather than acetate, in methanogenesis [12]. Biological CO_2 and CH_4 production from acetate were not observed among cells inhabiting BA3A waters (Supplementary Table 2).

Formate. Oxidation of formate to CO_2 and reduction of formate (or CO_2 generated from oxidation) to CH_4 were also measured in microcosm assays containing rocks and site waters from the Samail Ophiolite. Formate was chosen as a target substrate since it can be generated

abiotically following serpentinization reactions [15, 20, 21, 51, 52] and high rates of biological formate oxidation to CO_2, reduction to CH_4, and assimilation to biomass have been previously measured in Samail Ophiolite waters [5, 6]. Further, genes encoding formate dehydrogenases were abundantly detected in metagenomes generated from these same waters [6]. Lastly, a hydrogenotrophic methanogen population was shown to have adapted to be dependent on formate as an electron donor, since its oxidation in the cytoplasm presumably allowed it to generate reducing equivalents with similarly low reduction potential while at the same time generating CO_2 and allowing it to overcome CO_2 limitation [6]. Microcosm incubations containing pulverized rocks were again performed in sterilized site waters at 34°C to closely resemble the conditions experienced by the endolithic cells *in situ*, as described above. A 12-week incubation period was selected to evaluate whether potentially slow rates of metabolism among cells inhabiting BA3A rocks could be detected over a longer period than the 2-week incubation period used for microcosms amended with acetate. Microcosms amended with formate were incubated over a 12-week period with headspace gas samples taken at the 2, 4, 8, and 12-week timepoints to measure $HCOO^-$ transformation to CO_2 and CH_4 over time.

CO_2 and CH_4 production from $HCOO^-$ in the headspace of live replicates from BA4A (50 m) exceeded values observed in the processing control replicates at every timepoint throughout the 12-week incubation period (Fig. 5). This suggests that $HCOO^-$ oxidation to CO_2 and reduction to CH_4 were performed by cells endemic to the rocks rather than contaminants introduced during laboratory processing. Biological $HCOO^-$ oxidation to CO_2 and reduction to CH_4 have been previously observed among cells inhabiting waters from the Samail Ophiolite [5,6]. The difference between total CO_2 generation in the live samples versus processing controls was statistically significant ($p < 0.01$) when the microcosms were acidified after 12 weeks

incubation to volatilize and quantify dissolved inorganic carbon in addition to CO_2 accumulation in the headspace (Supplementary Table 3). This is a more accurate rate of $HCOO^-$ oxidation to CO_2 since very little of the CO_2 produced from $HCOO^-$ would be expected to be in the headspace in microcosms with a pH of 9.6. This value is referred herein as the "total rate of $HCOO^-$ oxidation."

The total rate of $HCOO^-$ oxidation to CO_2 among cells inhabiting the BA4A (50 m) rock sample was approximately 66 nmol gdw^{-1} day^{-1} and the maximum potential rate of formate reduction to CH_4 in this same sample was approximately 1.1 nmol gdw^{-1} day^{-1} (Supplementary Table 3). Given a bulk density of 2.7 g per cm^3 and 2% porosity of the BA4A sample at 50 m depth [36], these rates convert to 8,910 nmol mL^{-1} day^{-1} and 148.5 nmol mL^{-1} day^{-1}, respectively. Both of these values are considerably (> 3 orders of magnitude) higher than previous measurements of maximum potential rates of biological formate metabolism in alkaline to hyperalkaline waters sampled from wells in the Samail Ophiolite: formate oxidation to CO_2 has ranged from 0.3 – 13 nmol mL^{-1} day^{-1} and formate reduction to CH_4 has ranged from 0.2 – 1 nmol mL^{-1} day^{-1} [5,6]. Additionally, the rate of acetate oxidation to CO_2 was also considerably (~3 orders of magnitude) higher in the pulverized rock sample when compared with the water sample from well BA4A (50 m depth) (Fig. 4; Supplementary Table 1; Supplementary Table 2). These results collectively indicate that biological activities in microcosms containing pulverized rock are generally higher than those in microcosms containing non-sterilized site waters alone (without pulverized rock). To evaluate the hypothesis that this increased activity is due to nutrients or energy substrates generated via water-rock interactions from freshly exposed mineral surfaces and/or abundant colonizable surface area provided by pulverized rock, an experiment is underway in which microcosms containing sterilized rock from BA3A (80 m depth) and BA4A

(50 m depth) and non-sterilized site waters from BA3A (75 m depth) and BA4A (50 m depth) were amended with acetate (including [1,2]-^{14}C acetate). These values will be compared to activities in the pulverized rock and in the waters alone to determine whether the addition of a rock matrix accounts for the difference in activities between the microcosms containing pulverized rock and the microcosms containing water alone. It would additionally be desirable to identify whether differences in activities were associated with differences in microbial community compositions between planktonic and rock-hosted phases. However, these efforts have been confounded thus far because DNA has not been successfully extracted from pulverized rock samples (DNA in extraction products is below detection limits when quantified via Qubit fluorometry) or amplified via PCR (there are no visible bands when amplification products are checked via gel electrophoresis).

Among the available potential oxidants to fuel acetate or $HCOO^-$ oxidation in the Samail Ophiolite is sulfate (SO_4^{2-}) [37]. Potential rates of SO_4^{2-} reduction in BA4A (50 m) core section were measured at 0.003 to 0.01 pmol cm^{-3} day^{-1} [29], which is at least 4 orders of magnitude lower than rates of acetate or $HCOO^-$ oxidation to CO_2. While these numbers include reduction of SO_4^{2-} in abiotic controls that at this time cannot be accounted for, they do indicate that SO_4^{2-} reduction is unlikely to be extensively coupled with acetate or $HCOO^-$ oxidation in this core section. As previously mentioned, hydrogenotrophic methanogens of the genus *Methanobacterium* in hyperalkaline waters in Oman have apparently replaced many of their H_2-dependent steps of methanogenesis (e.g., cofactor F_{420} reduction and Coenzyme M-Coenzyme B heterodisulfide reduction) with formate as electron donor [6]. Assuming a stoichiometry of 2 mols reduced cofactor F_{420} and 1 mol reduced heterodisulfide required per mol of CO_2 consumed/mol CH_4 produced during hydrogenotrophic methanogenesis [55], this would increase

the ratio of mols of $HCOO^-$ oxidized per mol CH_4 produced to 4 (1 mol of CO_2 is consumed as substrate for methanogenesis). This still does not account for the high rate of $HCOO^-$ oxidation to CO_2, suggesting involvement of a different oxidant such as nitrate, ferric iron, or oxygen. Such oxidants may also pair with acetate oxidation. This is potentially consistent with a sharp transition between oxidized and reduced fluids at 50 m depth in BA4A [29].

No biological activities were observed above background (detection limit of our assay is 4 pmol gdw^{-1} day^{-1}) in the microcosms containing water and rocks from BA3A at 80 m depth (Supplementary Table 3). This was a somewhat anticipated result given the extremophilic character of these fluids (pH ~ 11 and Eh ~ -650 mV), but is surprising considering that rates of SO_4^{2-} reduction in this core section ranged from 0.02 to 0.1 pmol cm^{-3} day^{-1}, which is roughly an order of magnitude higher than the rate of SO_4^{2-} reduction measured in the BA4A 50 m core section [37]. The far lower rates of acetate and $HCOO^-$ oxidation in BA3A at 80 m depth versus BA4A at 50 m depth is potentially consistent with cell counts from rocks from these depth intervals, which ranged from 10^4-10^5 cells gdw^{-1} versus 10^5-10^6 cells gdw^{-1} in core veins/fractures in BA3A versus BA4A core sections, respectively [29]. Together, the acetate and $HCOO^-$ oxidation and SO_4^{2-} reduction data suggests that a greater proportion of cells in BA3A (80 m) are reducing SO_4^{2-} and a lower proportion are oxidizing acetate or $HCOO^-$ when compared to BA4A (50 m). The sampling interval at 80 m in BA3A is highly reduced and is well below the zone where more oxidized waters mix with reduced waters [29, 36], at least relative to BA4A. It is possible that in such highly reduced waters, acetate and $HCOO^-$ oxidation are disfavored as a potential source of electrons capable of fueling SO_4^{2-} reducers. Rather, $HCOO^-$ oxidation may be more highly utilized in more oxidized waters where oxygen, nitrate or other more favorable electron donors are available (e.g., BA4A at 50 m). Further experimentation

where the effect of amendment of microcosms with various oxidants, including ferric iron, which can be generated abiotically via serpentinization reactions and is abundantly detected in core sections from the Samail Ophiolite [16], on rates of substrate oxidation are needed to evaluate potential coupling among electron donor/acceptor pairs in endolithic populations in the mafic and ultramafic rocks in the Samail Ophiolite.

Conclusions

The results presented herein support the hypothesis that viable cells inhabit microfractures or pore spaces of mafic and ultramafic rocks and contribute to carbon cycling activities. This includes rocks collected from both the Stillwater Mine (Montana, U.S.A.) and the Samail Ophiolite (Sultanate of Oman), which have contrasting geologic histories and have undergone different extents of serpentinization. To the authors' knowledge, this study is the first to measure microbial activities within subsurface mafic to ultramafic igneous rocks while effectively controlling for potential laboratory and drill-site contaminants that have confounded other efforts. Rates of acetate and formate metabolism were on the order of 3 orders of magnitude higher per unit habitable volume in a rock core section (BA4A at 50 m depth) than have ever been previously measured in waters of the Samail Ophiolite. This suggests that a focus upon the study of planktonic cells in subsurface environments could substantially underestimate the role of a subsurface biosphere in nutrient cycling, and warrants further study into the extent, distribution, and activities of cells inhabiting rock cores of the Samail Ophiolite and other subsurface rock-hosted sites.

The detection of microbial activities within rock cores of the Samail Ophiolite, an early-Earth analog environment that is undergoing active serpentinization, supports the proposition that pore spaces and/or microfractures in mafic to ultramafic rocks may have been inhabited on

early Earth. Such environments would have provided protection from solar radiation under the forming atmosphere of early Earth [56]. These results also suggest that ultramafic rocks proposed to be undergoing serpentinization elsewhere in the solar system such as Mars, Europa, and Enceladus [27-31], may be habitable. The ability to detect microbial activities in a low porosity (~2%) rock core section from the Samail Ophiolite that intersects waters with polyextremophilic character (i.e., pH 9.6 – 10.0, approximately -550 mV) but not in a higher porosity (~6%) rock core section that intersects waters with even more intense polyextremophilic character (i.e., pH 10.9 – 11.4, approximately - 650 mV) provides potential boundary conditions for application of activity assays as life detection strategies.

Acknowledgements

This work was supported by a grant from the NASA Astrobiology Institute (NNA15BB02A) to AST and ESB. X-ray diffraction, SEM imaging, and EDS analyses were performed at the Imaging and Chemical Analysis Laboratory, Montana State University. The authors wish to thank the Stillwater Mining Company for providing cores from the Stillwater Mine and the Oman Drilling Project for facilitating core sampling from the Samail Ophiolite. The authors are grateful to the Sultanate of Oman Ministry of Regional Municipalities and Water Resources and the Oman Public Authority of Mining for allowing sampling and export of rock cores and well waters.

Competing Interests.

The authors declare that they have no conflicts of interest.

Table 1. Characteristics of water and rock cores sampled from boreholes BA4A and BA3A in the Samail Ophiolite in 2018 and 2020. – Denotes values that were not collected in the 2018 or 2020 field season. [1]Values were previously reported in Kelemen et al., 2020 and Templeton et al., 2021 [29,36].

	BA3A		**BA4A**	
Year	2018	2020	2018	2020
Sample collected	Rock core	Water	Rock core	Water
Sampled depth (m)	80	75	50	50
Water pH	10.9[1]	11.4	10.0[1]	9.6
Water temperature (°C)	-	36	-	35
Eh (mV)	-650[1]	-	-550[1]	-

Supplementary Table 1. Amount of biological CO_2 and CH_4 production from acetate following incubation for two weeks in rock samples collected from wells BA3A and BA4A from the Samail Ophiolite in 2018 following pulverization. Filter-sterilized (0.1 µm) and autoclaved water from each well was used as the growth medium. The average amount of CO_2 or CH_4 production observed in three replicate processing controls was subtracted from the average CO_2 or CH_4 production in three replicate biological assays (Avg). The standard deviations (SD) of three replicates microcosms are indicated. CO_2 values refer to samples that were acidified at the 2-week timepoint to volatilize dissolved inorganic carbon to the headspace prior to sampling headspace gas for analysis. *P*-values were determined between biological assays and processing controls at each timepoint via Student's t-test assuming unequal variance for each condition.

CH_4 generation in microcosms supplied with acetate	
BA4A Avg (nmol CH_4 mL^{-1})	0
SD	-
p-value	-
BA3A Avg (nmol CH_4 mL^{-1})	0
SD	-
p-value	-
CO_2 generation in microcosms supplied with acetate	
BA4A Avg (nmol CO_2 mL^{-1})	2740
SD	441
p-value	<0.01
BA3A Avg (nmol CO_2 mL^{-1})	0
SD	-
p-value	-

Supplementary Table 2. Amount of biological CO_2 and CH_4 production from acetate following incubation for two weeks in water samples collected from wells BA3A and BA4A from the Samail Ophiolite in 2020. The average amount of CO_2 or CH_4 production observed in three replicate abiotic controls was subtracted from the average methane production in three replicate biological assays (Avg). The standard deviations (SD) of three replicates microcosms are indicated. CO_2 values refer to samples that were acidified at the 2-week timepoint to volatilize dissolved inorganic carbon to the headspace prior to sampling headspace gas for analysis. *P*-values were determined between biological assays and processing controls at each timepoint via Student's t-test assuming unequal variance for each condition.

CH_4 generation in microcosms supplied with acetate	
BA4A Avg (nmol CH_4 mL^{-1})	0.06
SD	0.03
p-value	0.12
BA3A Avg (nmol CH_4 mL^{-1})	0
SD	-
p-value	-
CO_2 generation in microcosms supplied with acetate	
BA4A Avg (nmol CO_2 mL^{-1})	4
SD	0.7
p-value	0.01
BA3A Avg (nmol CO_2 mL^{-1})	0
SD	-
p-value	-

Supplementary Table 3. Rates of biological CO_2 and CH_4 production from formate in rock samples collected from wells BA3A and BA4A from the Samail Ophiolite in 2018 following pulverization. Filter-sterilized (0.1 µm) and autoclaved water from each well was used as the growth medium. The average amount of CO_2 or CH_4 production per gram dry weight (gdw) observed in three replicate processing controls was subtracted from the average CO_2 or CH_4 production in three replicate biological assays (Avg). The standard deviations (SD) of three replicates microcosms are indicated. Total CO_2 values refer to samples that were acidified at the 12-week timepoint to volatilize dissolved inorganic carbon to the headspace prior to sampling headspace gas for analysis. *P*-values were determined between biological assays and processing controls at each timepoint via Student's t-test assuming unequal variance for each condition.

	2 weeks	4 weeks	8 weeks	12 weeks
Headspace CH_4 generation in microcosms supplied with H_2 + formate				
BA4A Avg (nmol CH_4 gdw^{-1})	11	24	55	65
SD	7	14	26	31
p-value	0.17	0.13	0.09	0.11
BA3A Avg (nmol CH_4 gdw^{-1})	0	0	0	0
SD	-	-	-	-
p-value	-	-	-	-
Headspace CO_2 generation in microcosms supplied with H_2 + formate				
BA4A Avg (nmol CO_2 gdw^{-1})	32	47	91	138
SD	22	30	44	44
p-value	0.18	0.15	0.09	0.09
BA3A Avg (nmol CO_2 gdw^{-1})	0	0	0	0
SD	-	-	-	-
p-value	-	-	-	-
Total CO_2 generation in microcosms supplied with H_2 + formate				
BA4A Avg (nmol CO_2 gdw^{-1})	-	-	-	5545
SD	-	-	-	170
p-value	-	-	-	<0.01
BA3A Avg (nmol CO_2 gdw^{-1})	-	-	-	0
SD	-	-	-	-
p-value	-	-	-	-

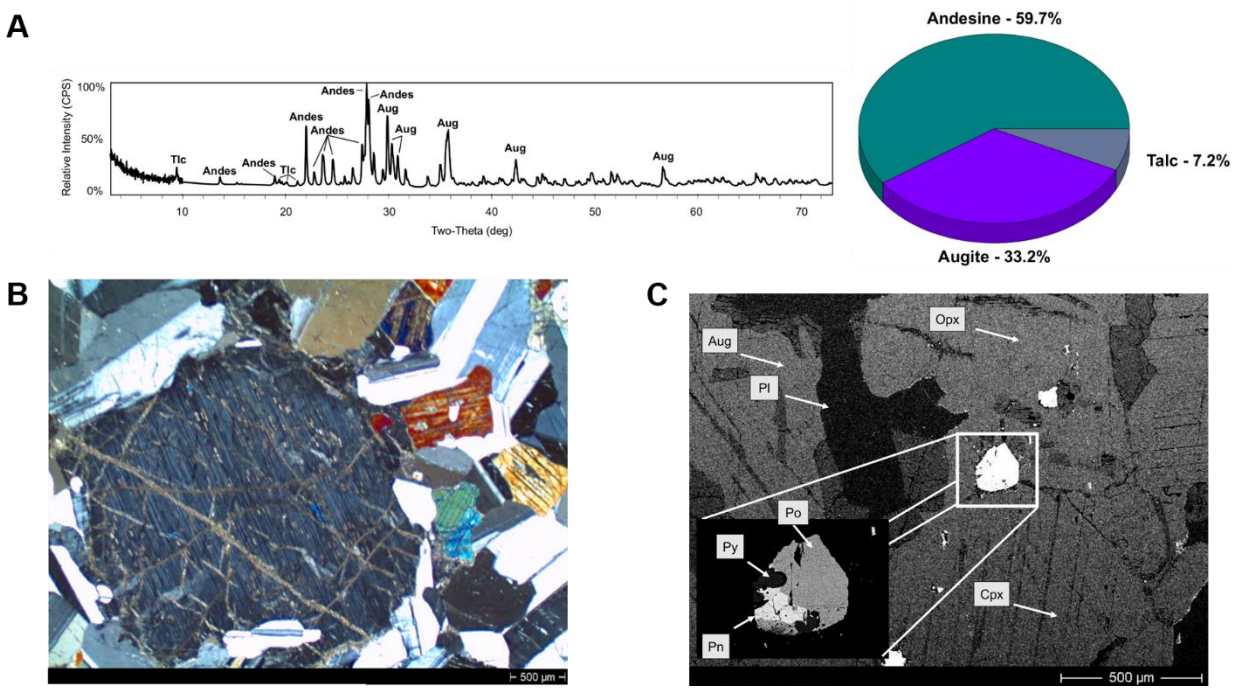

Figure 1. Mineralogical characterization of a gabbro core sample collected from the Stillwater Mine, Montana, U.S.A. (A) X-ray diffraction (XRD) results including XRD spectrum with major peaks identified and estimates of mineral percentages by weight depicted. (B) A photomicrograph using crossed-polarized light at 25x total magnification displaying a large central orthopyroxene grain crosscut with a talc vein and surrounded by clinopyroxene and plagioclase. (C) A scanning electron microscope (SEM) image collected in backscattered electron (BSE) mode showing a representative texture of the gabbro core sample. Major mineral phases were identified using SEM coupled with determination of elemental compositions by energy dispersive X-ray spectroscopy (EDS). All major mineral phases are denoted by standard abbreviations: Aug- augite, Andes- andesine, Cpx- clinopyroxene, Opx- orthopyroxene, Pl- plagioclase, Pn- pentlandite, Po- pyrrhotite, Py- pyrite, and Tlc- talc. Scale bars in panels B and C each represent 500µm. \

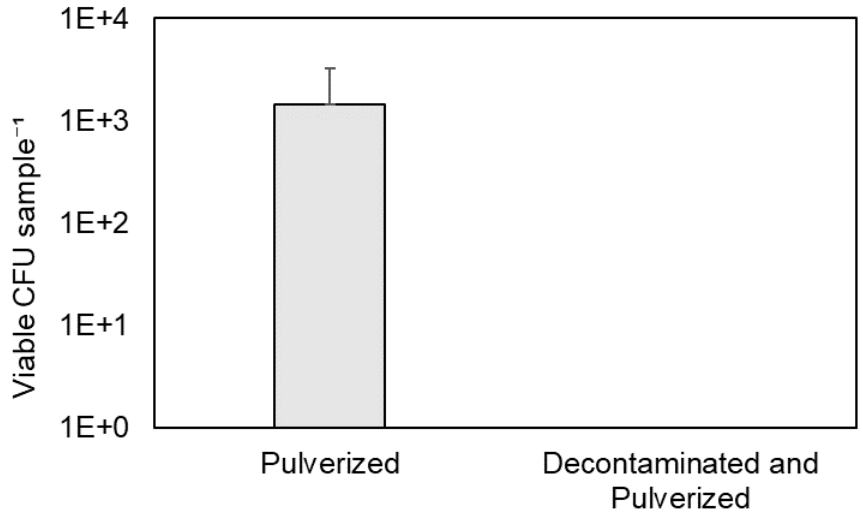

Figure 2. Viability of *Geobacillus stearothermophilus* cells introduced to the surface of a gabbro core to mimic contamination after application of surface decontamination and pulverization protocols. Replicate autoclaved gabbro core samples from the Stillwater Mine were coated in a dense (late log-phase) culture of *G. stearothermophilus* for 60 minutes. One core sample was then decontaminated by spraying with 70% ethanol and passing through a flame prior to pulverization with a jaw crusher (decontaminated and pulverized). The other core sample was pulverized without decontamination (pulverized). *G. stearothermophilus* viability was determined by plating aliquots of each sample on nutrient agar plates. Error bars reflect the standard deviations of ten analytical replicates for each condition.

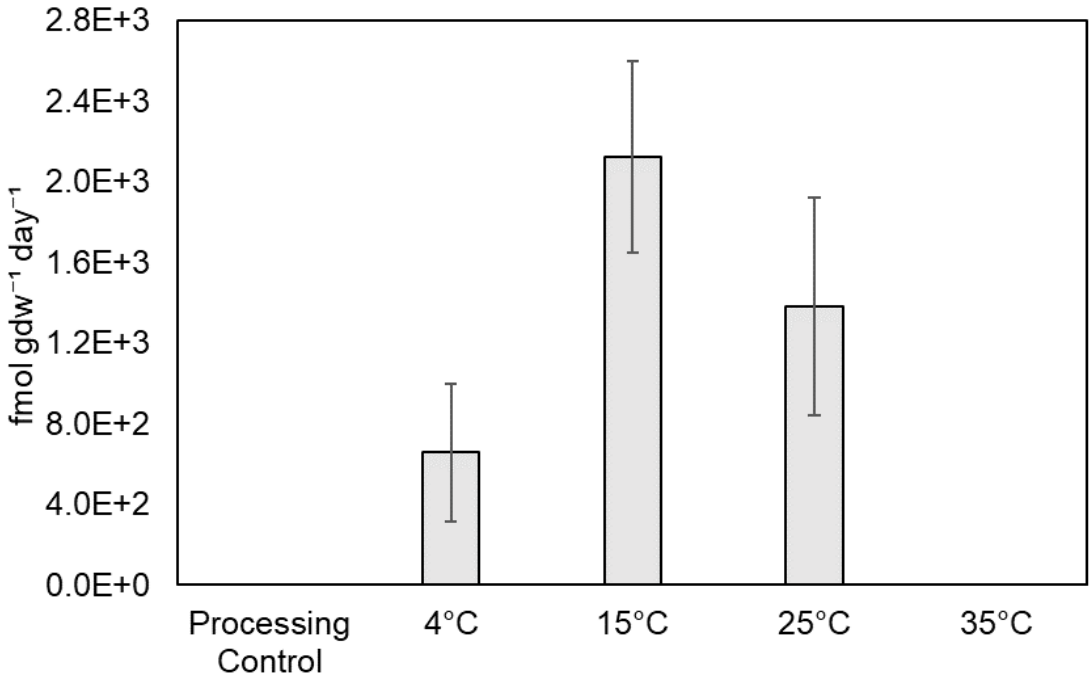

Figure 3. Rates of biological methane production from acetate in a surface decontaminated gabbro core from the Stillwater Mine incubated for 2 weeks at 4°C, 15°C, 25°C, and 35°C following pulverization. Rates of abiotic CH_4 production at each temperature were subtracted from biotic assays to arrive at rates of methanogenesis attributable to biological activity. The processing control depicts the rate of methanogenesis at 15°C attributable to contaminants introduced during laboratory processing of the core. Error bars reflect the standard deviation of three replicate microcosms for each condition.

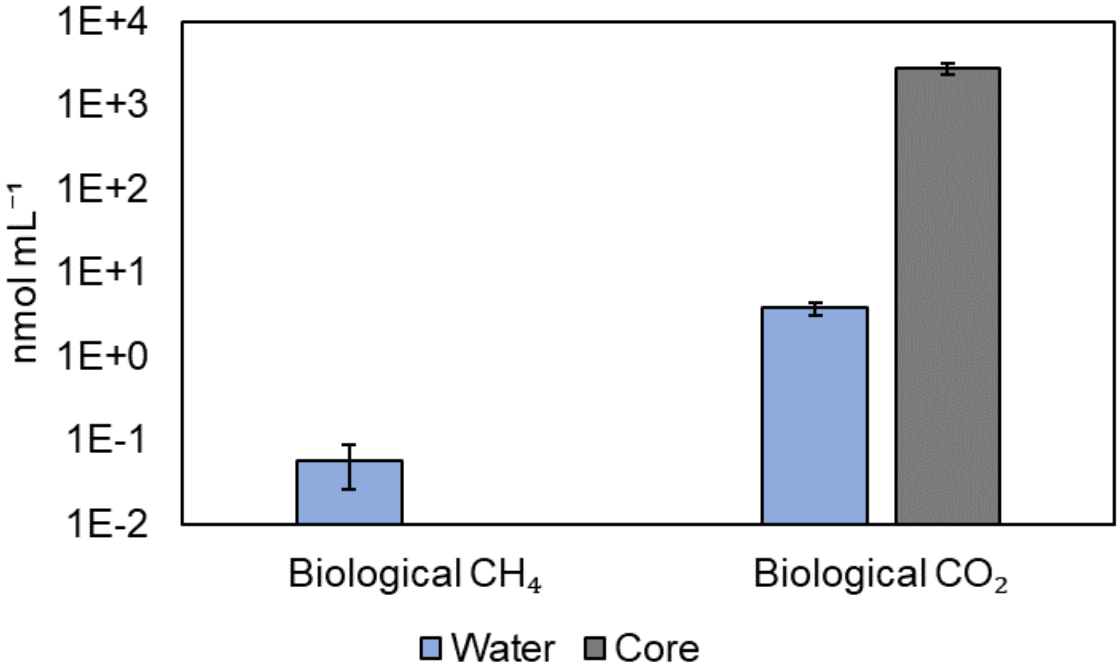

Figure 4. Biological production of headspace CO_2 and CH_4 from acetate in microcosms containing site waters or surface decontaminated and pulverized rock from a core collected from well BA4A (50 m depth) in the Samail Ophiolite, Oman. Water collected from BA4A that had been filter-sterilized (0.1 µm) and doubly autoclaved was used as the growth medium for microcosms containing pulverized rock. The average values of triplicate abiotic control microcosms (containing BA4A site waters that had been doubly autoclaved to account for abiotic reactivity) were subtracted from triplicate live microcosms to arrive at values attributable to microbial cells residing in the waters. The average values of triplicate processing control microcosms (containing BA4A rock core that had been doubly autoclaved prior to processing to account for contaminants added in the laboratory) were subtracted from triplicate live microcosms to arrive at values attributable to microbial cells in the rock that were not laboratory contaminants. Error bars represent the standard deviation of three replicate microcosms at each timepoint for each condition.

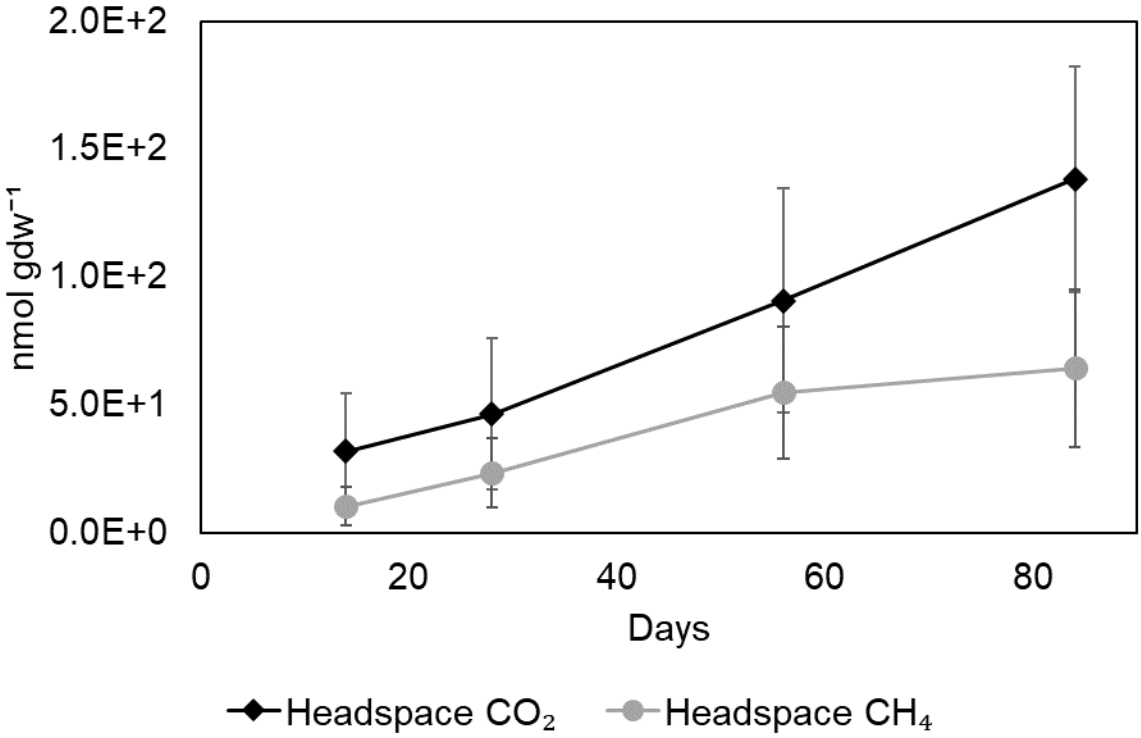

Figure 5. Biological production of headspace CO_2 and CH_4 from formate in microcosms containing surface decontaminated and pulverized rock from a core collected from well BA4A (50 m depth) in the Samail Ophiolite, Oman. Water collected from BA4A that had been filter-sterilized (0.1 µm) and doubly autoclaved was used as the growth medium. The average values of triplicate processing control microcosms (containing BA4A rock core that had been doubly autoclaved prior to processing to account for contaminants added in the laboratory) were subtracted from triplicate live microcosms to arrive at values attributable to microbial cells in the rock that were not laboratory contaminants. Error bars represent the standard deviation of three replicate microcosms at each timepoint for each condition.

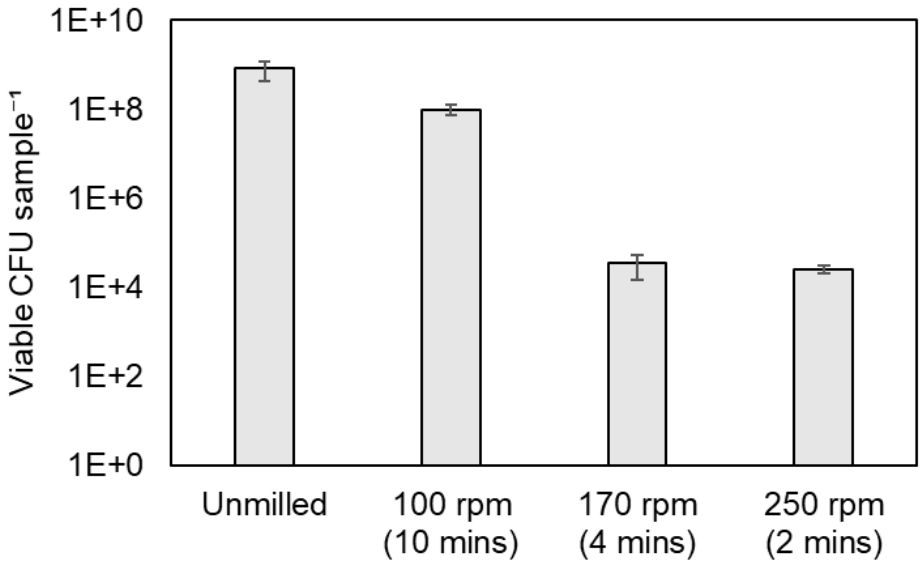

Supplementary Figure 1. Viability of *Escherichia coli* cells following milling at different speeds and milling times. Liquid *E. coli* cultures in the mid-logarithmic phase of growth were added to a gabbro core that had been coarsely pulverized via jaw crushing. Replicate samples were then milled at 100 rpm, 170 rpm, and 250 rpm until the gabbro exhibited a fine, homogenous powder (10, 4, and 2 minutes, respectively). Cell viability was determined by plating aliquots of each sample on Lennox Lysogeny Broth (LB) agar plates. Error bars reflect the standard deviations of three analytical replicates for each condition.

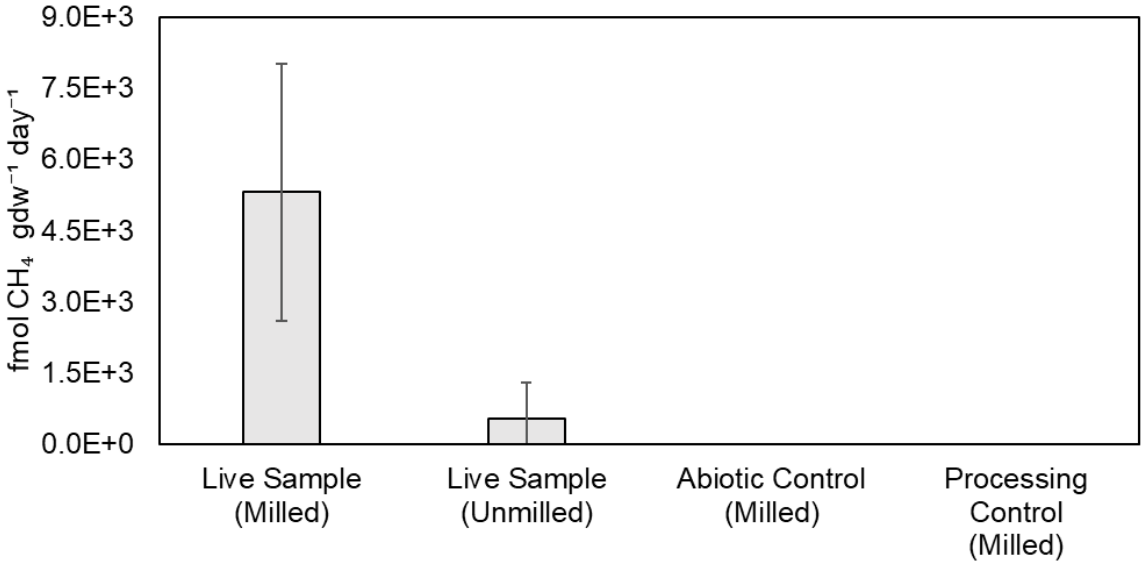

Supplementary Figure 2. Impact of milling on detection of biological methane production from acetate in gabbro cores from the Stillwater Mine, Montana. Rates of biological methane (CH_4) production from acetate were measured using radiolabeled acetate ($^{14}CH_3COO^-$) as a tracer. Gabbro samples had been pulverized via jaw crushing and milled under optimized conditions (100 rpm x 10 min.) or that were not subjected to additional milling are shown. The processing control describes the rate of methanogenesis attributable to contaminants introduced during laboratory processing and the abiotic control describes the rate of methanogenesis attributable to mineral-catalyzed reactivity. Error bars represent the standard deviation of three replicate samples for each condition.

References

1. McMahon S, Parnell J. Weighing the deep continental biosphere. FEMS Microbiol Ecol. 2014; 87(1): 113-20.

2. Carlson R. The abundance of ultramafic rocks in Atlantic Ocean crust. Geophys. J. Int. 2001; 144(1): 37-48.

3. Nisbet E, The geological setting of the earliest life forms. J. Mol. Evol. 1985; 21(3): 289-298.

4. Martin H, Albarede F, Claeys P, Garguad M, Marty B, Morbidelli A, *et al.*, 4. building of a habitable planet. Earth, Moon, and Planets 2006; 98(1-4): 97-151.

5. Fones, EM, Colman, DR, Kraus, EA, Nothaft, DB, Poudel, S, Rempfert, KR, *et al.* Physiological adaptations to serpentinization in the Samail Ophiolite, Oman. ISME J. 2019; 13: 1750-1762.

6. Fones, EM, Colman DR, Kraus EA, Stepanauskas R, Templeton AS, Spear JR, *et al.*, Diversification of methanogens into hyperalkaline serpentinizing environments through adaptations to minimize oxidant limitation. ISME J. 2021; 15: 1121–113.

7. Twing KI, Brazelton WJ, Kubo MD, Hyer AJ, Cardace D, Hoehler TM *et al*. Serpentinization-influenced groundwater harbors extremely low diversity microbial communities adapted to high pH. Front. Microbiol. 2017; 8: 308.

8. Brazelton WJ, Nelson B, Schrenk MO. Metagenomic evidence for H_2 oxidation and H_2 production by serpentinite-hosted subsurface microbial communities. Front. Microbiol. 2012; 2: 268.

9. Brazelton WJ, Thornton CN, Hyer A, Twing KI, Longino AA, Lang SQ *et al*. Metagenomic identification of active methanogens and methanotrophs in serpentinite springs of the Voltri Massif, Italy. PeerJ 2017; 5: e2945.

10. Crespo-Medina M, Twing KI, Sánchez-Murillo R, Brazelton WJ, McCollom TM, Schrenk MO. Methane dynamics in a tropical serpentinizing environment: the Santa Elena Ophiolite, Costa Rica. Front. Microbiol. 2017; 8: 916.

11. Woycheese KM, Meyer-Dombard DAR, Cardace D, Argayosa AM, Arcilla CA. Out of the dark: transitional subsurface-to-surface microbial diversity in a terrestrial serpentinizing seep (Manleluag, Pangasinan, the Philippines). Front. Microbiol. 2015; 6: 44.

12. Neubeck A, Sun L, Müller B, Ivarsson M, Hosgörmez H, Özcan D *et al*. Microbial community structure in a serpentine-hosted abiotic gas seepage at the Chimaera Ophiolite, Turkey. Appl. Environ. Microbiol. 2017; 83: e03430-03416.

13. Lang SQ, Früh-Green GL, Bernasconi SM, Lilley MD, Proskurowski G, Méhay S *et al*. Microbial utilization of abiogenic carbon and hydrogen in a serpentinite-hosted system. Geochim. Cosmochim. Acta. 2012; 92: 82-99.

14. Lang SQ, Früh-Green GL, Bernasconi SM, Brazelton WJ, Schrenk MO, McGonigle JM. Deeply-sourced formate fuels sulfate reducers but not methanogens at Lost City hydrothermal field. Sci. Rep. 2018; 8: 1-10

15. Miller HM, Mayhew LE, Ellison ET, Kelemen P, Kubo M, Templeton AS. Low temperature hydrogen production during experimental hydration of partially-serpentinized dunite. Geochim Cosmochim Ac 2017; 209: 161-183.

16. Ellison ET, Templeton AS, Zeigler SD, Mayhew L, Kelemen PB, Matter J. Low-Temperature Hydrogen Formation During Aqueous Alteration of Serpentinized Peridotite in the Samail Ophiolite. J. Geophys. Res. Solid Earth. 2021; *126*(6): e2021JB021981.

17. McCollom TM, Klein F, Solheid P, Moskowitz B. The effect of pH on rates of reaction and hydrogen generation during serpentinization. Philos. Trans. R. Soc. A. 2020; 378(2165): 20180428.

18. Templeton A, Ellison E. Formation and loss of metastable brucite: does Fe (II)-bearing brucite support microbial activity in serpentinizing ecosystems? Philos. Trans. R. Soc. A. 2020; 378(2165): 20180423.

19. Mayhew LE, Ellison ET, McCollom TM, Trainor TP, Templeton AS. Hydrogen generation from low-temperature water–rock reactions. Nat. Geosci. 2013; 6(6): 478-484.

20. Seewald JS, Zolotov MY, McCollom T. Experimental investigation of single carbon compounds under hydrothermal conditions. Geochim. Cosmochim. Acta. 2006; 70: 446-460.

21. McCollom TM, Seewald JS. Abiotic synthesis of organic compounds in deep-sea hydrothermal environments. Chem. Rev. 2007; 107: 382-401.

22. Russell M, Hall A, Martin W. Serpentinization as a source of energy at the origin of life. Geobiology 2010; 8: 355-371.

23. Chassefiére E, and Leblanc F, Constraining methane release due to serpentinization by the observed D/H ratio on Mars. Earth Planet. Sci. Lett. 2011; 310(3-4): 262-271.

24. Waite JH, Glein CR, Perryman RS, Teolis BD, Magee BA, Miller G, *et al.*, Cassini finds molecular hydrogen in the Enceladus plume: evidence for hydrothermal processes. Science 2017; 356(6334): 155-159.

25. Glein CR, Baross JA, and Waite JH. The pH of Enceladus' ocean. Geochim. Cosmochim. Acta. 2015; 162: 202-219.

26. Vance S, Hand K, and Pappalardo R. Geophysical controls of chemical disequilibria in Europa. Geophys. Res. Lett. 2016; 43(10): 4871-4879.

27. Vance S, Melwani Daswani M. Serpentinite and the search for life beyond Earth. Philos. Trans. R. Soc. A. 2020; 378: 20180421.

28. Morrill PL, Kuenen JG, Johnson OJ, Suzuki S, Rietze A, Sessions AL *et al*. Geochemistry and geobiology of a present-day serpentinization site in California: The Cedars. Geochim. Cosmochim. Acta. 2013; 109: 222-240.

29. Templeton A, Ellison ET, Glombitza C, Morono Y, Rempfert KR, Hoehler T, *et al.*, Accessing the subsurface biosphere within rocks undergoing active low-temperature serpentinization in the Samail Ophiolite (Oman Drilling Project). J Geophys. Res. Biogeosci., In review.

30. Früh-Green GL, Orcutt BN, Rouméjon S, Lilley MD, Morono Y, Cotterill C, *et al*. Magmatism, serpentinization and life: Insights through drilling the Atlantis Massif (IODP Expedition 357). Lithos 2018; 323: 137-155.

31. Motamedi S, Orcutt BN, Früh-Green GL, Twing KI, Pendleton HL, Brazelton WJ. Microbial residents of the Atlantis Massif's shallow serpentinite subsurface. Appl. Environ. Microbiol. 2020; 86(11): e00356-20.

32. Suzuki Y, Yamashita S, Kouduka M, Ao Y, Mukai H, Mitsunobu S, *et al.* Deep microbial proliferation at the basalt interface in 33.5–104 million-year-old oceanic crust. Commun. Biol. 2020; 3(1): 1-9.

33. Li J, Mara P, Schubotz F, Sylvan JB, Burgaud G, Klein F. *et al.* Recycling and metabolic flexibility dictate life in the lower oceanic crust. Nature 2020; 579(7798): 250-255.

34. Wall CJ, Scoates JS, Weis D, Friedman RM, Amini M, Meurer WP. The Stillwater Complex: integrating zircon geochronological and geochemical constraints on the age, emplacement history and crystallization of a large, open-system layered intrusion. J. Petrol. 2018; 59(1): 153-190.

35. Page NJ. Stillwater Complex, Montana: Structure, mineralogy, and petrology of the Basal Zone with emphasis on the occurrence of sulfides. Vol. 1038. 1978: Department of the Interior, Geological Survey.

36. Kelemen P, Matter JM, Teagle DAH, Coggon JA, *et al.* Proceedings of the Oman Drilling Project: Scientific Drilling in the Samail Ophiolite, Sultanate of Oman. International Ocean Discovery Program. 2020; Phase 1 and 2.

37. Rempfert KR, Miller HM, Bompard N, Nothaft D, Matter JM, Kelemen P *et al*. Geological and geochemical controls on subsurface microbial life in the Samail Ophiolite, Oman. Front. Microbiol. 2017; 8: 56.

38. Wells-Bennik MH, Janssen PWM, Klaus V, Yang C, Zwietering MH, Den Besten, HMW. Heat resistance of spores of 18 strains of Geobacillus stearothermophilus and impact of culturing conditions. Int. J. Food Microbiol. 2019; 291: 161-172.

39. Orcutt BN, Bach W, Becker K, Fisher AT, Hentscher M, Toner BM *et al*. Colonization of subsurface microbial observatories deployed in young ocean crust. ISME J. 2011; 5: 692-703.

40. Lever MA, Rouxel O, Alt JC, Shimizu N, Ono S, Coggon RM *et al*. Evidence for microbial carbon and sulfur cycling in deeply buried ridge flank basalt. Science 2013; 339: 1305-1308.

41. Schrenk MO, Kelley DS, Bolton SA, Baross JA. Low archaeal diversity linked to subseafloor geochemical processes at the Lost City Hydrothermal Field, Mid-Atlantic Ridge. Environ. Microbiol. 2004; 6: 1086-1095.

42. Urschel MR, Kubo MD, Hoehler TM, Peters JW, Boyd ES. Carbon source preference in chemosynthetic hot spring communities. Appl Environ Microbiol 2015; 81: 3834-3847.

43. Hamilton TL, Peters JW, Skidmore ML, Boyd ES. Molecular evidence for an active endogenous microbiome beneath glacial ice. ISME J. 2013; 7(7): 1402-12.

44. Neal C, Stanger G. Past and present serpentinisation of ultramafic rocks; an example from the Semail Ophiolite Nappe of Northern Oman. The Chemistry of Weathering. 1985. Springer. 249-275.

45. Paukert AN, Matter JM, Kelemen PB, Shock EL, Havig JR. Reaction path modeling of enhanced in situ CO_2 mineralization for carbon sequestration in the peridotite of the Samail Ophiolite, Sultanate of Oman. Chem. Geol. 2012; 330: 86-100.

46. Gómez M. and Moldenhauer J, Biological indicators for sterilization processes. 2009. Davis Healthcare International Publishing.

47. Magnabosco C, Lin LH, Dong H, Bomberg M, Ghiorse W, Stan-Lotter H, *et al.* The biomass and biodiversity of the continental subsurface. Nat. Geosci. 2018; 11(10): 707-717.

48. Miller HM, Matter JM, Kelemen P, Ellison ET, Conrad ME, Fierer N *et al*. Modern water/rock reactions in Oman hyperalkaline peridotite aquifers and implications for microbial habitability. Geochim. Cosmochim. Acta. 2016; 179: 217-241.

49. Kraus EA, Nothaft D, Stamps BW, Rempfert KR, Ellison ET, Matter JM, *et al.* Molecular evidence for an active microbial methane cycle in subsurface serpentinite-hosted groundwaters in the Samail Ophiolite, Oman. Appl. Environ. Microbiol. 2021; 87(2).

50. Chapelle FH, O'Neill K, Bradley PM, Methé BA, Ciufo SA, Knobel LL, *et al*. A hydrogen-based subsurface microbial community dominated by methanogens. Nature 2002; 415(6869): 312-315.

51. The Mineral Corporation, Competent Person's Report on the Montana Platinum Group Metal Mineral Assets of Sibanye Gold Limited, United States of America. 2017: Cramerview, South Africa.

52. Colman DR, Lindsay MR, and Boyd ES. Mixing of meteoric and geothermal fluids supports hyperdiverse chemosynthetic hydrothermal communities. Nat. Commun. 2019; 10(1): 1-13.

53. McCollom, T.M. and Seewald J.S. Experimental constraints on the hydrothermal reactivity of organic acids and acid anions: I. Formic acid and formate. Geochim. Cosmochim. Acta 2003; 67: 3625-3644.

54. Lang, S.Q., Butterfield, D.A., Schulte, M., Kelley, D.S., and Lilley, M.D. Elevated concentrations of formate, acetate and dissolved organic carbon found at the Lost City hydrothermal field. Geochim. Cosmochim. Acta 2010; 74: 941-952.

55. Thauer RK, Kaster AK, Seedorf H, Buckel W, and Hedderich, R. Methanogenic archaea: ecologically relevant differences in energy conservation. Nat. Rev. Microbiol. 2008; 6: 579-591.

56. Trevors J, The subsurface origin of microbial life on the Earth. Res. Microbiol. 2002; 153(8): 487-491.

CHAPTER FIVE

CONCLUSIONS AND FUTURE DIRECTIONS

Conclusions

In this dissertation, I aimed to characterize how serpentinization reaction progress shapes microbial life in subsurface fracture fluids and ultramafic rocks of the Samail Ophiolite, Sultanate of Oman. In Chapter 2, I began by analyzing the influence of serpentinization reaction progress on planktonic cell densities, community functional potentials, carbon cycling activities, and genomic features in waters spanning a range in pH values (a proxy for serpentinization reaction progress). I hypothesized that microbial cell densities would decrease with increasing pH and that microbial community functional potential would be shaped by geochemical characteristics. I further hypothesized that microbial cells would be able to metabolize single carbon substrates that can be formed as a result of serpentinization (i.e., formate and CO), but that the biological rates of utilization of these substrates would decrease with increasing serpentinization reaction progress.

Consistent with my first hypothesis, cell densities were higher in Type I waters as compared with Type II waters. However, cell densities were highest in a well where mixing occurs between Type I and Type II waters. Mixing may provide microorganisms with higher concentrations of oxidants and reductants that are in disequilibrium when compared with end-member waters, thereby providing additional chemical energy for cells to fuel their metabolisms and to replicate, as has been previously suggested (1, 2). Community functional potential, as inferred from metagenomic reconstructions of proteins annotated as involved in “metabolism,” clustered by water type (i.e., Type I, Type II, and mixing zones between end-member waters)

when ordinated on a PCoA plot. This suggests that waters influenced by similar degrees of serpentinization reaction progress harbored microbial communities with similar metabolism types, and genes involved in anaerobic microbial metabolisms were additionally found to be enriched among Type II waters. Consistent with my second hypothesis, metagenomes encoded homologues of select functional genes associated with formate metabolism (formate dehydrogenase), carbon monoxide metabolism (Mo- or Ni-carbon monoxide dehydrogenase), and inorganic carbon utilization via the Wood-Ljungdahl pathway (i.e., methyl-coenzyme M reductase and acetyl-CoA synthase). In line with these genomic predictions, biological oxidation of formate and carbon monoxide to carbon dioxide, reduction of inorganic carbon to methane, and assimilation of these substrates to biomass were observed in microcosms amended with ^{14}C-radiolabeled substrates (i.e., ^{14}C-$HCOO^-$, ^{14}C-CO, and ^{14}C-HCO_3^-, respectively). However, as expected, the rates of these biological substrate transformations generally decreased with increasing pH, as may be consistent with declining cell densities with slow metabolic rates due to increasingly extreme conditions in these waters.

Finally, I hypothesized that cells living in waters circulating through the subsurface of the Samail Ophiolite would exhibit a suite of adaptations allowing them to minimize stress associated with nutrient and energy limitation imposed by serpentinization. I hypothesized that carbon limitation in hyperalkaline wells would lead cells to assimilate a greater fraction of metabolized carbon than cells inhabiting circumneutral waters. A generally negative relationship between the ratio of HCO_3^- and $HCOO^-$ dissimilation to assimilation and pH was observed, with the lowest ratios observed in communities inhabiting Type II waters. This suggests that carbon limitation (substrate assimilation) may outweigh energy limitation (substrate dissimilation) for

autotrophic populations in Type II waters in Oman. Additionally, I observed a significant inverse relationship between the mean estimated size of metagenome assembled genomes (MAGs) reconstructed from communities inhabiting well waters in the Samail Ophiolite and the pH of those waters. This observation is consistent with genomic streamlining as a potential adaptation to energetic stress imposed on cells by increased serpentinization reaction progress. Furthermore, the average oxidation state of carbon (Z_c) in inferred proteomes was found to decrease with increasing pH of the waters hosting these microbial communities. This may reflect selection to minimize energetic costs and maximize protein stability during protein synthesis in cells subject to the highly reducing conditions of Type II waters.

A high relative abundance of 16S rRNA gene sequences affiliated with the hydrogenotrophic and autotrophic lineage of methanogens, *Methanobacterium*, had been previously detected in Type II waters of the Samail Ophiolite (2, 3) and other globally distributed sites of serpentinization (4-6). However, it was not understood how this putatively early-evolving lineage is able to overcome the extreme conditions, particularly inorganic carbon limitation, imposed by highly reacted waters in serpentinizing environments. Two distinct lineages affiliated with *Methanobacterium* were detected in metagenomes recovered from subsurface well waters spanning a range in pH values from the Samail Ophiolite. One MAG (Type I) represented an abundant microbial lineage in a well with circumneutral water (pH 7.6), whereas another MAG (Type II) represented a lineage that was abundant in a well with hyperalkaline water (pH 11.1 - 11.3). The Type I lineage encoded proteins to couple hydrogen oxidation to CO_2 reduction, typical of hydrogenotrophic methanogens. However, the Type II lineage branched from the Type I lineage and lacked homologs of two key oxidative [NiFe]-

hydrogenases. These functions of the absent hydrogenases were presumably replaced by formate dehydrogenases that oxidize formate to yield reductant and cytoplasmic CO_2, allowing cells to overcome CO_2/oxidant limitation in high pH waters via a pathway that is unique among characterized Methanobacteria. This prediction was supported by microcosm-based radiotracer experiments that showed significant biological methane generation from formate, but not bicarbonate, in waters where the Type II lineage was detected in highest relative abundance. In contrast, methane generation was observed from both formate and bicarbonate in waters where the Type I lineage was detected in highest relative abundance, as would be expected among canonical hydrogenotrophic methanogens. A combination of phylogenetic and gene distribution data relative to closely related taxa indicated that the Type II lineage was derived from the Type I lineage, suggesting that the replacement of H_2-based reductant by formate-based reductant is a derived trait. This suggests that the directionality of the diversification of *Methanobacterium* inhabiting the Samail Ophiolite was from circumneutral into hyperalkaline waters, the latter of which is likely to be limited in DIC, but where formate could be supplied by serpentinization reactions.

The observation that the Type II lineage of *Methanobacterium* appears to be derived from the Type I lineage and continues to diversify into increasingly hyperalkaline waters is potentially in line with the proposition that Earth's early oceans were mildly acidic (pH 5-6) and CO_2-rich, due to volcanism and magmatic degassing (7). The first methanogen cells therefore may have emerged in an environment that is reminiscent of Type I waters, where mildly acidic CO_2-rich waters (sourced either from oceanic or rainwaters) react with mafic to ultramafic rocks to generate anoxic circumneutral to alkaline waters. Instead of suggesting that methanogens and

acetogens emerged in a hyperalkaline environment with extremely limiting concentrations of DIC, the higher relative abundance of methanogenic and putatively acetogenic populations commonly detected in Type II waters as compared with Type I waters in modern serpentinizing environments may reflect the diversification of other cell types throughout Earth's history to exploit the larger relative niche space present in Type I waters as compared with Type II waters.

Finally, I evaluated the hypothesis that microbial cells are present within the pore spaces and microfractures of the mafic to ultramafic rocks of the Samail Ophiolite and that their activities can be measured via laboratory experiments. Microcosm assays were developed and optimized to detect the activities of cells residing in pore spaces and microfractures of mafic to ultramafic igneous rocks. Application of this optimized assay to gabbro core from the Stillwater Mine, Montana, USA revealed maximal methane production from acetate in 2-week incubations at *in situ* temperature. Controls indicate that these activities are not attributable to contamination introduced during drilling, exhumation, or laboratory processing of the core. This assay was then applied to two rock cores from the Samail Ophiolite, Sultanate of Oman, which is undergoing low temperature serpentinization. Higher rates of formate and acetate metabolism by habitable volume were observed among cells inhabiting a dunite core interfacing waters of pH 9.6 than have ever been measured among cells inhabiting subsurface waters of the Samail Ophiolite. Collectively, these results indicate that active microbial communities inhabit the rock pore spaces and/or microfractures of igneous rocks and raise new questions about the size and contribution of the subsurface biosphere to global nutrient cycles. The development of methods to sensitively detect endolithic life in igneous rocks has implications for life detection on other planetary bodies where similar rock types prevail, such as Mars, Europa, and Enceladus.

However, evidence of biological acetate and formate metabolism was not observed in a peridotite core interfacing waters of pH 11.4, suggesting the latter may not host a robust population of cells capable of metabolizing these substrates and providing potential boundary conditions for future life detection strategies.

Future Directions

Ongoing efforts will be made to extract DNA, amplify marker genes, and identify microbial community members inhabiting pulverized rock from the Samail Ophiolite, including intact biofilm polymerase chain reactions [8] and separating cells from mineral surfaces per the methods of Morono et al., 2013, before subjecting them to bulk DNA extraction or single cell genomic sequencing [9]. To evaluate the hypothesis that the increased activity observed in microcosms containing pulverized rock, as compared with microcosms containing waters alone, is due to nutrients or energy substrates generated via water-rock interactions from freshly exposed mineral surfaces and/or abundant colonizable surface area provided by pulverized rock, an experiment is underway in which microcosms containing sterilized rock from BA3A (80 m depth) and BA4A (50 m depth) and non-sterilized site waters from BA3A (75 m depth) and BA4A (50 m depth) were amended with acetate (including [1,2]-^{14}C acetate). Additionally, further study is needed to comprehensively characterize the distribution and activities of subsurface life inhabiting pore spaces and microfractures in mafic to ultramafic rocks of the Samail Ophiolite. Thus, future studies could apply the methods developed in Chapter 4 to additional core sections that have been collected and preserved from every 10 m depth (up to 300 m or 400 m depth) from boreholes BA3A/BA4A and borehole BA1B (coordinates: 22°52.874' N 58°42.035' E) in the Samail Ophiolite to robustly evaluate the influence of geology and

geochemistry upon the activities of endolithic cells. Additionally, genomic insights into the metabolism of *Methanobacterium* Type II described in Chapter 3 and previous geochemical data have guided cultivation efforts for this organism from BA3A site waters. Boyd lab members are successfully growing an enrichment culture containing approximately three cell morphologies and generating methane that will be used in further attempts to isolate and characterize *Methanobacterium* Type II. Additionally, 16S rRNA gene sequences will be amplified from DNA extracted from this co-culture and affiliation of these sequences to cultured representatives will be used to begin investigating the potential interactions between microbial community members inhabiting Type II waters.

The results of Chapter 3 also suggested that, despite extreme DIC limitation, cells affiliated with *Methanobacterium* are active in waters sampled from deep wells intersecting the Samail Ophiolite, Oman and appear to be actively diversifying. The prevalence of divergent transposases and viral signatures (CRISPR/Cas loci) in single cell genomes (SCG) within the *Methanobacterium* Type II population suggest that viral infection and horizontal gene transfer have and continue to mediate diversification of methanogens through acquisition of physiological capabilities that provide a competitive advantage in hyperalkaline conditions. To further understand the recent evolution of *Methanobacterium* lineages and other microbial populations in subsurface waters of the Samail Ophiolite, 198 single-cell genomes and a metagenome from each of seven samples spanning a range in pH and depth conditions will be generated via a project entitled “Microbial Carbon Cycling in the Samail Ophiolite” that was selected for the Joint Genome Institute’s Community Science Program Award, led by Dr. Rachel Spietz, Dr. Eric Boyd, and me. Additionally, boreholes NSHQ14 and BA3A were drilled only a

few meters from one another and both exhibit fluids of high pH (approximately 11.2 in NSHQ14 and 11.5 in BA3A). The single cell genomics and metagenomics data generated through this project will help us to investigate the dynamics of evolutionary ecology and local diversification of cell populations inhabiting these waters.

References

1. Canovas PA, Hoehler T, Shock EL. Geochemical bioenergetics during low-temperature serpentinization: An example from the Samail ophiolite, Sultanate of Oman. J. Geophys. Res. Biogeosci. 2017; 122: 1821-1847.

2. Rempfert KR, Miller HM, Bompard N, Nothaft D, Matter JM, Kelemen P *et al*. Geological and geochemical controls on subsurface microbial life in the Samail Ophiolite, Oman. Front. Microbiol. 2017; 8: 56.

3. Miller HM, Matter JM, Kelemen P, Ellison ET, Conrad ME, Fierer N *et al*. Modern water/rock reactions in Oman hyperalkaline peridotite aquifers and implications for microbial habitability. Geochim. Cosmochim. Acta. 2016; 179: 217-241.

4. Crespo-Medina M, Twing KI, Sánchez-Murillo R, Brazelton WJ, McCollom TM, Schrenk MO. Methane dynamics in a tropical serpentinizing environment: the Santa Elena Ophiolite, Costa Rica. Front. Microbiol. 2017; 8: 916.

5. Woycheese KM, Meyer-Dombard DAR, Cardace D, Argayosa AM, Arcilla CA. Out of the dark: transitional subsurface-to-surface microbial diversity in a terrestrial serpentinizing seep (Manleluag, Pangasinan, the Philippines). Front. Microbiol. 2015; 6: 44.

6. Brazelton WJ, Thornton CN, Hyer A, Twing KI, Longino AA, Lang SQ *et al*. Metagenomic identification of active methanogens and methanotrophs in serpentinite springs of the Voltri Massif, Italy. PeerJ 2017; 5: e2945.

7. Russell MJ, Martin W. The rocky roots of the acetyl-CoA pathway. Trends Biochem. Sci. 2004; 29: 358-363.

8. Boyd ES, Cummings DE, Geesey GG. Mineralogy influences structure and diversity of bacterial communities associated with geological substrata in a pristine aquifer. Microb. Ecol. 2007; 54(1): 170-182.

9. Morono Y, Terada T, Kallmeyer J, Inagaki F. An improved cell separation technique for marine subsurface sediments: applications for high-throughput analysis using flow cytometry and cell sorting. Environ. Microbiol. 2013; 15(10), 2841-2849.

CUMULATIVE REFERENCES

1. Schulte M, Blake D, Hoehler T, McCollom T. Serpentinization and its implications for life on the early Earth and Mars. Astrobiology 2006; 6: 364-376.

2. Russell M, Hall A, Martin W. Serpentinization as a source of energy at the origin of life. Geobiology 2010; 8: 355-371.

3. McCollom TM, Klein F, Robbins M, Moskowitz B, Berquó TS, Jöns N *et al*. Temperature trends for reaction rates, hydrogen generation, and partitioning of iron during experimental serpentinization of olivine. Geochim. Cosmochim. Acta. 2016; 181: 175-200.

4. Seewald JS, Zolotov MY, McCollom T. Experimental investigation of single carbon compounds under hydrothermal conditions. Geochim. Cosmochim. Acta. 2006; 70: 446-460.

5. McCollom TM, Seewald JS. Abiotic synthesis of organic compounds in deep-sea hydrothermal environments. Chem. Rev. 2007; 107: 382-401.

6. Rempfert KR, Miller HM, Bompard N, Nothaft D, Matter JM, Kelemen P *et al*. Geological and geochemical controls on subsurface microbial life in the Samail Ophiolite, Oman. Front. Microbiol. 2017; 8: 56.

7. Canovas PA, Hoehler T, Shock EL. Geochemical bioenergetics during low-temperature serpentinization: An example from the Samail ophiolite, Sultanate of Oman. J. Geophys. Res. Biogeosci. 2017; 122: 1821-1847.

8. Leong JAM, Shock EL. Thermodynamic constraints on the geochemistry of low-temperature, continental, serpentinization-generated fluids. Am. J. Sci. 2020; 320: 185-235.

9. Crespo-Medina M, Twing KI, Sánchez-Murillo R, Brazelton WJ, McCollom TM, Schrenk MO. Methane dynamics in a tropical serpentinizing environment: the Santa Elena Ophiolite, Costa Rica. Front. Microbiol. 2017; 8: 916.

10. Twing KI, Brazelton WJ, Kubo MD, Hyer AJ, Cardace D, Hoehler TM *et al*. Serpentinization-influenced groundwater harbors extremely low diversity microbial communities adapted to high pH. Front. Microbiol. 2017; 8: 308.

11. Brazelton WJ, Morrill PL, Szponar N, Schrenk MO. Bacterial communities associated with subsurface geochemical processes in continental serpentinite springs. Appl. Environ. Microbiol. 2013; 79: 3906-3916.

12. Lang SQ, Früh-Green GL, Bernasconi SM, Lilley MD, Proskurowski G, Méhay S *et al*. Microbial utilization of abiogenic carbon and hydrogen in a serpentinite-hosted system. Geochim. Cosmochim. Acta. 2012; 92: 82-99.

13. Schrenk MO, Kelley DS, Bolton SA, Baross JA. Low archaeal diversity linked to subseafloor geochemical processes at the Lost City Hydrothermal Field, Mid-Atlantic Ridge. Environ. Microbiol. 2004; 6: 1086-1095.

14. Brazelton WJ, Thornton CN, Hyer A, Twing KI, Longino AA, Lang SQ *et al*. Metagenomic identification of active methanogens and methanotrophs in serpentinite springs of the Voltri Massif, Italy. PeerJ 2017; 5: e2945.

15. Morrill PL, Kuenen JG, Johnson OJ, Suzuki S, Rietze A, Sessions AL *et al*. Geochemistry and geobiology of a present-day serpentinization site in California: The Cedars. Geochim. Cosmochim. Acta. 2013; 109: 222-240.

16. Tiago I, Chung AP, Veríssimo A. Bacterial diversity in a nonsaline alkaline environment: heterotrophic aerobic populations. Appl. Environ. Microbiol. 2004; 70: 7378-7387.

17. Brazelton WJ, Nelson B, Schrenk MO. Metagenomic evidence for H_2 oxidation and H_2 production by serpentinite-hosted subsurface microbial communities. Front. Microbiol. 2012; 2: 268.

18. Morrill PL, Brazelton WJ, Kohl L, Rietze A, Miles SM, Kavanagh H *et al*. Investigations of potential microbial methanogenic and carbon monoxide utilization pathways in ultra-basic reducing springs associated with present-day continental serpentinization: the Tablelands, NL, CAN. Front. Microbiol. 2014; 5: 613.

19. Woycheese KM, Meyer-Dombard DAR, Cardace D, Argayosa AM, Arcilla CA. Out of the dark: transitional subsurface-to-surface microbial diversity in a terrestrial serpentinizing seep (Manleluag, Pangasinan, the Philippines). Front. Microbiol. 2015; 6: 44.

20. Neubeck A, Sun L, Müller B, Ivarsson M, Hosgörmez H, Özcan D *et al*. Microbial community structure in a serpentine-hosted abiotic gas seepage at the Chimaera Ophiolite, Turkey. Appl. Environ. Microbiol. 2017; 83: e03430-03416.

21. Lang SQ, Früh-Green GL, Bernasconi SM, Brazelton WJ, Schrenk MO, McGonigle JM. Deeply-sourced formate fuels sulfate reducers but not methanogens at Lost City hydrothermal field. Sci. Rep. 2018; 8: 1-10.

22. Suzuki S, Ishii Si, Wu A, Cheung A, Tenney A, Wanger G *et al*. Microbial diversity in The Cedars, an ultrabasic, ultrareducing, and low salinity serpentinizing ecosystem. Proc. Natl. Acad. Sci. 2013; 110: 15336-15341.

23. Miller HM, Matter JM, Kelemen P, Ellison ET, Conrad ME, Fierer N *et al*. Modern water/rock reactions in Oman hyperalkaline peridotite aquifers and implications for microbial habitability. Geochim. Cosmochim. Acta. 2016; 179: 217-241.

24. Weiss MC, Sousa FL, Mrnjavac N, Neukirchen S, Roettger M, Nelson-Sathi S *et al*. The physiology and habitat of the last universal common ancestor. Nat. Microbiol. 2016; 1: 1-8.

25. Martin WF, Weiss MC, Neukirchen S, Nelson-Sathi S, Sousa FL. Physiology, phylogeny, and LUCA. Microb. Cell 2016; 3: 582.

26. Russell MJ, Martin W. The rocky roots of the acetyl-CoA pathway. Trends Biochem. Sci. 2004; 29: 358-363.

27. Berg IA. Ecological aspects of the distribution of different autotrophic CO_2 fixation pathways. Appl. Environ. Microbiol. 2011; 77: 1925.

28. Ljungdahl L. The autotrophic pathway of acetate synthesis in acetogenic bacteria. Annu. Rev. Microbiol. 1986; 40: 415-450.

29. Moore EK, Jelen BI, Giovannelli D, Raanan H, Falkowski PG. Metal availability and the expanding network of microbial metabolisms in the Archaean eon. Nat. Geosci. 2017; 10: 629-636.

30. Lyons TW, Reinhard CT, Planavsky NJ. The rise of oxygen in Earth's early ocean and atmosphere. Nature 2014; 506: 307-315.

31. Martin W, Baross J, Kelley D, Russell MJ. Hydrothermal vents and the origin of life. Nat. Rev. Microbiol. 2008; 6: 805-814.

32. Sojo V, Herschy B, Whicher A, Camprubi E, Lane N. The origin of life in alkaline hydrothermal vents. Astrobiology 2016; 16: 181-197.

33. Martin WF, Sousa FL. Early microbial evolution: the age of anaerobes. Cold Spring Harb. Perspect. Biol. 2016; 8: a018127.

34. Chassefiére E, and Leblanc, F. Constraining methane release due to serpentinization by the observed D/H ratio on Mars. Earth Planet. Sci. Lett. 2011; 310: 262-271.

35. Glein CR, Baross JA, Waite JH. The pH of Enceladus' ocean. Geochim. Cosmochim. Acta. 2015; 162: 202-219.

36. Waite JH, Glein CR, Perryman RS, Teolis BD, Magee BA, Miller G *et al*. Cassini finds molecular hydrogen in the Enceladus plume: evidence for hydrothermal processes. Science 2017; 356: 155-159.

37. Vance S, Melwani Daswani M. Serpentinite and the search for life beyond Earth. Philos. Trans. R. Soc. A. 2020; 378: 20180421.

38. Kelemen P, Matter J, Teagle D, Coggon J, Team ODPS. Proceedings of the Oman Drilling Project: Scientific Drilling in the Samail Ophiolite, Sultanate of Oman. International Ocean Discovery Program 2020; Phase 1 and 2.

39. Paukert AN, Matter JM, Kelemen PB, Shock EL, Havig JR. Reaction path modeling of enhanced in situ CO_2 mineralization for carbon sequestration in the peridotite of the Samail Ophiolite, Sultanate of Oman. Chem. Geol. 2012; 330: 86-100.

40. Barnes I, O'Neil JR. The relationship between fluids in some fresh alpine-type ultramafics and possible modern serpentinization, western United States. Geol. Soc. Am. Bull. 1969; 80: 1947-1960.

41. Neal C, Stanger G. Past and present serpentinisation of ultramafic rocks; an example from the Semail Ophiolite Nappe of Northern Oman. The Chemistry of Weathering. 1985. Springer. 249-275.

42. Boyd ES, Amenabar MJ, Poudel S, Templeton AS. Bioenergetic constraints on the origin of autotrophic metabolism. Philos. Trans. R. Soc. A. 2020; 378: 1471-2962.

43. Buckel W, Thauer RK. Energy conservation via electron bifurcating ferredoxin reduction and proton/Na+ translocating ferredoxin oxidation. Biochim. Biophys. Acta Bioenerg. 2013; 1827: 94-113.

44. Orcutt BN, Bach W, Becker K, Fisher AT, Hentscher M, Toner BM *et al*. Colonization of subsurface microbial observatories deployed in young ocean crust. ISME J. 2011; 5: 692-703.

45. Lever MA, Rouxel O, Alt JC, Shimizu N, Ono S, Coggon RM *et al*. Evidence for microbial carbon and sulfur cycling in deeply buried ridge flank basalt. Science 2013; 339: 1305-1308.

46. Sousa FL, Martin WF. Biochemical fossils of the ancient transition from geoenergetics to bioenergetics in prokaryotic one carbon compound metabolism. Biochim Biophys Acta 2014; 1837: 964-981.

47. Kelemen PB, Matter J, Streit EE, Rudge JF, Curry WB, Blusztajn J. Rates and mechanisms of mineral carbonation in peridotite: natural processes and recipes for enhanced, in situ CO2 capture and storage. Annu Rev Earth Pl Sc 2011; 39: 545-576.

48. Clark ID, Fontes JC. Paleoclimatic Reconstruction in northern Oman based on carbonates from hyperalkaline groundwaters. Quaternary Res 1990; 33: 320-336.

49. Nicolas A, Boudier E, Ildefonse B, Ball E. Accretion of Oman and United Arab Emirates ophiolite - discussion of a new structural map. Mar Geophys Res 2000; 21: 147-179.

50. Okland I, Huang S, Dahle H, Thorseth IH, Pedersen RB. Low temperature alteration of serpentinized ultramafic rock and implications for microbial life. Chem Geol 2012; 318: 75-87.

51. Kampbell D, Wilson J, McInnes D. Determining dissolved hydrogen, methane, and vinyl chloride concentrations in aqueous solution on a nanomolar scale with the bubble strip method. Proceedings of the 1998 Conference on Hazardous Waste Research 1998: 176-190.

52. Fu L, Niu B, Zhu Z, Wu S, Li W. CD-HIT: accelerated for clustering the next-generation sequencing data. J Bioinform 2012; 28: 3150-3152.

53. Colman DR, Poudel S, Hamilton TL, Havig JR, Selensky MJ, Shock EL et al. Geobiological feedbacks and the evolution of thermoacidophiles. ISME J 2018; 12: 225-236.

54. Kanehisa M. Enzyme annotation and metabolic reconstruction using KEGG. Protein Function Prediction: Methods and Protocols 2017; 1611: 135-145.

55. Moriya Y, Itoh M, Okuda S, Yoshizawa AC, Kanehisa M. KAAS: an automatic genome annotation and pathway reconstruction server. Nucleic Acids Res 2007; 35: W182-W185.

56. Team RC. R: a language and environment for statistical computing. Version 3.0. 1. R Foundation for Statistical Computing. Vienna, Austria 2013.

57. Oksanen J, Blanchet FG, Kindt R, Legendre P, O'hara R, Simpson GL et al. vegan: community ecology package. R package version 2.3 edn 2015.

58. Markowitz VM, Chen IMA, Palaniappan K, Chu K, Szeto E, Grechkin Y et al. IMG: the integrated microbial genomes database and comparative analysis system. Nucleic Acids Res 2012; 40: D115-D122.

59. Parks DH, Imelfort M, Skennerton CT, Hugenholtz P, Tyson GW. CheckM: assessing the quality of microbial genomes recovered from isolates, single cells, and metagenomes. Genome Res 2015; 25: 1043-1055.

60. Dick JM, Shock EL. Calculation of the relative chemical stabilities of proteins as a function of temperature and redox chemistry in a hot spring. PLoS One 2011; 6: e22782.

61. Urschel MR, Kubo MD, Hoehler TM, Peters JW, Boyd ES. Carbon source preference in chemosynthetic hot spring communities. Appl Environ Microbiol 2015; 81: 3834-3847.

62. Schrenk MO, Brazelton WJ, Lang SQ. Serpentinization, carbon, and deep life. Rev Mineral Geochem 2013; 75: 575-606.

63. Suzuki S, Ishii S, Hoshino T, Rietze A, Tenney A, Morrill PL et al. Unusual metabolic diversity of hyperalkaliphilic microbial communities associated with subterranean serpentinization at The Cedars. ISME J 2017; 11: 2584-2598.

64. Colman DR, Lindsay M. R., and E.S. Boyd. Mixing of meteoric and geothermal fluids supports hyperdiverse chemosynthetic hydrothermal communities. Nat Commun 2019; 10: 681.

65. Adam PS, Borrel G, Gribaldo S. Evolutionary history of carbon monoxide dehydrogenase/acetyl-CoA synthase, one of the oldest enzymatic complexes. PNAS 2018; 115: E1166-1173.

66. Jeoung JH, Fesseler J, Goetzl S, Dobbek H. Carbon monoxide. toxic gas and fuel for anaerobes and aerobes: carbon monoxide dehydrogenases. Met Ions Life Sci 2014; 14: 37-69.

67. Can M, Armstrong FA, Ragsdale SW. Structure, function, and mechanism of the nickel metalloenzymes, CO dehydrogenase, and acetyl-CoA synthase. Chem Rev 2014; 114: 4149-4174.

68. Nielsen MB, Kjeldsen KU, Ingvorsen K. Desulfitibacter alkalitolerans gen. nov., sp. nov., an anaerobic, alkalitolerant, sulfite-reducing bacterium isolated from a district heating plant. Int J Syst Evol Microbiol 2006; 56: 2831-2836.

69. McCollom TM, Seewald JS. A reassessment of the potential for reduction of dissolved CO_2 to hydrocarbons during serpentinization of olivine. Geochim Cosmochim Ac 2001; 65: 3769-3778.

70. Miller HM, Mayhew LE, Ellison ET, Kelemen P, Kubo M, Templeton AS. Low temperature hydrogen production during experimental hydration of partially-serpentinized dunite. Geochim Cosmochim Ac 2017; 209: 161-183.

71. Brazelton WJ, Schrenk MO, Kelley DS, Baross JA. Methane- and sulfur-metabolizing microbial communities dominate the Lost City hydrothermal field ecosystem. Appl Environ Microbiol 2006; 72: 6257-6270.

72. Kohl L, Cumming E, Cox A, Rietze A, Morrissey L, Lang SQ et al. Exploring the metabolic potential of microbial communities in ultra-basic, reducing springs at The Cedars, CA, USA: Experimental evidence of microbial methanogenesis and heterotrophic acetogenesis. J Geophys Res-Biogeo 2016; 121: 1203-1220.

73. Postec A, Quemeneur M, Bes M, Mei N, Benaissa F, Payri C et al. Microbial diversity in a submarine carbonate edifice from the serpentinizing hydrothermal system of the Prony Bay (New Caledonia) over a 6-year period. Front Microbiol 2015; 6.

74. Ermler U, Grabarse W, Shima S, Goubeaud M, Thauer RK. Crystal structure of methyl coenzyme M reductase: The key enzyme of biological methane formation. Science 1997; 278: 1457-1462.

75. Boone DR. Methanobacterium. Bergey's Manual of Systematics of Archaea and Bacteria 2015. Bergey's Manual Trust: New York, NY.

76. Becraft ED, Woyke T, Jarett J, Ivanova N, Godoy-Vitorino F, Poulton N et al. Rokubacteria: genomic giants among the uncultured bacterial phyla. Front in Microbiol 2017; 8: 2264.

77. Takami H, Noguchi H, Takaki Y, Uchiyama I, Toyoda A, Nishi S et al. A deeply branching thermophilic bacterium with an ancient acetyl-CoA pathway dominates a subsurface ecosystem. PLoS One 2012; 7.

78. Giovannoni SJ, Thrash JC, Temperton B. Implications of streamlining theory for microbial ecology. ISME J 2014; 8: 1553-1565.

79. Valentine DL. Adaptations to energy stress dictate the ecology and evolution of the Archaea. Nat Rev Microbiol 2007; 5: 316-323.

80. Baker-Austin C, Dopson M. Life in acid: pH homeostasis in acidophiles. Trends Microbiol 2007; 15: 165-171.

81. Poudel S, Colman DR, Fixen KR, Ledbetter RN, Zheng YN, Pence N et al. Electron transfer to nitrogenase in different genomic and metabolic backgrounds. J Bacteriol 2018; 200: 00757-00717.

82. Thauer RK, Jungermann K, Decker K. Energy-conservation in chemotropic anaerobic bacteria. Bacteriol Rev 1977; 41: 100-180.

83. Boyd, E.S., Schut, G.J., Adams, M.W.W., and Peters, J.W. Hydrogen metabolism and the evolution of biological respiration. Microbe 2014; 9: 361-367.

84. Hoehler, T.M. Biogeochemistry of dihydrogen (H_2). In: Sigel, H., and Sigel, R. (eds) Metal Ions in Biological Systems. Vol 43. (Taylor & Francis Group, Boca Raton, FL, 2005) pp 9-48.

85. Fones, E.M., Colman, D.R., Kraus, E.A., Nothaft, D.B., Poudel, S., Rempfert, K.R., *et al.* Physiological adaptations to serpentinization in the Samail Ophiolite, Oman. ISME J. 2019; 13: 1750-1762.

86. Ueno, Y., Yamada, K., Yoshida, N., Maruyama, S., and Isozake, Y. Evidence from fluid inclusions for microbial methanogenesis in the early Archaean era. Nature 2006; 440: 516-519.

87. Etiope, G., Vadillo, I., Whiticar, M.J, Marques, J.M., Carreira, P.M, Tiago, I. *et al.* Abiotic methane seepage in the Ronda peridotite massif, southern Spain. Geochem. 2016; 66: 101-113.

88. Proskurowski, G., Lilley, M.D., Seewald, J.S., Früh-Green, G., Olson, E.J., Lupton, J.E., *et al.* Abiogenic hydrocarbon production at Lost City hydrothermal field. Science 2008; 319: 604-607.

89. Etiope, G. Methane origin in the Samail ophiolite: Comment on "Modern water/rock reactions in Oman hyperalkaline peridotite aquifers and implications for microbial habitability." Geochim. Cosmochim. Acta 2017; 197: 467-470.

90. Miller, H.M., Matter, J.M., Kelemen, P., Ellison, E.T., Conrad, M.E., Fierer, N. *et al.* Reply to "Methane origin in the Samail ophiolite: Comment on 'Modern water/rock reactions in Oman hyperalkaline peridotite aquifers and implications for microbial habitability.'" Geochim. Cosmochim. Acta 2017; 197: 471-473.

91. Miller, H.M., Chaudhry, N., Conrad, M.E., Markus, B., Kopf, S.H., and Templeton, A.S. Large carbon isotope variability during methanogenesis under alkaline conditions. Geochim. Cosmochim. Acta 2018; 237: 18-31.

92. Bradley, A.S., Hayes, J.M., and Summons, R.E. Extraordinary ^{13}C enrichment of diether lipids at the Lost City Hydrothermal Field indicates a carbon-limited ecosystem. Geochim. Cosmochim. Acta 2009; 73: 102-118.

93. Zwicker, J., Birgel, D., Bach, W., Richoz, S., Smrzka, D., Grasemann, B. *et al.* Evidence for archaeal methanogenesis within veins at the onshore serpentinite-hosted Chimaera seeps, Turkey. Chem. Geol. 2018; 483: 567-580.

94. Kraus, E.A., Stamps, B.W., Rempfert, K.R., Nothaft D.B., Boyd, E.S., Matter, J.M. *et al.* Biological methane cycling in serpentinization-impacted fluids of the Samail ophiolite of Oman. AGU Fall Meeting Abstracts. 2018; (abstract #V13E-0139).

95. Neal, C. and Stanger, G. Hydrogen generation from mantle source rocks in Oman. Earth Planet. Sci. Lett. 1983; 66: 315-320.

96. Streit, E., Kelemen P., and Eiler J. Coexisting serpentine and quartz from carbonate- bearing serpentinized peridotite in the Samail Ophiolite, Oman. Contrib. Mineral. Petr. 2012; 164: 821-837.

97. Chavagnac, V., Monnin, C., Ceuleneer, G., Boulart, C., and Hoareau, G. Characterization of hyperalkaline fluids produced by lowtemperature serpentinization of mantle peridotites in the Oman and Ligurian ophiolites. Geochem. Geophys. 2013; 14: 2496-2522.

98. Mervine, E.M., Humphris, S.E., Sims, K.W.W., Kelemen, P.B., and Jenkins, W.J. Carbonation rates of peridotite in the Samail Ophiolite, Sultanate of Oman, constrained through ^{14}C dating and stable isotopes. Geochim. Cosmochim. Acta 2014; 126: 371-397.

99. Kang, D.W.D., Froula, J., Egan, R., and Wang, Z. MetaBAT, an efficient tool for accurately reconstructing single genomes from complex microbial communities. PeerJ 2015; 3: e1165.

100. Stepanauskas, R., Fergusson, E.A., Brown, J., Poulton, N.J., Tupper, B., Labonté, J.M. *et al.* Improved genome recovery and integrated cell-size analyses of individual uncultured microbial cells and viral particles. Nat. Commun. 2017; 8: 84.

101. Wu, M. and Scott, A.J., Phylogenomic analysis of bacterial and archaeal sequences with AMPHORA2. J. Bioinform. 2012; 28: 1033-1034.

102. Sievers, F., Wilm, A., Dineen, D., Gibson, T.J., Karplus, K., Li, W. *et al.* Fast, scalable generation of high quality protein multiple sequence alignments using Clustal Omega. Mol. Syst. Biol. 2011; 7: 539.

103. Nguyen, L.T., Schmidt, H.A., von Haesler, A., and Minh, B.Q. IQ-TREE: a fast and effective stochastic algorithm for estimating maximum-likelihood phylogenies. Mol. Biol. Evol. 2015; 32: 268-274.

104. Kalyaanamoorthy, S., Minh, B.Q., Wong, T.K.F., von Haesler, A., and Jermiin, L.S. ModelFinder: fast model selection for accurate phylogenetic estimates. Nat. Methods 2017; 14: 587.

105. Hyatt, D., Chen, G.L., LoCascio, P.F., Land, M.L., Larimer, F.W., and Hauser, L.J. Prodigal: prokaryotic gene recognition and translation initiation site identification. BMC Bioinformatics 2010; 11: 119.

106. Seemann, T. Prokka: rapid prokaryotic genome annotation. J. Bioinform. 2014; 30: 2068-9.

107. Kanehisa, M. and Goto, S. KEGG: Kyoto Encyclopedia of Genes and Genomes. Nucleic Acids Res. 2000; 28: 27-30.

108. Altschul, S.F., Gish, W., Miller, W., Myers, E.W., and Lipman, D.J. Basic local alignment search tool. J. Mol. Biol. 1990; 215: 403-410.

109. Greening, C., Biswas, A., Carere, C.R., Jackson, C.J., Taylor, M.C., Stott, M.B. *et al.* Genomic and metagenomic surveys of hydrogenase distribution indicate H_2 is a widely utilized energy source for microbial growth and survival. ISME J. 2016; 10: 761-777.

110. Peters, J.W., Schut, G.J., Boyd, E.S., Mulder, D.W., Shepard, E.M., Broderick, J.B. *et al.* [FeFe]-and [NiFe]-hydrogenase diversity, mechanism, and maturation. BBA-Mol. Cell Res. 2015; 1853: 1350-1369.

111. Marchler-Bauer, A., Bo, Y., Han, L., He, J., Lanczycki, C.J., Lu, S. *et al.* CDD/SPARCLE: functional classification of proteins via subfamily domain architectures. Nucleic Acids Res. 2016; 45: D200-D203.

112. Marçais, G., Delcher, A.L., Phillippy, A.M., Coston, R., Salzberg, S.L., and Zimin, A. MUMmer4: a fast and versatile genome alignment system. PLoS Comput. Biol. 2018; 14: e1005944.

113. Leplae, R., Lima-Mendez, G., and Toussaint, A. ACLAME: a CLAssification of Mobile genetic Elements, update 2010. Nucleic Acids Res. 2010; 38: D57-D61.

114. Lefort, V., Longueville, J.-E., and Gascuel, O. SMS: smart model selection in PhyML. Mol. Biol. Evol. 2017; 34: 2422-2424.

115. Guindon, S., Dufayard, J.-F., Lefort, V., Anisimova, M., Hordijk, W., and Gascuel, O. New algorithms and methods to estimate maximum-likelihood phylogenies: assessing the performance of PhyML 3.0. Syst. Biol. 2010; 59: 307-321.

116. Darling, A.E., Mau, B., and Perna, N.T. progressiveMauve: multiple genome alignment with gene gain, loss and rearrangement. PloS One 2010; 5: e11147.

117. Harrison, K.J., Crécy-Lagard, V., and Zallot, R. Gene Graphics: a genomic neighborhood data visualization web application. J. Bioinform. 2018; 34: 1406-1408.

118. Bowers, R.M., Kyrpides, N.C, Stepanauskas, R., Harmon-Smith, M., Doud, D., Reddy, T.B.K. *et al.* Minimum information about a single amplified genome (MISAG) and a metagenome-assembled genome (MIMAG) of bacteria and archaea. Nat. Biotechnol. 2017; 25: 725-731.

119. Thauer, R.K., Kaster, A.K., Seedorf, H., Buckel, W., and Hedderich, R. Methanogenic archaea: ecologically relevant differences in energy conservation. Nat. Rev. Microbiol. 2008; 6: 579-591.

120. Hendrickson, E.L. and Leigh, J.A. Roles of coenzyme F_{420}-reducing hydrogenases and hydrogen-and F_{420}-dependent methylenetetrahydromethanopterin dehydrogenases in reduction of F_{420} and production of hydrogen during methanogenesis. J. Bacteriol. 2008; 190: 4818-4821.

121. Goldman, A.D., Leigh, J.A., and Samudrala, R. Comprehensive computational analysis of Hmd enzymes and paralogs in methanogenic Archaea. BMC Evol. Biol. 2009; 9: 199.

122. Tersteegen, A. and Hedderich, R. Methanobacterium thermoautotrophicum encodes two multisubunit membrane-bound [NiFe] hydrogenases: Transcription of the operons and sequence analysis of the deduced proteins. Eur. J. Biochem. 1999; 264: 930-943.

123. Lie, T.J., Costa, K.C., Lupa, B., Korpole, S., Whitman, W.B., and Leigh, J.A. Essential anaplerotic role for the energy-converting hydrogenase Eha in hydrogenotrophic methanogenesis. Proc. Natl. Acad. Sci. U.S.A. 2012; 109: 15473-15478.

124. Thauer, R.K. The Wolfe cycle comes full circle. Proc. Natl. Acad. Sci. U.S.A. 2012; 109: 15084-15085.

125. Costa, K.C., Wong, P.M., Wang, T., Lie, T.J., Dodsworth, J.A., Swanson, I. *et al*. Protein complexing in a methanogen suggests electron bifurcation and electron delivery from formate to heterodisulfide reductase. Proc. Natl. Acad. Sci. U.S.A. 2010; 107: 11050-11055.

126. Greening, C., Ahmed, F.A., Mohamed, A.E., Lee, B.M., Pandey, G., Warden, A.C. *et al.* Physiology, biochemistry, and applications of F_{420}-and Fo-dependent redox reactions. Microbiol. Mol. Biol. Rev. 2016; 80: 451-493.

127. Yan, Z. and Ferry, J.G. Electron bifurcation and confurcation in methanogenesis and reverse methanogenesis. Front. Microbiol. 2018; 9: 1322.

128. Costa, K.C., Lie, T.J., Xia, Q., and Leigh, J.A. VhuD facilitates electron flow from H_2 or formate to heterodisulfide reductase in Methanococcus maripaludis. J. Bacteriol. 2013; 195: 5160-5165.

129. Schauer, N.L. and Ferry, J.G. Properties of formate dehydrogenase in Methanobacterium formicicum. J. Bacteriol. 1982; 150: 1-7.

130. Schauer, N.L., Ferry, J.G., Honek, J.F., Orme-Johnson, W.H., and Walsh, C. Mechanistic studies of the coenzyme F420-reducing formate dehydrogenase from Methanobacterium formicicum. Biochemistry 1986; 25: 7163-7168.

131. Mills, D.J., Vitt, S., Strauss, M., Shima, S., and Vonck, J. De novo modeling of the F_{420}-reducing [NiFe]-hydrogenase from a methanogenic archaeon by cryo-electron microscopy. Elife 2013; 2: e00218.

132. Schut, G.J., Boyd, E.S., Peters, J.W., and Adams, M.W.W. The modular respiratory complexes involved in hydrogen and sulfur metabolism by heterotrophic hyperthermophilic archaea and their evolutionary implications. FEMS Microbiol. Rev. 2013; 37: 182-203.

133. Hamamoto, T., Hashimoto, M., Hino, M., Kitada, M., Seto, Y., Kudo, T. *et al.* Characterization of a gene responsible for the Na^+/H^+ antiporter system of alkalophilic Bacillus species strain C125. Mol. Microbiol. 1994; 14: 939-946.

134. Boone, D.R., Johnson, R.L., and Liu, Y. Diffusion of the interspecies electron carriers H_2 and formate in methanogenic ecosystems and its implications in the measurement of K_m for H_2 or formate uptake. Appl. Environ. Microbiol. 1989; 55: 1735-1741.

135. McCollom, T.M. and Seewald J.S. Experimental constraints on the hydrothermal reactivity of organic acids and acid anions: I. Formic acid and formate. Geochim. Cosmochim. Acta 2003; 67: 3625-3644.

136. Lang, S.Q., Butterfield, D.A., Schulte, M., Kelley, D.S., and Lilley, M.D. Elevated concentrations of formate, acetate and dissolved organic carbon found at the Lost City hydrothermal field. Geochim. Cosmochim. Acta 2010; 74: 941-952.

137. Zeng, Y. and Liu, J. Short-chain carboxylates in fluid inclusions in minerals. Appl. Geochemistry 2000; 15: 13-25.

138. Suzuki, S., Nealson, K.H., and Ishii, S. Genomic and in-situ transcriptomic characterization of the candidate phylum NPL-UPL2 from highly alkaline highly reducing serpentinized groundwater. Front. Microbiol. 2018; 9: 3141.

139. Brazelton, W.J. and Baross, J.A. Abundant transposases encoded by the metagenome of a hydrothermal chimney biofilm. ISME J. 2009; 3: 1420-1424.

140. Zhang, J., Kasciukovic, T., and White, M.F. The CRISPR associated protein Cas4 Is a 5′ to 3′ DNA exonuclease with an iron-sulfur cluster. PloS One 2012; 7: e47232.

141. Rath, D., Amlinger, L., Rath, A., and Lundgren, M. The CRISPR-Cas immune system:biology, mechanisms and applications. Biochimie 2015; 117: 119-128.

142. Jansen, R., van Embden, J.D.A., Gaastra, W., and Schouls, L.M. Identification of genes that are associated with DNA repeats in prokaryotes. Mol. Microbiol. 2002; 43: 1565-1575.

143. Reno, M.L., Held, N.L., Fields, C.J., Burke, P.V., and Whitaker, R.J. Biogeography of the *Sulfolobus islandicus* pan-genome. Proc. Natl. Acad. Sci. U.S.A. 2009; 106: 8605-8610.

144. Tettelin, H., Masignani, V., Cieslewicz, M.J., Donati, C., Medini, D., Ward, N.L. *et al.* Genome analysis of multiple pathogenic isolates of *Streptococcus agalactiae:* implications for the microbial "pan-genome." Proc. Natl. Acad. Sci. U.S.A. 2005; 102: 13950-13955.

145. Labonté, J.M., Field, E.K., Lau, M., Chivian, D., Van Heerden, E., Wommack, K.E. *et al.* Single cell genomics indicates horizontal gene transfer and viral infections in a deep subsurface Firmicutes population. Front. Microbiol. 2015; 6: 349.

146. Karnachuk, O.V., Frank, Y.A., Lukina, A.P., Kadnikov, V.V., Beletsky, A.V., Mardanov, A.V. *et al.* Domestication of previously uncultivated *Candidatus* Desulforudis audaxviator from a deep aquifer in Siberia sheds light on its physiology and evolution. ISME J. 2019; 13: 1947-1959.

147. Paul, B.G., Burstein, D., Castelle, C.J., Handa, S., Arambula, D., Czornyj, E. *et al.* Retroelement-guided protein diversificiation abounds in vast lineages of Bacteria and Archaea. Nat. Microbiol. 2017; 2: 17045.

148. Dirix, G., Monsieurs, P., Dombrecht, B., Daniels, R., Marchal, K., Vanderleyden, J. *et al.* Peptide signal molecules and bacteriocins in Gram-negative bacteria: a genome-wide in silico screening for peptides containing a double-glycine leader sequence and their cognate transporters. Peptides 2004; 25: 1425-1440.

149. McMahon S, Parnell J. Weighing the deep continental biosphere. FEMS Microbiol Ecol. 2014; 87(1): 113-20.

150. Carlson R. The abundance of ultramafic rocks in Atlantic Ocean crust. Geophys. J. Int. 2001; 144(1): 37-48.

151. Nisbet E, The geological setting of the earliest life forms. J. Mol. Evol. 1985; 21(3): 289-298.

152. Martin H, Albarede F, Claeys P, Garguad M, Marty B, Morbidelli A, *et al.*, 4. building of a habitable planet. Earth, Moon, and Planets 2006; 98(1-4): 97-151.

153. Fones, EM, Colman DR, Kraus EA, Stepanauskas R, Templeton AS, Spear JR, *et al.*, Diversification of methanogens into hyperalkaline serpentinizing environments through adaptations to minimize oxidant limitation. ISME J. 2021; 15: 1121–113.

154. Ellison ET, Templeton AS, Zeigler SD, Mayhew L, Kelemen PB, Matter J. Low-Temperature Hydrogen Formation During Aqueous Alteration of Serpentinized Peridotite in the Samail Ophiolite. J. Geophys. Res. Solid Earth. 2021; *126*(6): e2021JB021981.

155. McCollom TM, Klein F, Solheid P, Moskowitz B. The effect of pH on rates of reaction and hydrogen generation during serpentinization. Philos. Trans. R. Soc. A. 2020; 378(2165): 20180428.

156. Templeton A, Ellison E. Formation and loss of metastable brucite: does Fe (II)-bearing brucite support microbial activity in serpentinizing ecosystems? Philos. Trans. R. Soc. A. 2020; 378(2165): 20180423.

157. Mayhew LE, Ellison ET, McCollom TM, Trainor TP, Templeton AS. Hydrogen generation from low-temperature water–rock reactions. Nat. Geosci. 2013; 6(6): 478-484.

158. Chassefiére E, and Leblanc F, Constraining methane release due to serpentinization by the observed D/H ratio on Mars. Earth Planet. Sci. Lett. 2011; 310(3-4): 262-271.

159. Waite JH, Glein CR, Perryman RS, Teolis BD, Magee BA, Miller G, *et al.*, Cassini finds molecular hydrogen in the Enceladus plume: evidence for hydrothermal processes. Science 2017; 356(6334): 155-159.

160. Glein CR, Baross JA, and Waite JH. The pH of Enceladus' ocean. Geochim. Cosmochim. Acta. 2015; 162: 202-219.

161. Vance S, Hand K, and Pappalardo R. Geophysical controls of chemical disequilibria in Europa. Geophys. Res. Lett. 2016; 43(10): 4871-4879.

162. Templeton A, Ellison ET, Glombitza C, Morono Y, Rempfert KR, Hoehler T, *et al.*, Accessing the subsurface biosphere within rocks undergoing active low-temperature serpentinization in the Samail Ophiolite (Oman Drilling Project). J Geophys. Res. Biogeosci., In review.

163. Früh-Green GL, Orcutt BN, Rouméjon S, Lilley MD, Morono Y, Cotterill C, *et al*. Magmatism, serpentinization and life: Insights through drilling the Atlantis Massif (IODP Expedition 357). Lithos 2018; 323: 137-155.

164. Motamedi S, Orcutt BN, Früh-Green GL, Twing KI, Pendleton HL, Brazelton WJ. Microbial residents of the Atlantis Massif's shallow serpentinite subsurface. Appl. Environ. Microbiol. 2020; 86(11), e00356-20.

165. Suzuki Y, Yamashita S, Kouduka M, Ao Y, Mukai H, Mitsunobu S, *et al*. Deep microbial proliferation at the basalt interface in 33.5–104 million-year-old oceanic crust. Commun. Biol. 2020; 3(1), 1-9.

166. Li J, Mara P, Schubotz F, Sylvan JB, Burgaud G, Klein F. *et al.* Recycling and metabolic flexibility dictate life in the lower oceanic crust. Nature 2020; 579(7798): 250-255.

167. Wall CJ, Scoates JS, Weis D, Friedman RM, Amini M, Meurer WP. The Stillwater Complex: integrating zircon geochronological and geochemical constraints on the age, emplacement history and crystallization of a large, open-system layered intrusion. J. Petrol. 2018; 59(1): 153-190.

168. Page, N.J., Stillwater Complex, Montana: Structure, mineralogy, and petrology of the Basal Zone with emphasis on the occurrence of sulfides. Vol. 1038. 1978: Department of the Interior, Geological Survey.

169. Kelemen P, Matter JM, Teagle DAH, Coggon JA, *et al.*, Proceedings of the Oman Drilling Project: Scientific Drilling in the Samail Ophiolite, Sultanate of Oman. International Ocean Discovery Program. 2020; Phase 1 and 2.

170. Wells-Bennik MH, Janssen PWM, Klaus V, Yang C, Zwietering MH, Den Besten, HMW. Heat resistance of spores of 18 strains of Geobacillus stearothermophilus and impact of culturing conditions. Int. J. Food Microbiol. 2019; 291: 161-172.

171. Hamilton TL, Peters JW, Skidmore ML, Boyd ES. Molecular evidence for an active endogenous microbiome beneath glacial ice. ISME J. 2013; 7(7): 1402-12.

172. Gómez M. and Moldenhauer J, Biological indicators for sterilization processes. 2009. Davis Healthcare International Publishing.

173. Magnabosco C, Lin LH, Dong H, Bomberg M, Ghiorse W, Stan-Lotter H, *et al.* The biomass and biodiversity of the continental subsurface. Nat. Geosci. 2018; 11(10): 707-717.

174. Kraus EA, Nothaft D, Stamps BW, Rempfert KR, Ellison ET, Matter JM, *et al.* Molecular evidence for an active microbial methane cycle in subsurface serpentinite-hosted groundwaters in the Samail Ophiolite, Oman. Appl. Environ. Microbiol. 2021; 87(2).

175. Chapelle FH, O'Neill K, Bradley PM, Methé BA, Ciufo SA, Knobel LL, *et al*. A hydrogen-based subsurface microbial community dominated by methanogens. Nature 2002; 415(6869): 312-315.

176. The Mineral Corporation, Competent Person's Report on the Montana Platinum Group Metal Mineral Assets of Sibanye Gold Limited, United States of America. 2017: Cramerview, South Africa.

177. Trevors J, The subsurface origin of microbial life on the Earth. Res. Microbiol. 2002; 153(8): 487-491.

178. Boyd ES, Cummings DE, Geesey GG. Mineralogy influences structure and diversity of bacterial communities associated with geological substrata in a pristine aquifer. Microb. Ecol. 2007; 54(1): 170-182.

179. Morono Y, Terada T, Kallmeyer J, Inagaki F. An improved cell separation technique for marine subsurface sediments: applications for high-throughput analysis using flow cytometry and cell sorting. Environ. Microbiol. 2013; 15(10), 2841-2849.

APPENDIX A

COPIES OF PERMISSIONS TO REPRINT

Article | Open Access | Published: 12 March 2019

Physiological adaptations to serpentinization in the Samail Ophiolite, Oman

Elizabeth M. Fones, Daniel R. Colman, Emily A. Kraus, Daniel B. Nothaft, Saroj Poudel, Kaitlin R. Rempfert, John R. Spear, Alexis S. Templeton & Eric S. Boyd

Rights and permissions

Article | Open Access | Published: 30 November 2020

Diversification of methanogens into hyperalkaline serpentinizing environments through adaptations to minimize oxidant limitation

Elizabeth M. Fones, Daniel R. Colman, Emily A. Kraus, Ramunas Stepanauskas, Alexis S. Templeton, John R. Spear & Eric S. Boyd

Rights and permissions